Diplomarbeit

Using an inverted Spin Ensemble as a Photon Source

ausgeführt am

Atominstitut
der Technischen Universität Wien

Institute for Atomic and Subatomic Physics
Vienna University of Technology

unter der Anleitung von

Dipl.-Ing. Wenzel Kersten,

Dipl.-Ing. Dr. rer. nat. Andreas Angerer
und

Univ.-Prof. Dipl.-Ing. Dr. techn. Hannes-Jörg Schmiedmayer
durch

Nikolaus de Zordo
Matrikelnummer: 01526242
[redacted]

Hannes-Jörg Schmiedmayer

Nikolaus de Zordo

Ebreichsdorf/Wien, am 13. Dezember 2021

Die approbierte gedruckte Originalversion dieser Diplomarbeit ist an der TU Wien Bibliothek verfügbar
The approved original version of this thesis is available in print at TU Wien Bibliothek.
TU Bibliothek Your knowledge hub WIEN

Die approbierte gedruckte Originalversion dieser Diplomarbeit ist an der TU Wien Bibliothek verfügbar
The approved original version of this thesis is available in print at TU Wien Bibliothek.

Abstract

In the most recent century a technological breakthrough in information-technology, using hybrid quantum systems, is expected. To be able to use such systems in daily life, however, the controlled manipulation of them needs to be understood. For future technological implementations the usage of solid state spin ensembles in cavities seems a very promising approach since these systems can be scaled up easily. Therefore, the controlled manipulation of defects in diamond, so-called negatively charged nitrogen vacancy centers, with a single mode microwave cavity is studied in the present thesis.

At first, we design microwave pulses with which we invert our macroscopic spin system with high fidelity. Then, in the main part of the thesis, it is shown that by changing the magnetic field and as a consequence the transition frequency between the excited and the ground state such an inverted spin system can be stabilized. Moreover, after bringing the spin system back into resonance, one observes a photon burst caused by superradiant spin decay. By doing so, we are able to hold the spins inverted for some milliseconds. This controlled decay can therefore be used to build a "quantum battery". We furthermore demonstrate, how such an inverted spin system can be used as a quantum detector which can detect arbitrary weak pulses since its physical limit is given by the blackbody radiation.

Additionally, we numerically demonstrate a second stabilization method for the inverted spin ensemble by which one can extend the time in which a detection is possible. This time is now only limited by the inherent spin decay caused by spin-spin interactions.

Die approbierte gedruckte Originalversion dieser Diplomarbeit ist an der TU Wien Bibliothek verfügbar
The approved original version of this thesis is available in print at TU Wien Bibliothek.
TU Bibliothek Your knowledge hub WIEN

Die approbierte gedruckte Originalversion dieser Diplomarbeit ist an der TU Wien Bibliothek verfügbar
The approved original version of this thesis is available in print at TU Wien Bibliothek.

Zusammenfassung

In diesem Jahrhundert wird ein technologischer Durchbruch in der Informationstechnologie mit Hilfe von hybriden Quantensystemen erwartet. Um solche Systeme auch im täglichen Leben verwenden zu können, muss jedoch die kontrollierte Manipulation dieser verstanden werden. Für zukünftige technologische Anwendungen scheint die Verwendung von Spinensembles von Festkörpern in Resonatoren ein sehr vielversprechender Ansatz zu sein, da solche Systeme recht einfach vergrößert werden können. Daher wird die kontrollierte Manipulation von Defekten im Diamant, sogenannte negativ geladene Stickstofffehlstellenzentren, mit einem Resonator in dieser Arbeit untersucht.

Zuerst designen wir Mikrowellenpulse, mit denen wir das makroskopische Spinensemble mit hoher Genauigkeit invertieren. Dann wird im Hauptteil der Arbeit gezeigt, dass durch das Ändern des Magnetfeldes und in weiterer Folge durch die Änderung der Übergangsfrequenz zwischen angeregtem und Grundzustand solch ein invertiertes Spinensemble stabilisiert werden kann. Zusätzlich lässt sich, nachdem man das Spinsystem zurück in Resonanz gebracht hat, eine Photonenlawine, ausgelöst durch superradianten Spinzerfall, beobachten. Auf diese Art und Weise können wir die Spins für einige Millisekunden invertiert halten. Dieser kontrollierte Zerfall kann daher verwendet werden, um eine "Quantenbatterie" zu bauen. Außerdem zeigen wir, dass ein solches invertiertes Spinsystem als Quantendetektor zu nutzen ist, der beliebig schwache Mikrowellenpulse detektieren kann, da sein physikalisches Limit durch Schwarzkörperstrahlung gegeben ist.

Zusätzlich zeigen wir numerisch eine zweite Art wie das invertierte Spinensemble stabilisiert werden kann wodurch die Zeit in der eine Detektion möglich ist verlängert wird. Diese Zeit ist jetzt nur durch den inhärenten Spinzerfall, welcher durch Spin-Spin Wechselwirkungen verursacht wird, limitiert.

Die approbierte gedruckte Originalversion dieser Diplomarbeit ist an der TU Wien Bibliothek verfügbar
The approved original version of this thesis is available in print at TU Wien Bibliothek.
TU Bibliothek Your knowledge hub WIEN

Die approbierte gedruckte Originalversion dieser Diplomarbeit ist an der TU Wien Bibliothek verfügbar
The approved original version of this thesis is available in print at TU Wien Bibliothek.

Contents

Abstract **iii**

Zusammenfassung **v**

1 Introduction **1**

2 Cavity Quantum Electrodynamics **3**
2.1 Quantization of Electromagnetic Field 3
2.2 Ideal Cavity - Quantized LC Oscillator 9
2.3 Jaynes-Cummings Hamiltonian 11
2.4 Tavis-Cummings Hamiltonian - Interaction of a Spin Ensemble with a Cavity 16
2.5 Driven Tavis-Cummings Hamiltonian 20
2.6 Numerical Simulation of our System - Maxwell-Bloch Equations . . . 21

3 Experimental Setup **25**
3.1 Real Cavity 25
3.2 NV Center 28
3.3 Dilution Refrigerator 34
3.4 Experimental Measurement Methods 34
3.5 Homodyne Measurement and IQ Mixing 38
3.6 Design of OCT Pulse 39
3.7 Simulation of the System 41

4 Experiment **45**
4.1 Constant Spin Detuning - Detection of Thermal Microwave Background 47
4.2 Periodic Spin Detuning - Detection of Short Microwave Pulses 61

5 Conclusion and Outlook **69**

A Cavity QED Calculations **71**
A.1 Quantization of Electromagnetic Field - Evaluate Integral 71
A.2 Unitary Operator Transformation 71
A.3 Calculating Eigenenergies and Eigenvectors of the Jaynes-Cummings Hamiltonian 73

Die approbierte gedruckte Originalversion dieser Diplomarbeit ist an der TU Wien Bibliothek verfügbar
The approved original version of this thesis is available in print at TU Wien Bibliothek.
TU Bibliothek Your knowledge hub WIEN

A.4 Unitary Transformation of driven Tavis-Cummings Hamiltonian . . . 75
A.5 Derivation of the Lindblad Master Equation 78
A.6 Derivation of the Maxwell-Bloch Equations 86

Bibliography **91**

Acknowledgments **97**

Die approbierte gedruckte Originalversion dieser Diplomarbeit ist an der TU Wien Bibliothek verfügbar
The approved original version of this thesis is available in print at TU Wien Bibliothek.
TU WIEN Bibliothek Your knowledge hub

1 Introduction

One of the most important equations in physics are Maxwell's equations describing electrodynamics [1]. By exploring the interaction of light and matter, the photoelectric effect (besides many others) was discovered. This effect is only explainable if one assumes that the light is quantized as done by Albert Einstein [2] for which explanation he received the 1921 Nobel Prize in Physics [3]. Based on that insight, a completely new framework of quantum mechanics was developed [4] which led to the quantization of the electromagnetic field and opened a new research area named quantum electro dynamics (QED) [5]. This was honored with the 1965 Nobel Prize in Physics [6–8]. In the following, the interaction of such a quantized field with matter, which is nowadays realized by putting atoms or other emitters inside a cavity (cavity QED), is studied. This experimental setup lead to a Nobel Price in Physics in 2012 [9, 10].
Such experimental setups paved the way for a wide range of applications. The possibility of controlling individual qubits led to the experimental realization of quantum information technologies. In such setups, a lower number of emitters which ranges from trapped cold atoms and ions [11] to localized solid state quantum emitters such as superconducting circuits [12], quantum dots [13, 14] and color centers [15], are coupled to the cavity mode. Besides that, another research direction is to couple to a larger ensemble of emitters [16, 17] which allows to study and observe non linear effects as well. By coupling to a larger ensemble, many new effects like non-Markovian spin dynamics [18], the protection of a spin ensemble against decoherence [19], coherent coupling between two spin ensembles [20], spectral hole burning [21], bistable hybrid quantum systems [22], collective strong coupling [23] and superradiant spin decay [24], just to name a few, are observable.

Based on the quite recent success of observing a superradiant spin decay [24], which is a collective effect [25] and therefore only observable when dealing with a larger ensemble, we asked us whether it is possible to keep the spins inverted for some time and then let them decay in a controlled way. In other words, we asked us if it is possible to store the energy in the inverted spin system and then discharge our "quantum battery". The decay of such a stabilized inverted ensemble can in principle be triggered by a (very) weak pulse as well which means that such a setup can be additionally used as a detector. As said before, also when coupling to a larger spin ensemble one has a plethora of emitters which one can use in cavity QED experiments. In this thesis, we are working with nitrogen vacancy centers in diamond since they are very stable and robust. The large number of centers in such

Die approbierte gedruckte Originalversion dieser Diplomarbeit ist an der TU Wien Bibliothek verfügbar
The approved original version of this thesis is available in print at TU Wien Bibliothek.
TU Bibliothek Your knowledge hub WIEN

a crystal gives us the possibility to work in the strong coupling regime and therefore to observe non-linear effects like superradiant emission. Besides that, by working at cryogenic temperatures we can easily initialize our spin system in its ground state. The transition frequency of 2.88 GHz simplifies things as well since one can work in the S-band of the microwave regime.

The thesis consists of three main chapters. In the first chapter, the mathematical framework of cavity quantum electrodynamics is derived. We start with quantizing the electromagnetic field and how a cavity can be described mathematically. Then, we derive the interaction term between the photons and a single two level system which afterwards get generalized to a larger number of emitters. At the end of this chapter, we extend the Hamiltonian once more and include a cavity driving term and derive the Maxwell-Bloch equations with which our system can be modeled. The second chapter is dedicated to the experimental setup. We explain how a real cavity differs from an ideal one and what properties our nitrogen vacancy centers exhibit. Next, the working principle of the dilution refrigerator and our experimental measurement methods including IQ mixing are explained. We conclude that chapter with the design of our optimal control pulse and how we can simulate the experiment numerically. Last but not least the obtained experimental results are presented.

Die approbierte gedruckte Originalversion dieser Diplomarbeit ist an der TU Wien Bibliothek verfügbar
The approved original version of this thesis is available in print at TU Wien Bibliothek.
TU Bibliothek Your knowledge hub WIEN

2 Cavity Quantum Electrodynamics

In this chapter we want to derive the mathematical framework with which one can describe our experiment. First, we start with the quantization of the electromagnetic field and then continue with quantizing the field of a cavity which is equivalent to an LC circuit. Next, we derive an equation which describes the interaction between a cavity and a single two level system, for example a single spin which afterwards gets extended to a model describing the interaction between the cavity and many spins. Lastly, we include a driving term and derive equations of motion, the so-called Maxwell-Bloch equations. For further reading the reader is referred to the books [26–30] on which parts of the following chapter are based as well.

2.1 Quantization of Electromagnetic Field

The starting point for the quantization of the electromagnetic field in vacuum are the corresponding Maxwell equations,

$$\nabla \cdot \boldsymbol{B} = 0, \tag{2.1a}$$

$$\nabla \cdot \boldsymbol{E} = 0, \tag{2.1b}$$

$$\nabla \times \boldsymbol{B} = \mu_0 \varepsilon_0 \frac{\partial \boldsymbol{E}}{\partial t}, \tag{2.1c}$$

$$\nabla \times \boldsymbol{E} = -\frac{\partial \boldsymbol{B}}{\partial t}, \tag{2.1d}$$

where the spatial and time dependence of the vector fields have been dropped for better readability. The homogeneous Maxwell equations can be solved by introducing new potentials. For example, the vector potential $\boldsymbol{A}$ with

$$\boldsymbol{B} = \nabla \times \boldsymbol{A}, \tag{2.2}$$

automatically solves $\nabla \cdot \boldsymbol{B} = 0$ since the divergence of the curl of a vector field is zero. This can be seen by writing this in index notation, i.e., $\nabla \cdot (\nabla \times \boldsymbol{A}) = \partial_i \partial_j \epsilon_{ijk} A_k$, where the spatial derivatives are symmetric and the epsilon tensor antisymmetric with respect to i and j which immediately leads to the aforementioned relation.

Die approbierte gedruckte Originalversion dieser Diplomarbeit ist an der TU Wien Bibliothek verfügbar
The approved original version of this thesis is available in print at TU Wien Bibliothek.
TU Bibliothek Your knowledge hub WIEN

Next, we want to find a relation between $\boldsymbol{A}$ and $\boldsymbol{E}$. Therefore, we insert Eq. (2.2) into Eq. (2.1d) and get

$$\nabla \times \left(\boldsymbol{E} + \frac{\partial \boldsymbol{A}}{\partial t} \right) = 0, \tag{2.3}$$

where we exchanged the partial and time derivative. Because the curl of a gradient-field vanishes as well ($\nabla \times (\nabla \phi) = \partial_j \epsilon_{ijk} \partial_k \phi$ for which the same symmetry arguments hold as before), we can write

$$\boldsymbol{E} = -\nabla \phi - \frac{\partial \boldsymbol{A}}{\partial t}, \tag{2.4}$$

where ϕ is a new introduced scalar field which solves Eq. (2.3). Inserting the new potentials into Eq. (2.1c) leads to

$$\nabla \times (\nabla \times \boldsymbol{A}) = -\mu_0 \epsilon_0 \frac{\partial}{\partial t} \left(\nabla \phi + \frac{\partial \boldsymbol{A}}{\partial t} \right). \tag{2.5}$$

Using the relation $\nabla \times (\nabla \times \boldsymbol{A}) = \nabla(\nabla \cdot \boldsymbol{A}) - \Delta \boldsymbol{A}$ yields

$$\nabla \left(\nabla \cdot \boldsymbol{A} + \epsilon_0 \mu_0 \frac{\partial \phi}{\partial t} \right) - \Delta \boldsymbol{A} + \mu_0 \epsilon_0 \frac{\partial^2 \boldsymbol{A}}{\partial t^2} = 0. \tag{2.6}$$

Up to now we have not set up any conditions for the above introduced potentials $\boldsymbol{A}$ and ϕ. Actually, this set is overcomplete. One can easily see this by performing a gauge transformation, i.e., by introducing an additional scalar field $\Lambda(t, r)$ and transform the potentials

$$\begin{aligned} \phi'(t, r) &= \phi(t, r) + \frac{\partial}{\partial t} \Lambda(t, r), \\ \boldsymbol{A}'(t, r) &= \boldsymbol{A}(t, r) - \nabla \Lambda(t, r), \end{aligned} \tag{2.7}$$

under which the $\boldsymbol{E}$ and $\boldsymbol{B}$ field remain unchanged. By using the Coulomb gauge $\nabla \cdot \boldsymbol{A} = 0$ (if the potential does not satisfy this equation one can choose a suitable $\Lambda(t, r)$ such that it is fulfilled) and assume furthermore that there are no sources present, i.e., $\phi = 0$, one gets rid of this overcompleteness and Eq. (2.6) gives

$$\nabla^2 \boldsymbol{A}(r, t) - \mu_0 \epsilon_0 \frac{\partial^2 \boldsymbol{A}(r, t)}{\partial t^2} = 0, \tag{2.8}$$

which is a wave equation and has plane wave solutions of the form $\boldsymbol{A} = \boldsymbol{\alpha} \mathrm{e}^{\mathrm{i}(\boldsymbol{kr} - \omega t)}$. Since a wave equation in general reads like $\frac{\partial^2 u}{\partial x^2} - \frac{1}{c^2} \frac{\partial^2 u}{\partial t^2} = 0$ we know that $\mu_0 \epsilon_0$ has the dimension of an inverse velocity squared and since electromagnetic waves in vacuum propagate with the speed of light we end up with $c = \frac{1}{\sqrt{\mu_0 \epsilon_0}}$. Inserting that and the plane wave solution into Eq. (2.8) reveals the dispersion relation $\omega = kc$.

Die approbierte gedruckte Originalversion dieser Diplomarbeit ist an der TU Wien Bibliothek verfügbar
The approved original version of this thesis is available in print at TU Wien Bibliothek.
TU Bibliothek Your knowledge hub WIEN

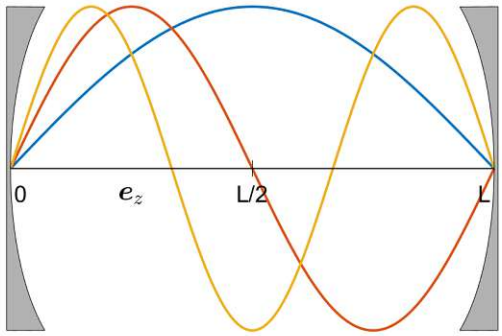

Figure 2.1: By limiting the mode volume of electromagnetic waves with two conducting walls at $z = 0$ and $z = L$, only certain wave vectors, namely $k\vec{e}_z = \frac{n\pi}{L}$ with $n \in \mathbb{N}$ are allowed. The first three modes of the electric field ($n = 1, 2, 3$) are shown in blue, red and yellow, respectively.

In the following, we assume a one dimensional conducting box in the z direction with length L. Because of the boundary conditions (the electric field has to be zero at $z = 0$ and $z = L$), only certain wave vectors $\boldsymbol{k}$, namely those that fulfill $k\vec{e}_z = \frac{n\pi}{L}$ with $n \in \mathbb{N}$ are allowed. The first three modes of an electric field in such a box can be seen in Fig. 2.1. Therefore, we decompose the vector field $\boldsymbol{A}$ in components of the different wave vectors $k\vec{e}_z$ and additionally make a separation ansatz

$$\boldsymbol{A}(z,t) = \alpha \sum_k \boldsymbol{u}_k(z) a_k(t), \tag{2.9}$$

with a variable α which can be fixed by dimensional analysis. Please note, that by assuming a one dimensional box in z direction, the direction of the wave vector $\boldsymbol{k} = k\vec{e}_z$ is fixed as well. Therefore, from now onwards, we will not use bold symbols for vectors as it should be clear from the context in which direction they are pointing. Inserting that separation ansatz into Eq. (2.8) leads to

$$\begin{aligned} a_k(t)\nabla^2 \boldsymbol{u}_k(z) - \frac{1}{c^2}\boldsymbol{u}_k(z)\frac{\partial^2}{\partial t^2}a_k(t) &= 0, \\ c^2\frac{\nabla^2 \boldsymbol{u}_k(z)}{\boldsymbol{u}_k(z)} = \frac{\frac{\partial^2}{\partial t^2}a_k(t)}{a_k(t)} &= -\omega_k^2 = \text{const.} \end{aligned} \tag{2.10}$$

Since the left side depends only on z and the right side only on t, the equation has to be constant which we set to $-\omega_k^2$. Therefore, one can separate that expression and solve the corresponding equations,

$$\left[\nabla^2 + \frac{w_k^2}{c^2}\right] \boldsymbol{u}_k(z) = 0, \tag{2.11a}$$

Die approbierte gedruckte Originalversion dieser Diplomarbeit ist an der TU Wien Bibliothek verfügbar
The approved original version of this thesis is available in print at TU Wien Bibliothek.
TU Bibliothek Your knowledge hub WIEN

$$\left[\frac{\partial^2}{\partial t^2} + \omega_k^2\right] a_k(t) = 0, \tag{2.11b}$$

for themselves. The solution of Eq. (2.11b) is given by

$$a_k(t) = a_k \mathrm{e}^{-\mathrm{i}\omega_k t} + a_k^* \mathrm{e}^{\mathrm{i}\omega_k t}, \tag{2.12}$$

where the complex conjugated amplitudes assure that we get a real vector field. Since we assume, as mentioned above, a one dimensional conducting box in the z direction and therefore the electric field has to be zero at the boundaries, the solution of Eq. (2.11a) is

$$\boldsymbol{u}_k(z) = \beta \vec{e}_k \sin(kz), \tag{2.13}$$

with $k = \frac{n\pi}{L}$, $\vec{e}_k$ being the polarization vector and β a normalization constant. By postulating $\int_0^L |\boldsymbol{u}_k(z)|^2 = 1$, we get $\beta = \sqrt{\frac{2}{L}}$. Inserting the solutions for $a(t)$ and $\boldsymbol{u}_k(z)$ into Eq. (2.9) our vector potential $\boldsymbol{A}$ reads like

$$A = \alpha \sqrt{\frac{2}{L}} \sum_k \vec{e}_x \left[a_k \mathrm{e}^{-\mathrm{i}\omega_k t} \sin(kz) + a_k^* \mathrm{e}^{\mathrm{i}\omega_k t} \sin(kz)\right], \tag{2.14}$$

where we, with no loss of generality, assume, that the vector potential A points in the x direction. With Eq. (2.2), Eq. (2.4) and $\phi = 0$, we find the following expressions for the electric and magnetic field

$$\begin{aligned} E_x &= \mathrm{i}\alpha \sqrt{\frac{2}{L}} \sum_k \omega_k \vec{e}_x \left[a_k \mathrm{e}^{-\mathrm{i}\omega_k t} \sin(kz) - a_k^* \mathrm{e}^{\mathrm{i}\omega_k t} \sin(kz)\right], \\ B_y &= \alpha \sqrt{\frac{2}{L}} \sum_k (k\vec{e}_z \times \vec{e}_x) \left[a_k \mathrm{e}^{-\mathrm{i}\omega_k t} \cos(kz) + a_k^* \mathrm{e}^{\mathrm{i}\omega_k t} \cos(kz)\right]. \end{aligned} \tag{2.15}$$

The electromagnetic mode with $k = \frac{3\pi}{L}$ at $t = \frac{\pi}{2\omega_k}$ is visualized in Fig. 2.2.

After we derived both fields, we want to calculate the energy of the electromagnetic waves, i.e.,

$$H = \frac{1}{2} \int_V \left(\epsilon_0 E^2 + \frac{1}{\mu_0} B^2\right). \tag{2.16}$$

Since we have a one dimensional problem we do not integrate over the whole volume but only in the respective dimension z from 0 to L. For the electric field energy we get

$$\begin{aligned} \int_0^L |E_x|^2 \,\mathrm{d}z = \int_0^L \frac{\alpha^2}{4} \sum_{k,k'} \omega_k \left[a_k \mathrm{e}^{-\mathrm{i}\omega_k t} \sin(kz) - a_k^* \mathrm{e}^{\mathrm{i}\omega_k t} \sin(kz)\right] \\ \omega_{k'} \left[a_{k'}^* \mathrm{e}^{\mathrm{i}\omega_{k'} t} \sin(k'z) - a_{k'} \mathrm{e}^{-\mathrm{i}\omega_{k'} t} \sin(k'z)\right] \mathrm{d}z. \end{aligned} \tag{2.17}$$

Die approbierte gedruckte Originalversion dieser Diplomarbeit ist an der TU Wien Bibliothek verfügbar
The approved original version of this thesis is available in print at TU Wien Bibliothek.
TU Bibliothek Your knowledge hub WIEN

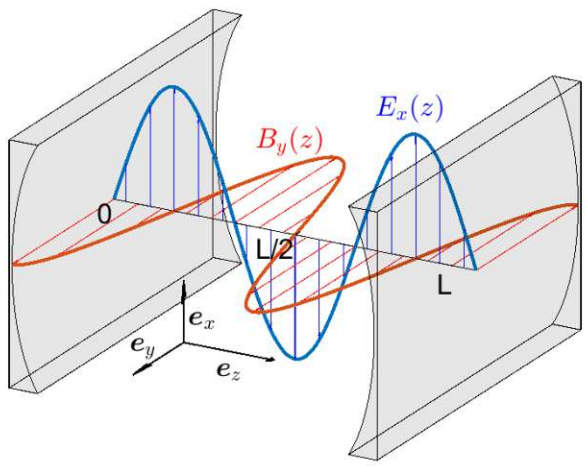

Figure 2.2: Visualization of the third electromagnetic mode (i.e. $k = \frac{3\pi}{L}$) at $t = \frac{\pi}{2\omega_k}$ inside a box with conducting walls placed at $z = 0$ and $z = L$.

Using $k = \frac{n\pi}{L}$ and $k' = \frac{m\pi}{L}$ we get terms like (the coefficients which do not depend on the spatial component are not relevant for this integral and are therefore dropped for better readability)

$$\begin{aligned}&\int_0^L \sin\left(\frac{n\pi}{L}z\right)\sin\left(\frac{m\pi}{L}z\right)\mathrm{d}z\\&= \frac{1}{2}\int_0^L \cos\left(\frac{(n-m)\pi}{L}z\right)\mathrm{d}z - \frac{1}{2}\int_0^L \cos\left(\frac{(n+m)\pi}{L}z\right)\mathrm{d}z = \frac{L}{2}\delta_{nm} = \frac{L}{2}\delta_{kk'},\end{aligned} \tag{2.18}$$

where we used $\sin(x)\sin(y) = \frac{1}{2}\left[\cos(x-y) - \cos(x+y)\right]$ and in the last step we resubstitute the expressions for k and k'. The exact calculation is shown in the appendix, Sec. A.1. Now we return to the original problem and by using Eq. (2.18) we get

$$\int_0^L |E_x|^2\,\mathrm{d}x = \sum_k \frac{\alpha^2\omega_k^2}{4}\left(a_k a_k^* - a_k^2 \mathrm{e}^{-2\mathrm{i}\omega_k t} - a_k^{*2}\mathrm{e}^{2\mathrm{i}\omega_k t} + a_k^* a_k\right). \tag{2.19}$$

After calculating the energy of the electric field we now want to calculate the energy of the magnetic field, i.e.,

$$\begin{aligned}\int_0^L |B_y|^2\,\mathrm{d}x = \int_0^L \frac{\alpha^2}{4}\sum_{k,k'} k\left[a_k \mathrm{e}^{-\mathrm{i}\omega_k t}\cos(kz) + a_k^*\mathrm{e}^{\mathrm{i}\omega_k t}\cos(kz)\right]\\ k'\left[a_{k'}^*\mathrm{e}^{\mathrm{i}\omega_{k'} t}\cos(k'z) + a_{k'}\mathrm{e}^{-\mathrm{i}\omega_{k'} t}\cos(k'z)\right]\mathrm{d}x,\end{aligned} \tag{2.20}$$

Die approbierte gedruckte Originalversion dieser Diplomarbeit ist an der TU Wien Bibliothek verfügbar
The approved original version of this thesis is available in print at TU Wien Bibliothek.
TU Bibliothek Your knowledge hub WIEN

where terms like $\cos(x)\cos(y)$ are remaining to be integrated. Using $\cos(x)\cos(y) = \frac{1}{2}\left[\cos(x-y)+\cos(x+y)\right]$ and integrating over it leads to the same result as before (the second term was zero in both cases), namely $\delta_{kk'}$. Overall, we get

$$\int_0^L |B_y|^2 \,\mathrm{d}x = \sum_k \frac{\alpha^2 k^2}{4}\left(a_k a_k^* + a_k^2 \mathrm{e}^{-2\mathrm{i}\omega_k t} + a_k^{*2}\mathrm{e}^{2\mathrm{i}\omega_k t} + a_k^* a_k\right). \tag{2.21}$$

Now we are ready to insert the results into Eq. (2.16) which leads to

$$\begin{aligned} H = \frac{1}{2}\epsilon_0 \sum_k \frac{\alpha^2\omega_k^2}{4}\left(a_k a_k^* - a_k^2 \mathrm{e}^{-2\mathrm{i}\omega_k t} - a_k^{*2}\mathrm{e}^{2\mathrm{i}\omega_k t} + a_k^* a_k\right) \\ + \frac{1}{2\mu_0}\sum_k \frac{\alpha^2\omega_k^2\epsilon_0\mu_0}{4}\left(a_k a_k^* + a_k^2 \mathrm{e}^{-2\mathrm{i}\omega_k t} + a_k^{*2}\mathrm{e}^{2\mathrm{i}\omega_k t} + a_k^* a_k\right), \end{aligned} \tag{2.22}$$

where we used $k = \frac{\omega_k}{c}$ and $c = \frac{1}{\sqrt{\epsilon_0\mu_0}}$. We see that the a_k^2 and a_k^{*2} terms cancel each other which gives

$$H = \sum_k \frac{\epsilon_0\alpha^2\omega_k^2}{4}\left(a_k a_k^* + a_k^* a_k\right). \tag{2.23}$$

Finally, by identifying $\alpha^2 = \frac{2\hbar}{\epsilon_0\omega_k}$, we end up with

$$H = \sum_k \frac{\hbar\omega_k}{2}\left(a_k a_k^* + a_k^* a_k\right), \tag{2.24}$$

which looks like the Hamiltonian of a harmonic oscillator. Therefore, we can now make the following identification

$$a_k \to \hat{a}_k \qquad \text{and} \qquad a_k^* \to \hat{a}_k^\dagger, \tag{2.25}$$

i.e., interpret the field amplitudes as operators. Since the quanta of the electromagnetic field are photons which have an integer spin, the operators have to obey the bosonic commutation relation, i.e.,

$$\left[\hat{a}, \hat{a}^\dagger\right] = 1. \tag{2.26}$$

With that commutation relation the result resembles the Hamiltonian of the harmonic oscillator

$$\hat{H} = \sum_k \hbar\omega_k\left(\hat{a}_k^\dagger \hat{a}_k + \frac{1}{2}\right). \tag{2.27}$$

After quantizing the electromagnetic field and showing that it can be described with the Hamiltonian of a harmonic oscillator, we want to continue our quantization procedure and introduce corresponding creation and annihilation operators in the regime of LC circuits. This will be done in the following section.

Die approbierte gedruckte Originalversion dieser Diplomarbeit ist an der TU Wien Bibliothek verfügbar
The approved original version of this thesis is available in print at TU Wien Bibliothek.
TU Bibliothek Your knowledge hub WIEN

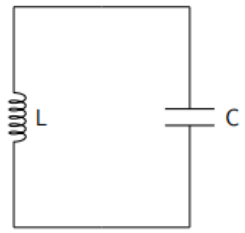

Figure 2.3: An ideal cavity can be understood as a simple LC circuit.

2.2 Ideal Cavity - Quantized LC Oscillator

After quantizing the electromagnetic field we now want to take a step further and look at a cavity, which can be understood as a simple LC circuit shown in Fig. 2.3. In order to do that, we want to show that the Hamiltonian describing such an LC circuit resembles one of a harmonic oscillator when quantized.

From Kirchhoffs voltage law we know that the voltage drop over the capacitor plus the voltage drop over the inductance has to be zero, i.e., $u_L + u_C = 0$. We further know, according to Kirchhoffs knot rule, that the current through the capacitor has to be equal to that through the inductance, i.e., $i_C = i_L$. We also know that

$$u_L(t) = L\frac{\mathrm{d}i_L}{\mathrm{d}t}, \tag{2.28a}$$

$$i_C(t) = C\frac{\mathrm{d}u_C}{\mathrm{d}t}. \tag{2.28b}$$

Inserting Eq. (2.28a) into Eq. (2.28b) and taking into account that $u_C = u_L$, leads to the following differential equation

$$\frac{\mathrm{d}^2 i(t)}{\mathrm{d}t^2} + \frac{1}{LC} i(t) = 0, \tag{2.29}$$

where we drop the indices of the current because $i_C = i_L$. By using $\omega = \frac{1}{\sqrt{LC}}$, the solution of Eq. (2.29) can be written as

$$i(t) = \alpha \left(a\mathrm{e}^{-\mathrm{i}\omega t} + a^* \mathrm{e}^{\mathrm{i}\omega t} \right), \tag{2.30}$$

where α is a normalization constant which needs to be determined. The complex conjugated amplitudes assure that we get a real current. The total energy of the system, i.e., its Hamiltonian, can be written as

$$H = \frac{1}{2} L i^2 + \frac{1}{2}\frac{q^2}{C}. \tag{2.31}$$

Die approbierte gedruckte Originalversion dieser Diplomarbeit ist an der TU Wien Bibliothek verfügbar
The approved original version of this thesis is available in print at TU Wien Bibliothek.
TU Bibliothek Your knowledge hub WIEN

To get the energy of the LC circuit, we now evaluate the first term, i.e. i^2 for which we find

$$|i|^2 = \alpha \left(a\mathrm{e}^{-\mathrm{i}\omega t} + a^*\mathrm{e}^{\mathrm{i}\omega t}\right) \alpha \left(a^*\mathrm{e}^{\mathrm{i}\omega t} + a\mathrm{e}^{-\mathrm{i}\omega t}\right) = \alpha^2 \left(aa^* + a^2\mathrm{e}^{-2\mathrm{i}\omega t} + a^{*2}\mathrm{e}^{2\mathrm{i}\omega t} + a^*a\right). \tag{2.32}$$

To get the contribution of the second term, we first have to determine q. With

$$i = \frac{\mathrm{d}q}{\mathrm{d}t}, \tag{2.33}$$

one obtains

$$q = \frac{\mathrm{i}}{\omega}\left(a\mathrm{e}^{-\mathrm{i}\omega t} - a^*\mathrm{e}^{\mathrm{i}\omega t}\right). \tag{2.34}$$

Now we are able to evaluate q^2 which is

$$\begin{aligned} |q|^2 &= \frac{\mathrm{i}\alpha}{\omega}\left(a\mathrm{e}^{-\mathrm{i}\omega t} - a^*\mathrm{e}^{\mathrm{i}\omega t}\right)\frac{-\mathrm{i}\alpha}{\omega}\left(a^*\mathrm{e}^{\mathrm{i}\omega t} - a\mathrm{e}^{-\mathrm{i}\omega t}\right) \\ &= \frac{\alpha^2}{\omega^2}\left(aa^* - a^2\mathrm{e}^{-2\mathrm{i}\omega t} - a^{*2}\mathrm{e}^{2\mathrm{i}\omega t} + a^*a\right). \end{aligned} \tag{2.35}$$

After we derived the expressions for i^2 and q^2 we can insert Eqs. (2.32) and (2.35) into Eq. (2.31) and calculate the total energy of the system,

$$\begin{aligned} H &= \frac{1}{2}L\alpha^2\left(aa^* + a^2\mathrm{e}^{-2\mathrm{i}\omega t} + a^{*2}\mathrm{e}^{2\mathrm{i}\omega t} + a^*a\right) \\ &+ \frac{1}{2C}\frac{\alpha^2}{\omega^2}\left(aa^* - a^2\mathrm{e}^{-2\mathrm{i}\omega t} - a^{*2}\mathrm{e}^{2\mathrm{i}\omega t} + a^*a\right) = L\alpha^2\left(aa^* + a^*a\right), \end{aligned} \tag{2.36}$$

where we used $\omega = \frac{1}{\sqrt{LC}}$. As before, if we assume $\alpha^2 = \frac{\hbar\omega}{2L}$ and interpret the amplitudes a as operators,

$$a \to \hat{a}, \qquad a^* \to \hat{a}^\dagger, \tag{2.37}$$

we end up with

$$\hat{H} = \hbar\omega\left(\hat{a}\hat{a}^\dagger + \hat{a}^\dagger\hat{a}\right) = \hbar\omega\left(\hat{a}^\dagger\hat{a} + \frac{1}{2}\right), \tag{2.38}$$

where we used the commutation relation $[\hat{a}, \hat{a}^\dagger] = 1$. As we can clearly see, a resonator, which is the same as an LC circuit, is equivalent to a harmonic oscillator and, therefore, has a certain (and measurable) number of photons in the cavity. We will use this result later on. Please note that the use of the above bosonic commutation relation is justified since we here quantize electromagnetic fields (caused by moving electrons) whose quanta are photons. In contrast to the quantization shown in Sec. 2.1 now only a single mode with frequency $\omega = \frac{1}{\sqrt{LC}}$ is allowed, we therefore do not have a sum in Eq. (2.31) anymore. This frequency is fixed and depends on geometric factors like the size of the capacitor plates and the distance between them. Such a fixed mode at a certain time t can be seen in Fig. 2.2.

After deriving the Hamiltonian of a cavity, the next step is to describe the interaction of the electromagnetic field in a cavity with a two level system, for example an electronic spin. This will be done in the following.

Die approbierte gedruckte Originalversion dieser Diplomarbeit ist an der TU Wien Bibliothek verfügbar
The approved original version of this thesis is available in print at TU Wien Bibliothek.
TU Bibliothek Your knowledge hub WIEN

2.3 Jaynes-Cummings Hamiltonian

In cavity QED, the interaction of the electromagnetic field with atoms or other emitters like spins is studied. For this system we want to derive a Hamiltonian in the following. The Hamiltonian consists of three terms: the energy of the cavity, the energy of the emitter under investigation (usually assumed to be a two level system) and the interaction of these two. As shown before, the energy of the cavity is the same as for a harmonic oscillator. The energy of a two level system is given by $E_{\mathrm{TLS}} = \frac{\hbar\omega_s\hat{\sigma}_z}{2}$, where we assume that our two level system is an electron spin with transition frequency ω_s and $\hat{\sigma}_z$ is the Pauli spin operator. The last term is the interaction energy of the magnetic dipole moment of the spin with a magnetic field (in our experiment we only couple to this field, see Sec. 3.1 for more information) and can be written as

$$E_{\mathrm{int}} = -\boldsymbol{\mu}\cdot\boldsymbol{B} = -\frac{g_e\mu_B}{\hbar}\boldsymbol{S}\cdot\boldsymbol{B}. \tag{2.39}$$

Here the newly introduced constants are g_e, the gyro magnetic ratio of an electron and μ_B, the Bohr magneton in which units the magnetic moment gets quantified. We now assume, with no loss of generality, that the quantization axis of the spin is the z direction and that the magnetic field of the cavity (as calculated before) points in the y direction. By doing so, we obtain

$$\hat{H}_{\mathrm{int}} = -\frac{g_e g_B}{2}\hat{\sigma}_y\hat{B}_y = -\frac{g_e g_B}{2}\frac{1}{\mathrm{i}}\left(\hat{\sigma}_+ - \hat{\sigma}_-\right)\hat{B}_y, \tag{2.40}$$

where we expressed the $\hat{\sigma}_y$ operator in terms of spin raising and lowering operators, given by $\hat{\sigma}_\pm = \frac{1}{2}\left(\hat{\sigma}_x \pm \mathrm{i}\hat{\sigma}_y\right)$. Please note that this definition (which will be used in the whole thesis) is different to the general convention where the factor $\frac{1}{2}$ is missing. This ensures that only one spin is raised or lowered, if one would use the general convention then two spins would be raised or lowered at the same time, respectively. Inserting the expression for the $\boldsymbol{B}$ field from Eq. (2.15) into Eq. (2.40) leads to

$$\begin{aligned}\hat{H}_{\mathrm{int}} &= -2\sqrt{\frac{\hbar\omega_k\mu_0}{L}}\cos(kz)\left(\hat{a}\mathrm{e}^{-\mathrm{i}\omega_c t} + \hat{a}^\dagger\mathrm{e}^{\mathrm{i}\omega_c t}\right)\frac{g_e g_B}{2}\frac{1}{\mathrm{i}}\left(\hat{\sigma}_+\mathrm{e}^{\mathrm{i}\omega_s t} - \hat{\sigma}_-\mathrm{e}^{-\mathrm{i}\omega_s t}\right)\\ &= -\mathrm{i}\hbar g\left(\hat{a}\mathrm{e}^{-\mathrm{i}\omega_c t} + \hat{a}^\dagger\mathrm{e}^{\mathrm{i}\omega_c t}\right)\left(\hat{\sigma}_+\mathrm{e}^{\mathrm{i}\omega_s t} - \hat{\sigma}_-\mathrm{e}^{-\mathrm{i}\omega_s t}\right),\end{aligned} \tag{2.41}$$

with g being $g = \sqrt{\frac{\hbar\omega_k\mu_0}{L}}\frac{\cos(kz)g_e g_B}{\hbar}$. Please note that the creation and annihilation operators $\hat{a}$ and $\hat{a}^\dagger$ of Eq. (2.15) with the additional exponential factors can be interpreted as time dependent operators and we therefore have transformed the spin raising and lowering operators as well. This transformation can be done with $\hat{A}_I(t) = \hat{U}_0^\dagger\hat{A}\hat{U}_0$ (where $\hat{A}$ is an arbitrary operator) with $\hat{U}_0 = \exp\left(-\mathrm{i}\left(\omega_c\hat{a}^\dagger\hat{a} + \frac{\omega_s}{2}\hat{\sigma}_z\right)t\right)$. The new picture we obtain is called Interaction picture for which we get $\hat{\sigma}_\pm(t) = \hat{\sigma}_\pm\mathrm{e}^{\pm\mathrm{i}\omega_s t}$

Die approbierte gedruckte Originalversion dieser Diplomarbeit ist an der TU Wien Bibliothek verfügbar
The approved original version of this thesis is available in print at TU Wien Bibliothek.
TU Bibliothek Your knowledge hub WIEN

(the calculation is shown in the appendix Sec. A.2). By multiplying the two brackets, Eq. (2.41) yields

$$\hat{H}_{\text{int}} = -\mathrm{i}\hbar g \left(\hat{a}\hat{\sigma}_+ \mathrm{e}^{\mathrm{i}(\omega_s-\omega_c)t} - \hat{a}\hat{\sigma}_- \mathrm{e}^{-\mathrm{i}(\omega_c+\omega_s)t} + \hat{a}^\dagger\hat{\sigma}_+ \mathrm{e}^{\mathrm{i}(\omega_c+\omega_s)t} - \hat{a}^\dagger\hat{\sigma}_- \mathrm{e}^{\mathrm{i}(\omega_c-\omega_s)t} \right). \tag{2.42}$$

There are terms where two quanta are created or destroyed ($\hat{\sigma}_+\hat{a}^\dagger$ and $\hat{\sigma}_-\hat{a}$) which are therefore not energy conserving. To get rid of them we do the so-called rotating wave approximation, i.e., neglect the fast rotating terms with frequency $\pm(\omega_c + \omega_s)$ and only keep the slower rotating terms with frequency $\pm(\omega_s - \omega_c)$. To get rid of the time dependence of the operators, we transform them back into the Schrödinger picture ($\hat{A} = \hat{U}_0 \hat{A}_I(t) \hat{U}_0^\dagger$) and get an expression for the interaction Hamiltonian

$$\hat{H}_{\text{int}} = \mathrm{i}\hbar g(\hat{\sigma}_-\hat{a}^\dagger - \hat{\sigma}_+\hat{a}). \tag{2.43}$$

This interaction term either creates a photon in the cavity and destroys one excitation in the spin system or vice versa. The interaction Hamiltonian is now energy conserving. By adding up all terms, this gives the final Hamiltonian of our system

$$\hat{H} = \hat{H}_{\text{cavity}} + \hat{H}_{\text{spin}} + \hat{H}_{\text{int}} = \hbar\omega_c \hat{a}^\dagger\hat{a} + \frac{\hbar\omega_s}{2}\hat{\sigma}_z + \mathrm{i}\hbar g \left(\hat{\sigma}_-\hat{a}^\dagger - \hat{\sigma}_+\hat{a} \right), \tag{2.44}$$

which is called Jaynes-Cummings Hamiltonian and named after the first developers of the model [31]. The eigenenergies of this Hamiltonian are calculated in the appendix (Sec. A.3) and read like

$$E_\pm = \hbar\omega_c \left(n + \frac{1}{2} \right) \pm \frac{\hbar}{2}\sqrt{\Omega_n^2 + \delta^2}, \tag{2.45}$$

with $\Omega_n = 2g\sqrt{n+1}$ and $\delta = \omega_c - \omega_s$. The energy splitting for different values of n as well as a comparison with the energy values of the uncoupled states is shown in Fig. 2.4. In Fig. 2.5, the eigenenergies in units of $\hbar\omega_c$ are plotted for different detunings $\delta = \omega_c - \omega_s$ and $n = 0$. By calculating the difference between the two energy values on resonance one gets the value for the coupling g.

The calculation of the eigenvectors can be found in the appendix as well (Sec. A.3) and we obtain

$$\begin{aligned} |n,+\rangle &= \sin(\theta)\,|g,n+1\rangle + \mathrm{i}\cos(\theta)\,|e,n\rangle\,, \\ |n,-\rangle &= \cos(\theta)\,|g,n+1\rangle - \mathrm{i}\sin(\theta)\,|e,n\rangle\,, \end{aligned} \tag{2.46}$$

where θ can be calculated with $\tan(2\theta) = \frac{\Omega_n}{\delta}$. Since the Hilbert space of the system can be written as $\hat{H}_{\text{cavity}} \otimes \hat{H}_{\text{spin}}$, we choose the vectors $|g, n+1\rangle$ and $|e, n\rangle$ as basis vectors. The spin is either in the ground (g) or excited (e) state, the number of photons in the cavity is denoted by n and $n+1$, respectively.

Please note that the oscillating field of the cavity has to have a component orthogonal to the quantization axis of the spins (which for example can be a strong

Die approbierte gedruckte Originalversion dieser Diplomarbeit ist an der TU Wien Bibliothek verfügbar
The approved original version of this thesis is available in print at TU Wien Bibliothek.
TU Bibliothek Your knowledge hub WIEN

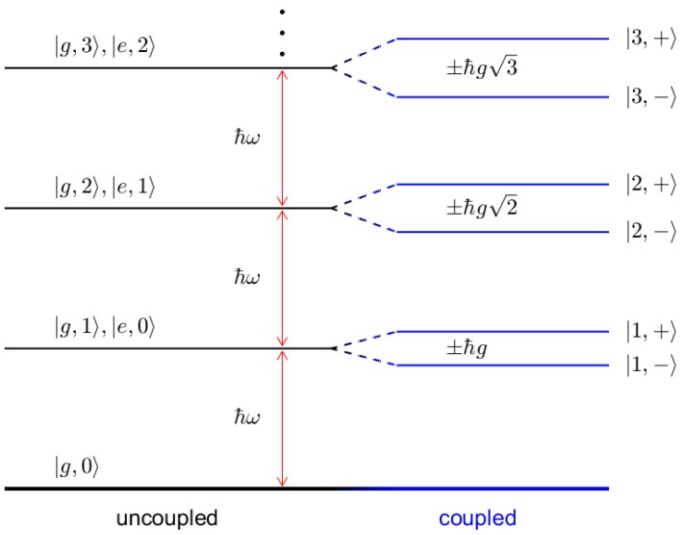

Figure 2.4: Comparison of energies of uncoupled (left) and coupled (right) states on resonance (i.e. $\omega_s = \omega_c$). The splitting of the coupled states is $\propto \sqrt{n}$ as can be seen from Eq. (2.45) as well.

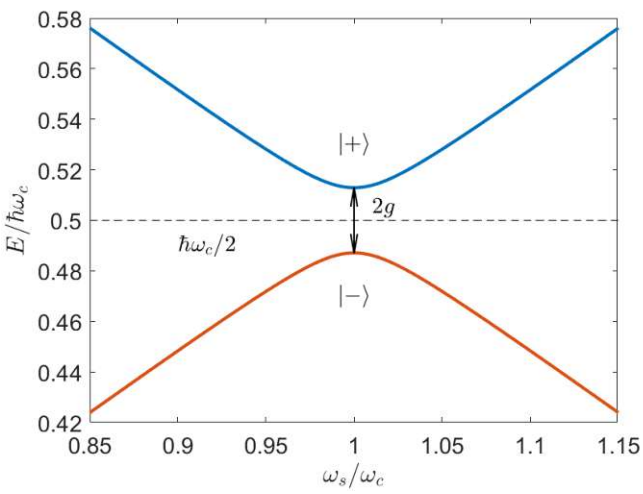

Figure 2.5: Calculated eigenenergies of the Jaynes-Cummings Hamiltonian in units of $\hbar\omega_c$ as a function of spin detuning $\delta = \omega_c - \omega_s$. E_+ with the corresponding eigenvector $|+\rangle$ is shown in blue, E_- with the corresponding eigenvector $|-\rangle$ is shown in red, respectively. For that calculation we set $n = 0$. On resonance, the difference between the two eigenvalues is $2g$ as can be seen from Eq. (2.45) as well.

Die approbierte gedruckte Originalversion dieser Diplomarbeit ist an der TU Wien Bibliothek verfügbar
The approved original version of this thesis is available in print at TU Wien Bibliothek.
TU Bibliothek Your knowledge hub WIEN

external magnetic field) in order to induce transitions in the spin system. If that is not the case then the spin system will stay forever in its initial state because the magnetic field of the cavity cannot change the spin states. It would instead lead to a Zeeman shift of the energy levels, i.e., the energy of the lower level would get reduced and the energy of the upper level increased.

Besides that it is important to note that the choice of the magnetic field direction (in our derivation it points in the y direction) is not unique. The only requirement the vectors $\boldsymbol{k}$, $\boldsymbol{E}$ and $\boldsymbol{B}$ have to fulfill is that they have to form a right-handed trihedron. By fixing $\boldsymbol{k} = k_z$, E can point in the x direction (as before) or in the $(-)y$ direction. When pointing in the $-y$ direction, then the $\boldsymbol{B}$ field points in the x direction and we end up with terms like $\hat{\sigma}_x(t)\hat{B}_x(t)$ (now only the direction of the B field is different, besides that it is still given by Eq. (2.15)). By expressing, as done before, the Pauli spin operator in terms of raising and lowering operators, i.e., $\hat{\sigma}_x = \hat{\sigma}_+ + \hat{\sigma}_-$ and transform the operators into the interaction picture (see appendix Sec. A.2), we get an interaction term which is proportional to

$$\hat{\sigma}_x(t)\hat{B}_x(t) \propto (\hat{\sigma}_+ + \hat{\sigma}_-)\left(\hat{a} + \hat{a}^\dagger\right) = \left(\hat{\sigma}_+\hat{a} + \hat{\sigma}_+\hat{a}^\dagger + \hat{\sigma}_-\hat{a} + \hat{\sigma}_-\hat{a}^\dagger\right) \approx \left(\hat{\sigma}_+\hat{a} + \hat{\sigma}_-\hat{a}^\dagger\right), \tag{2.47}$$

where we again have made use of the rotating wave approximation and dropped the non energy conserving terms. By comparing that expression with the expression we had before (see Eqs. (2.42) and (2.43)), i.e.,

$$\begin{aligned}\hat{\sigma}_y(t)\hat{B}_y(t) \propto \frac{1}{\mathrm{i}}(\hat{\sigma}_+ - \hat{\sigma}_-)\left(\hat{a} + \hat{a}^\dagger\right) &= \frac{1}{\mathrm{i}}\left(\hat{\sigma}_+\hat{a} + \hat{\sigma}_+\hat{a}^\dagger - \hat{\sigma}_-\hat{a} - \hat{\sigma}_-\hat{a}^\dagger\right) \\ &\approx \mathrm{i}\left(\hat{\sigma}_-\hat{a}^\dagger - \hat{\sigma}_+\hat{a}\right),\end{aligned} \tag{2.48}$$

they look quite different but it does not make any physical difference because none of the directions orthogonal to the quantization axis is preferable. Before discussing this in more detail, we want to point out a different way of obtaining these different terms of the interaction Hamiltonian. Since the zero point of time can be chosen arbitrarily, we can shift time. According to Eq. (2.15), the electric field is

$$\hat{E} \propto \mathrm{i}\left(\hat{a}\mathrm{e}^{-\mathrm{i}\omega t} + \hat{a}^\dagger\mathrm{e}^{\mathrm{i}\omega t}\right) = \hat{a}\mathrm{e}^{-\mathrm{i}\omega\left(t - \frac{\pi}{2\omega}\right)} - \hat{a}^\dagger\mathrm{e}^{\mathrm{i}\omega\left(t + \frac{\pi}{2\omega}\right)}, \tag{2.49}$$

which, by introducing a time offset $t \to t' + \frac{\pi}{2\omega}$, leads to

$$\hat{E} \propto \hat{a}\mathrm{e}^{-\mathrm{i}\omega t'} - \hat{a}^\dagger\mathrm{e}^{\mathrm{i}\omega t' + \mathrm{i}\pi} = \hat{a}\mathrm{e}^{-\mathrm{i}\omega t'} + \hat{a}^\dagger\mathrm{e}^{\mathrm{i}\omega t'}. \tag{2.50}$$

The magnetic field which originally was

$$\hat{B}(t) \propto \left(\hat{a}\mathrm{e}^{-\mathrm{i}\omega t} + \hat{a}^\dagger\mathrm{e}^{\mathrm{i}\omega t}\right), \tag{2.51}$$

therefore becomes

$$\begin{aligned}\hat{B}(t') \propto \left(\hat{a}\mathrm{e}^{-\mathrm{i}\omega\left(t' + \frac{\pi}{2\omega}\right)} + \hat{a}^\dagger\mathrm{e}^{\mathrm{i}\omega\left(t' + \frac{\pi}{2\omega}\right)}\right) &= \mathrm{e}^{-\mathrm{i}\frac{\pi}{2}}\left(\hat{a}\mathrm{e}^{-\mathrm{i}\omega t'} + \hat{a}^\dagger\mathrm{e}^{\mathrm{i}\omega t'}\mathrm{e}^{\mathrm{i}\pi}\right) \\ &= -\mathrm{i}\left(\hat{a}\mathrm{e}^{-\mathrm{i}\omega t'} - \hat{a}^\dagger\mathrm{e}^{\mathrm{i}\omega t'}\right).\end{aligned} \tag{2.52}$$

Die approbierte gedruckte Originalversion dieser Diplomarbeit ist an der TU Wien Bibliothek verfügbar
The approved original version of this thesis is available in print at TU Wien Bibliothek.
TU Bibliothek WIEN Your knowledge hub

Now we want to calculate the same expressions as before but with the time shifted magnetic field, i.e., $\hat{\sigma}_x(t')\hat{B}_x(t')$ and $\hat{\sigma}_y(t')\hat{B}_y(t')$. We find

$$\begin{aligned}\hat{\sigma}_x(t')\hat{B}_x(t') \propto \mathrm{i}\left(\hat{\sigma}_+ + \hat{\sigma}_-\right)\left(\hat{a} - \hat{a}^\dagger\right) &= -\mathrm{i}\left(\hat{\sigma}_+\hat{a} + \hat{\sigma}_-\hat{a} - \hat{\sigma}_+\hat{a}^\dagger - \hat{\sigma}_-\hat{a}^\dagger\right) \\ &\approx \mathrm{i}\left(\hat{\sigma}_-\hat{a}^\dagger - \hat{\sigma}_+\hat{a}\right),\end{aligned} \tag{2.53}$$

and

$$\begin{aligned}\hat{\sigma}_y(t')\hat{B}_y(t') \propto \frac{1}{\mathrm{i}}\left(\hat{\sigma}_+ - \hat{\sigma}_-\right)(-\mathrm{i})\left(\hat{a} - \hat{a}^\dagger\right) &= -\left(\hat{\sigma}_+\hat{a} - \hat{\sigma}_-\hat{a} - \hat{\sigma}_+\hat{a}^\dagger + \hat{\sigma}_-\hat{a}^\dagger\right) \\ &\approx -\left(\hat{\sigma}_-\hat{a}^\dagger + \hat{\sigma}_+\hat{a}\right),\end{aligned} \tag{2.54}$$

which are in fact the same expressions as before (with a possible additional overall sign change). This means that the change of the direction of the electromagnetic fields yield the same changes as a time shift.

To see if either of these transformations lead to a physical difference, we calculate the eigenenergies and the eigenvectors of the Jaynes-Cummings Hamiltonian written in the form

$$\hat{H} = \hat{H}_{\text{cavity}} + \hat{H}_{\text{spin}} + \hat{H}_{\text{int}} = \hbar\omega_c\hat{a}^\dagger\hat{a} + \frac{\hbar\omega_s}{2}\hat{\sigma}_z + \hbar g\left(\hat{\sigma}_-\hat{a}^\dagger + \hat{\sigma}_+\hat{a}\right), \tag{2.55}$$

which is shown in the appendix Sec. A.3. We find that this Hamiltonian has the same eigenenergies as before (written in Eq. (2.45)), but the eigenvectors are a little bit different now, we obtain

$$|n,+\rangle = \sin(\theta)\,|g,n+1\rangle + \cos(\theta)\,|e,n\rangle\,, \tag{2.56a}$$

$$|n,-\rangle = \cos(\theta)\,|g,n+1\rangle - \sin(\theta)\,|e,n\rangle\,. \tag{2.56b}$$

As stated before, we see that the new Hamiltonian does not change anything about the physical behavior of the system. The eigenenergies (which are the physical observables) are exactly the same and the different coefficients of $|e,n\rangle$ in the eigenvector equations (once with and the other time without imaginary unit) are physically irrelevant because the relevant information is in the probability of being in such a state and by calculating that the imaginary unit drops out; one always gets $P(|e,n\rangle) = \cos^2(\theta)$ and $P(|e,n\rangle) = \sin^2(\theta)$, respectively. A possible overall sign change (as can be seen in Eq. (2.54)) is, for the same reasons, irrelevant as well.

To gain better understanding we now do an energy shift of the aforementioned Jaynes-Cummings Hamiltonian. This is also necessary, since we in the experiment do not observe an energy spectrum as shown in Fig. 2.5 but a different one as depicted and explained in Sec. 3.4. To get qualitatively the same pictures, we add $\frac{\hbar\omega_s}{2}$ to the Jaynes-Cummings Hamiltonian so that the spin in the ground and excited

Die approbierte gedruckte Originalversion dieser Diplomarbeit ist an der TU Wien Bibliothek verfügbar
The approved original version of this thesis is available in print at TU Wien Bibliothek.
TU Bibliothek Your knowledge hub WIEN

states have an energy of 0 and $\hbar\omega_s$ instead of $\pm\frac{\hbar\omega_s}{2}$. This is equivalent to replacing the $\hat{\sigma}_z$ operator with the spin raising and lowering operators $\hat{\sigma}_\pm = \frac{1}{2}(\hat{\sigma}_x \pm \mathrm{i}\hat{\sigma}_y)$, i.e.,

$$\begin{aligned}\hat{\sigma}_+\hat{\sigma}_- &= \frac{1}{4}(\hat{\sigma}_x + \mathrm{i}\hat{\sigma}_y)(\hat{\sigma}_x - \mathrm{i}\hat{\sigma}_y) = \frac{1}{4}\left(\hat{\sigma}_x^2 + \mathrm{i}\hat{\sigma}_y\hat{\sigma}_x - \mathrm{i}\hat{\sigma}_x\hat{\sigma}_y + \hat{\sigma}_y^2\right) \\ &= \frac{1}{2}\cdot\mathbb{1} + \frac{\mathrm{i}}{4}[\hat{\sigma}_y, \hat{\sigma}_x] = \frac{1}{2}\cdot\mathbb{1} + \frac{\mathrm{i}}{4}(-2\mathrm{i}\hat{\sigma}_z) = \frac{1}{2}(\mathbb{1} + \hat{\sigma}_z)\,,\end{aligned} \tag{2.57}$$

where we used the commutator relations for Pauli spin operators, i.e., $[\hat{\sigma}_i, \hat{\sigma}_j] = 2\mathrm{i}\epsilon_{ijk}\hat{\sigma}_k$. After adding the above mentioned energy offset our Hamiltonian looks like

$$\frac{\hbar\omega_s\hat{\sigma}_z}{2} + \frac{\hbar\omega_s}{2}\mathbb{1} = \frac{\hbar\omega_s}{2}(\mathbb{1} + \hat{\sigma}_z) = \hbar\omega_s\hat{\sigma}_+\hat{\sigma}_-. \tag{2.58}$$

This energy offset leads to new eigenvalues. If we have a look on the new Hamiltonian and the corresponding eigenvalue equations of the old and new Hamiltonian, i.e.,

$$\hat{H}_{\text{new}} = \hat{H} + \alpha\mathbb{1}, \qquad \det\left(\hat{H} + \alpha\mathbb{1} - \lambda_{\text{new}}\mathbb{1}\right) = 0, \qquad \det\left(\hat{H} - \lambda_{\text{old}}E\right) = 0, \tag{2.59}$$

we find that $\lambda_{\text{old}} = \lambda_{\text{new}} - \alpha$ or $\lambda_{\text{new}} = \lambda_{\text{old}} + \alpha$ and the new eigenenergies are

$$E_\pm = \hbar\omega_c\left(n + \frac{1}{2}\right) + \frac{1}{2}\hbar\omega_s \pm \frac{\hbar}{2}\sqrt{\Omega_n^2 + \delta^2}, \tag{2.60}$$

which are shown in Fig. 2.6 in units of $\hbar\omega_c$ for different detunings $\delta = \omega_c - \omega_s$ and $n = 0$ as well. By calculating the difference between the two energy values on resonance, one gets the value for the coupling g. For comparison, the energies of the states $|1, g\rangle$ and $|0, e\rangle$ are depicted in black. Please note, however, that the eigenvectors stay unchanged. this can be seen by the eigenvalue equation

$$\left(\hat{H} - \lambda_{\text{old}}\right)x = 0 \qquad \left(\hat{H} + \alpha\mathbb{1} - \lambda_{\text{new}}\right)x = 0, \tag{2.61}$$

where the additional offset α is compensated by the now different eigenvalues and therefore the eigenvectors x stay unchanged.

Now we know how we can describe the interaction of a single spin with the electromagnetic field in a cavity. However, since we are dealing with a huge spin ensemble in our experiment, we have to generalize the Jaynes-Cummings Hamiltonian to be able to describe such a spin ensemble. This will be done in the following.

2.4 Tavis-Cummings Hamiltonian - Interaction of a Spin Ensemble with a Cavity

After we have derived the Hamiltonian for a single spin interacting with photons in a cavity, we can quite easily extend this Hamiltonian to describe the energy in a

Die approbierte gedruckte Originalversion dieser Diplomarbeit ist an der TU Wien Bibliothek verfügbar
The approved original version of this thesis is available in print at TU Wien Bibliothek.
TU Bibliothek Your knowledge hub WIEN

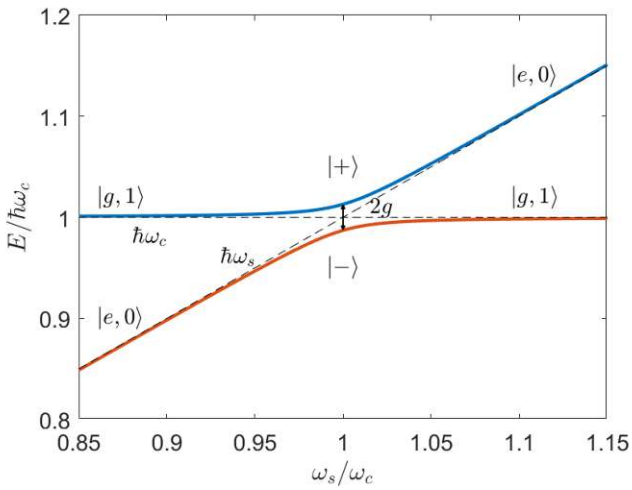

Figure 2.6: Calculated eigenenergies of the energy shifted Jaynes-Cummings Hamiltonian in units of $\hbar\omega_c$ as a function of spin detuning $\delta = \omega_c - \omega_s$ (with $n = 0$). E_+ with the corresponding eigenvector $|+\rangle$ is shown in blue, E_- with the corresponding eigenvector $|-\rangle$ is shown in red, respectively. For comparison, the energies of the states $|1, g\rangle$ and $|0, e\rangle$ are depicted in black. On resonance, the difference between the two eigenvalues is $2g$ as can be seen from Eq. (2.60) as well.

system with more than one spin. We just sum over the second and third term and get the Tavis-Cummings Hamiltonian [32]

$$\hat{H}_{\mathrm{TC}} = \hbar\omega_c \hat{a}^\dagger \hat{a} + \sum_j \frac{\hbar\omega_s^j}{2} \hat{\sigma}_z^j + \sum_j \mathrm{i}\hbar g_j \left(\hat{\sigma}_-^j \hat{a}^\dagger - \hat{\sigma}_+^j \hat{a} \right) , \tag{2.62}$$

where we take into account that the transition frequency between ground and excited state can be different for different spins (also named inhomogeneous spin broadening) and that they can couple with a different strength to the cavity mode which is covered in the different coupling strengths g_j as well. Please note that we assume a system which is completely isolated from the environment and therefore no interactions with the environment are considered. We will introduce them later on (see Sec. 2.6 where we derive the Maxwell-Bloch equations).

To see what influence the inhomogeneous broadening, i.e. the different frequencies have on the eigenenergies of the system, we will calculate them. In contrast to before, where we had to calculate the eigenvalues of a (2×2) matrix we now have to calculate them for a $(N + 1) \times (N + 1)$ matrix where N is the number of spins. Even if we only take two spins into account, the corresponding eigenvalue problem is quite hard to solve so we do it numerically. For that calculation we assume $\omega_s^1 = \omega_c - 0.05\omega_c$ and $\omega_s^2 = \omega_c + 0.05\omega_c$, i.e. $\pm 5\%$ detuning from the cavity frequency.

Die approbierte gedruckte Originalversion dieser Diplomarbeit ist an der TU Wien Bibliothek verfügbar
The approved original version of this thesis is available in print at TU Wien Bibliothek.
TU Bibliothek Your knowledge hub WIEN

The obtained eigenenergies in units of $\hbar\omega_c$ as a function of spin detuning $\delta = \omega_c - \omega_s$ (with $n = 0$) can be seen in Fig. 2.7(a) where, as before, the energies of the states $|\downarrow\downarrow, 1\rangle$, $|\uparrow\downarrow, 0\rangle$ and $|\downarrow\uparrow, 0\rangle$ are depicted in black. In Fig. 2.7(b) and (c) the same calculation but with $\pm 2.5\%$ and $\pm 1.25\%$ detuning from the cavity frequency was carried out. One clearly sees that the distance between the two black lines which represent the spin energies get closer and closer. Finally, for zero detuning, both black depicted spin energy lines coincide and the picture looks like that obtained before (see Fig. 2.7(d) and Fig. 2.6 for comparison). At least they look qualitatively the same, since the collective coupling (i.e. the difference between the two outer energy curves) is increased by a factor of $\sqrt{2}$ which will be explained in the following.

By assuming the same frequencies and coupling strengths for all spins, i.e., $\omega_s^i = \omega_s$ and $g_j = g$, we can define collective operators for the spins which read like

$$\hat{J}_z = \sum_j \hat{\sigma}_z^j \qquad \text{and} \qquad \hat{J}_\pm = \frac{1}{\sqrt{N}} \sum_j \hat{\sigma}_\pm^j. \tag{2.63}$$

Inserting Eq. (2.63) into Eq. (2.62) leads to

$$\hat{H}_{\mathrm{TC}} = \hbar\omega_c \hat{a}^\dagger \hat{a} + \frac{\hbar\omega_s}{2} \hat{J}_z + \mathrm{i}\hbar g_{coll} \left(\hat{J}_- \hat{a}^\dagger - \hat{J}_+ \hat{a} \right), \tag{2.64}$$

which has very similar properties as the Jaynes-Cummings Hamiltonian. The eigenenergies of that system are

$$E_\pm = \hbar\omega_c \left(n + \frac{1}{2} \right) \pm \frac{\hbar}{2} \sqrt{\Omega_n^2 + \delta^2}, \tag{2.65}$$

with $\Omega_n = 2g_{coll}\sqrt{n+1}$, n being the number of photons in the cavity and $\delta = \omega_c - \omega_s$. Please note that g_{coll} now includes contributions from all spins of the system

$$g_{coll} = \sqrt{g_1^2 + g_2^2 + g_3^2 + \cdots} = g\sqrt{N}, \tag{2.66}$$

where N is the number of spins. This additional factor cancels the factor of the collective spin operators $J_\pm$ which is necessary for the equivalence of Eqs. (2.62) and (2.64). Therefore, $\Omega_n = 2g\sqrt{N}\sqrt{n+1}$ which means that the energy now scales not only with the square root of photon number n but with the number of spins N as well. For the single excitation regime we get the eigenenergies

$$\begin{aligned} |+\rangle &= \sin(\theta)\,|G, 1\rangle + \mathrm{i}\cos(\theta)\,|D_1, 0\rangle\,, \\ |-\rangle &= \cos(\theta)\,|G, 1\rangle - \mathrm{i}\sin(\theta)\,|D_1, 0\rangle\,, \end{aligned} \tag{2.67}$$

where θ is again given by $\tan(2\theta) = \frac{\Omega_n}{\delta}$. Here $|G\rangle$ denotes the spin ground state which for N spins can be written as $|G\rangle = |\downarrow\downarrow \ldots \downarrow\rangle$. $|D_1\rangle$ is the so called Dicke state [25] and can be calculated by applying $\hat{J}_+$ on $|G\rangle$. For 3 spins the first Dicke

Die approbierte gedruckte Originalversion dieser Diplomarbeit ist an der TU Wien Bibliothek verfügbar
The approved original version of this thesis is available in print at TU Wien Bibliothek.
TU Bibliothek Your knowledge hub WIEN

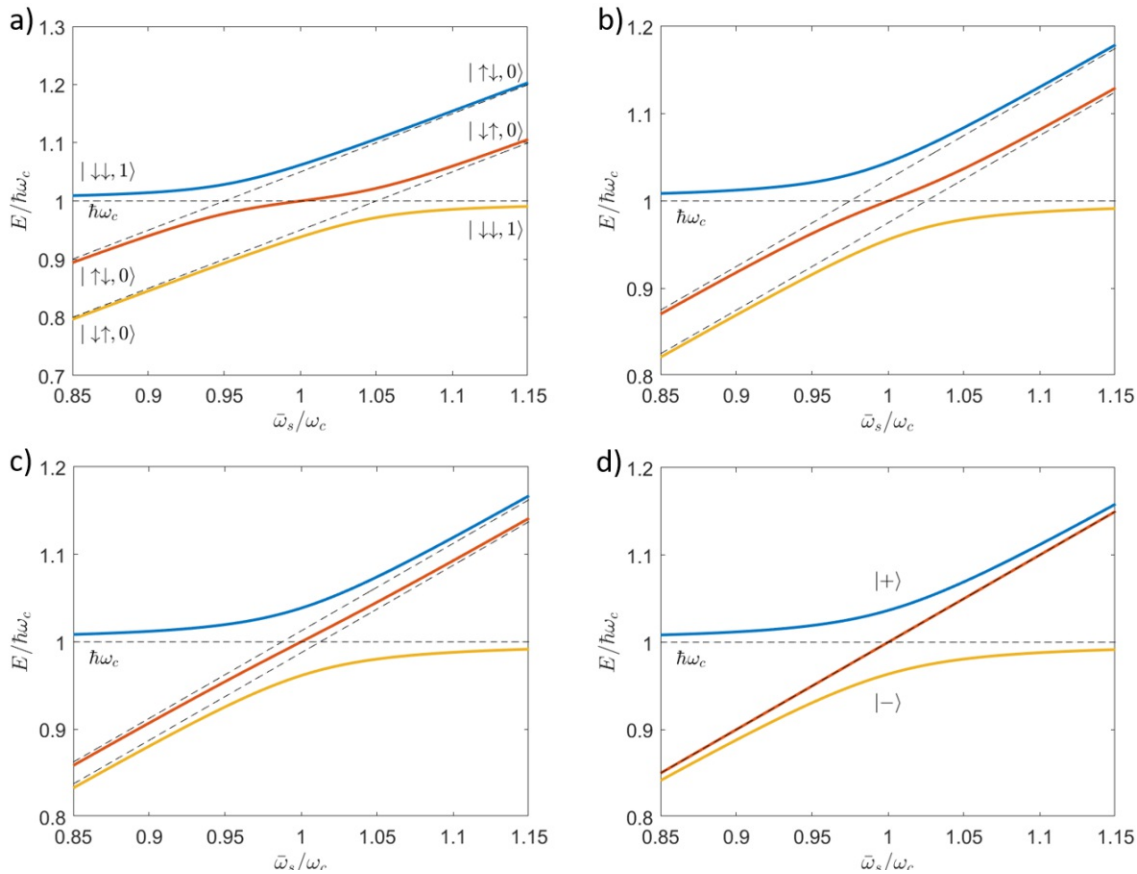

Figure 2.7: Here the eigenenergies of two spins with different frequencies ω_s^j coupled to a cavity are shown in units of $\hbar\omega_c$ as a function of the detuning $\bar{\omega}_s - \omega_c$ where $\bar{\omega}_s$ denotes the mean value of the spin frequency. In Fig. (a) the spins are detuned by $\pm 5\%$ from the cavity frequency. Besides the three eigenvalues which are shown in blue, red and yellow, the energies of the states $|\downarrow\downarrow,1\rangle$, $|\uparrow\downarrow,0\rangle$ and $|\downarrow\uparrow,0\rangle$ are depicted in black as well. As the detuning decreases ($\pm 2.5\%$ in Fig. (b) and $\pm 1.25\%$ in Fig. (c)), the distance between the two outer energy eigenvalues gets less and for zero detuning (Fig. (d)) the black depicted lines coincide, the distance between the outer energy values is minimal. It qualitatively resembles the picture of before but now with larger coupling which gets increased by a factor of $\sqrt{2}$ since it scales with the square root of the spins. Please note that as can be seen in Fig. (d), only the energy eigenvalues represented in blue and yellow can be measured in the experiment since they are the only ones which lead to a non zero photon number and are therefore the only visible ones. The red one is a mixture between $|\uparrow\downarrow,0\rangle$ and $|\downarrow\uparrow,0\rangle$ and is therefore invisible.

Die approbierte gedruckte Originalversion dieser Diplomarbeit ist an der TU Wien Bibliothek verfügbar
The approved original version of this thesis is available in print at TU Wien Bibliothek.
TU Bibliothek Your knowledge hub WIEN

state would therefore be $D_1 = \frac{1}{\sqrt{3}}\left(|\downarrow\downarrow\uparrow\rangle + |\downarrow\uparrow\downarrow\rangle + |\uparrow\downarrow\downarrow\rangle\right)$. In general, by applying $\hat{J}_+$ on $|G\rangle$, one always gets a symmetric spin state. Please note that these two eigenvectors are of course not the only ones (for N spins we get $N+1$ eigenvectors) but the only ones which lead to photons in the cavity and therefore are measurable in the experiment as can be seen in Fig. 2.7. Please note further that this single excitation regime is a special case. In contrast to the Jaynes-Cummings Hamiltonian where we couple to a single spin and therefore only one excitation in the spin system is possible, now more excitations are possible as well. By doing so and leaving the single excitation regime, the eigenvectors get complicated very fast but in principle analytic solutions exist [32].

After deriving the Hamiltonian for a larger spin system, we now want to extend it once more and include a cavity driving term. This will be done in the next section.

2.5 Driven Tavis-Cummings Hamiltonian

In our experiment we manipulate the spins with different microwave pulses which we send into our cavity. Until now, we cannot model this, since our Tavis-Cummings Hamiltonian does not have such a driving term. To include that, we add a term which describes the interaction of a quantized magnetic field inside the cavity with an external classical drive field, i.e.,

$$\hat{H}_{\text{drive}} = -2\sqrt{\frac{\hbar\omega_k\mu_0}{L}}\cos(kz)\left(\hat{a}\mathrm{e}^{-\mathrm{i}\omega_c t} + \hat{a}^\dagger\mathrm{e}^{\mathrm{i}\omega_c t}\right)A_0\sin(\omega_d t), \tag{2.68}$$

where the amplitude A_0 of our drive field can be complex and time dependent. Rewriting the expression leads to

$$\hat{H}_{\text{drive}} = \alpha\left(\hat{a}\mathrm{e}^{-\mathrm{i}\omega_c t} + \hat{a}^\dagger\mathrm{e}^{\mathrm{i}\omega_c t}\right)\left(\frac{-\mathrm{i}}{2}\right)\left(\mathrm{e}^{\mathrm{i}\omega_d t} - \mathrm{e}^{-\mathrm{i}\omega_d t}\right). \tag{2.69}$$

The parameters which are not relevant for the further calculation are represented by α. By neglecting terms with $\pm(\omega_c+\omega_d)$, i.e., doing the rotating wave approximation and by performing a transformation into the Schrödinger picture (the operators therefore are not time dependent any more, see Sec. A.2 for more information), we end up with

$$\hat{H}_{\text{drive}} = \mathrm{i}\hbar\eta\left(\hat{a}^\dagger\mathrm{e}^{-\mathrm{i}\omega_d t} - \hat{a}\mathrm{e}^{\mathrm{i}\omega_d t}\right), \tag{2.70}$$

where $\eta = \frac{\alpha}{2\hbar}$ and can be, as said before, time dependent and complex. Adding that term to our previous Hamiltonian finally gives

$$\hat{H} = \hbar\omega_c\hat{a}^\dagger\hat{a} + \sum_j \frac{\hbar\omega_s^j}{2}\hat{\sigma}_z^j + \sum_j \mathrm{i}\hbar g_j\left(\hat{\sigma}_-^j\hat{a}^\dagger - \hat{\sigma}_+^j\hat{a}\right) + \mathrm{i}\hbar\eta\left(\hat{a}^\dagger\mathrm{e}^{-\mathrm{i}\omega_d t} - \hat{a}\mathrm{e}^{\mathrm{i}\omega_d t}\right), \tag{2.71}$$

Die approbierte gedruckte Originalversion dieser Diplomarbeit ist an der TU Wien Bibliothek verfügbar
The approved original version of this thesis is available in print at TU Wien Bibliothek.
TU Bibliothek Your knowledge hub WIEN

i.e. the driven Tavis-Cummings Hamiltonian (in the Schrödinger picture). Please note that we assumed that our driving field is $\propto \sin(\omega_d t)$. With no loss of generality, we can assume it to be $\propto \cos(\omega_d t)$ as well which would lead to a driving Hamiltonian $\propto \left(\hat{a}^\dagger \mathrm{e}^{-\mathrm{i}\omega_d t} + \hat{a}\mathrm{e}^{\mathrm{i}\omega_d t}\right)$ which is physically equivalent (see discussion in Sec. 2.3).

To get rid of the time dependency, we do a unitary transformation of the Hamiltonian (i.e. we transform it into the rotating frame)

$$\tilde{\hat{H}} = \hat{U}^\dagger \hat{H} \hat{U} - \mathrm{i}\hbar \hat{U}^\dagger \dot{\hat{U}}, \tag{2.72}$$

with $\hat{U}$ being

$$\hat{U} = \mathrm{e}^{-\mathrm{i}\omega t\left(\hat{a}^\dagger \hat{a} + \sum_i \frac{\hat{\sigma}_z^i}{2}\right)}. \tag{2.73}$$

The derivation of the transformation law as well as the transformation itself is shown in appendix Sec. A.4. We finally end up with the Hamiltonian

$$\hat{H} = \hbar\Delta_c \hat{a}^\dagger \hat{a} + \sum_j \frac{\hbar\Delta_s^j}{2}\hat{\sigma}_z^j + \sum_j \mathrm{i}\hbar g_j \left(\hat{\sigma}_-^j \hat{a}^\dagger - \hat{\sigma}_+^j \hat{a}\right) + \mathrm{i}\hbar\eta\left(\hat{a}^\dagger - \hat{a}\right), \tag{2.74}$$

where $\Delta_j^{(i)} = \omega_j^{(i)} - \omega_d$ denote the corresponding detuning of the cavity or i^{th} spin frequency from the drive frequency.

As stated before, so far we have neglected any interactions of the spin system with its environment and the cavity was treated ideally, i.e., without any damping in the LC circuit. In the following, we will introduce corresponding terms and derive equations of motion for the operator expectation values which will describe our system and with which we can model our experiment.

2.6 Numerical Simulation of our System - Maxwell-Bloch Equations

Up to now, the aforementioned Hamiltonian (see Eq. (2.74)) does not include any terms - except the driving term - which describe an interaction with the environment or other ones like the interaction between spins. Because of the lack of other interactions the coherence in the spin system would remain forever which is of course unphysical. Since nitrogen vacancy (NV) centers in diamond (with which we are dealing in our experiment, see Sec. 3.2 for more details) are embedded in a crystalline structure, one has to take the processes which happen therein into account and cannot neglect them any more so that the equations reveal the real dynamics of the spin system. There are two major processes in such a crystal structure which we have not taken into account so far. The first one is the aforementioned spin-spin (between NV centers) and additionally spin-bath (between a NV center and nuclear spins in the host material) interaction which leads to decoherence, the other one

Die approbierte gedruckte Originalversion dieser Diplomarbeit ist an der TU Wien Bibliothek verfügbar
The approved original version of this thesis is available in print at TU Wien Bibliothek.
TU Bibliothek Your knowledge hub WIEN

interactions with phonons which lead to spin decay. Furthermore, the cavity is not perfect and therefore losses and damping occur (see Sec. 3.1 for more details) which are until now not covered in the equations as well. The equations of motion for an isolated system can be obtained from the von Neumann equation

$$\frac{\mathrm{d}\hat{\rho}}{\mathrm{d}t} = -\frac{\mathrm{i}}{\hbar}\left[\hat{H}, \hat{\rho}\right]. \tag{2.75}$$

To take the interactions with the environment into account, we have to add the corresponding terms for every coupling operator as derived in the appendix, Sec. A.5. By inserting the operators with their corresponding dissipation rates we get [33]

$$\begin{aligned}\hat{\mathcal{L}}\hat{\rho} = {} & \kappa(\bar{n}(\omega_c)+1)(2\hat{a}\hat{\rho}\hat{a}^\dagger - \hat{a}^\dagger\hat{a}\hat{\rho} - \hat{\rho}\hat{a}^\dagger\hat{a}) + \kappa\bar{n}(\omega_c)(2\hat{a}^\dagger\hat{\rho}\hat{a} - \hat{a}\hat{a}^\dagger\hat{\rho} - \hat{\rho}\hat{a}\hat{a}^\dagger) \\ & + \frac{\gamma_\parallel}{2}(\bar{n}(\omega_s)+1)\sum_j(2\hat{\sigma}_-^j\hat{\rho}\hat{\sigma}_+^j - \hat{\sigma}_+^j\hat{\sigma}_-^j\hat{\rho} - \hat{\rho}\hat{\sigma}_+^j\hat{\sigma}_-^j) \\ & + \frac{\gamma_\parallel}{2}\bar{n}(\omega_s)\sum_j(2\hat{\sigma}_+^j\hat{\rho}\hat{\sigma}_-^j - \hat{\sigma}_-\hat{\sigma}_+^j\hat{\rho} - \hat{\rho}\hat{\sigma}_-^j\hat{\sigma}_+^j) + \frac{\gamma_\perp}{2}\sum_j(\hat{\sigma}_z^j\hat{\rho}\hat{\sigma}_z^j - \hat{\rho}),\end{aligned} \tag{2.76}$$

where $\bar{n}(\omega)$ is the number of thermal photons, given by $\bar{n}(\omega) = \frac{1}{\mathrm{e}^{\hbar\omega/k_BT}-1}$. The first term describes the photon loss $\hat{a}$ in the cavity because of damping with the rate κ. The second term describes the decay of spins either through spontaneous emission processes or spin-phonon interactions with the coupling operator $\hat{\sigma}_-$ and a rate $\gamma_\parallel = 1/T_1$. the last term describes dephasing of the spin system because of spin-spin and spin-bath interactions which can be described with the operator $\hat{\sigma}_z$ and happens at a rate of $\gamma_\perp = 1/T_2$ [34].

Please note that the thermal photon distribution $\bar{n}$ depends on different frequencies. The thermal photon number which interacts with the cavity amplitude depends on the cavity frequency, the photon number which gets multiplied with the spin operators depends on the transition frequency of the spin levels. Since for our parameters ($\omega_c \approx \omega_s \approx 3.1 \cdot 2\pi\,\mathrm{GHz}$, $T \approx 1\,\mathrm{K}$ which is the approximated mode temperature) the thermal photon number is quite small (≈ 6) we can neglect these terms in first approximation.

By taking the additional terms coming from the Liouvillian into account, we obtain the Lindblad master equation

$$\begin{aligned}\frac{\mathrm{d}\hat{\rho}}{\mathrm{d}t} = -\frac{\mathrm{i}}{\hbar}[\hat{H},\hat{\rho}] + \hat{\mathcal{L}}\hat{\rho} = -\frac{\mathrm{i}}{\hbar}[\hat{H},\hat{\rho}] + \kappa(2\hat{a}\hat{\rho}\hat{a}^\dagger - \hat{a}^\dagger\hat{a}\hat{\rho} - \hat{\rho}\hat{a}^\dagger\hat{a}) \\ + \frac{\gamma_\parallel}{2}\sum_j(2\hat{\sigma}_-^j\hat{\rho}\hat{\sigma}_+^j - \hat{\sigma}_+^j\hat{\sigma}_-^j\hat{\rho} - \hat{\rho}\hat{\sigma}_+^j\hat{\sigma}_-^j) + \frac{\gamma_\perp}{2}\sum_j(\hat{\sigma}_z^j\hat{\rho}\hat{\sigma}_z^j - \hat{\rho}),\end{aligned} \tag{2.77}$$

where we neglected the terms which include thermal photons. By using $\mathrm{Tr}[\hat{O}\hat{\rho}] = \langle\hat{O}\rangle$ and $\mathrm{Tr}[\hat{O}\dot{\hat{\rho}}] = \frac{\mathrm{d}}{\mathrm{d}t}\langle\hat{O}\rangle$ (the exchange is allowed since the trace is a linear operator) one can calculate the equations of motion, i.e., the expectation values of the operators.

Die approbierte gedruckte Originalversion dieser Diplomarbeit ist an der TU Wien Bibliothek verfügbar
The approved original version of this thesis is available in print at TU Wien Bibliothek.
TU Bibliothek WIEN Your knowledge hub

This calculation is shown in the appendix, Sec. A.6. We get coupled differential equations

$$\begin{aligned}
\langle \dot{\hat{a}} \rangle &= -\mathrm{i}\Delta_c \langle \hat{a} \rangle + \sum_j g_j \langle \hat{\sigma}_-^j \rangle + \eta - \kappa \langle \hat{a} \rangle \,, \\
\langle \dot{\hat{\sigma}}_-^j \rangle &= -\mathrm{i}\Delta_s^j \langle \hat{\sigma}_-^j \rangle + g_j \langle \hat{a}\hat{\sigma}_z^j \rangle - \left(\frac{\gamma_\parallel}{2} + \gamma_\perp \right) \langle \hat{\sigma}_-^j \rangle \,, \\
\langle \dot{\hat{\sigma}}_z^j \rangle &= -2g_j \left(\langle \hat{a}^\dagger \hat{\sigma}_-^j \rangle + \langle \hat{a}\hat{\sigma}_+^j \rangle \right) - \gamma_\parallel \left(1 + \langle \hat{\sigma}_z^j \rangle \right) .
\end{aligned} \tag{2.78}$$

Please note that since we are in the Schrödinger picture, we obtain solutions for the expectation values but not for the operators themselves. By assuming that we are dealing with a large spin number and a relatively small coupling between the cavity mode and the spins, one can do the approximation $\langle a\sigma_z^j \rangle = \langle a \rangle \langle \sigma_z^j \rangle$, i.e., the quantum effects encoded in the correlations are negligibly small [34]. Therefore, we end up with the Maxwell-Bloch equations

$$\begin{aligned}
\langle \dot{\hat{a}} \rangle &= -\mathrm{i}\Delta_c \langle \hat{a} \rangle + \sum_j g_j \langle \hat{\sigma}_-^j \rangle + \eta - \kappa \langle \hat{a} \rangle \,, \\
\langle \dot{\hat{\sigma}}_-^j \rangle &= -\mathrm{i}\Delta_s^j \langle \hat{\sigma}_-^j \rangle + g_j \langle \hat{a} \rangle \langle \hat{\sigma}_z^j \rangle - \left(\frac{\gamma_\parallel}{2} + \gamma_\perp \right) \langle \hat{\sigma}_-^j \rangle \,, \\
\langle \dot{\hat{\sigma}}_z^j \rangle &= -2g_j \left(\langle \hat{a}^\dagger \rangle \langle \hat{\sigma}_-^j \rangle + \langle \hat{a} \rangle \langle \hat{\sigma}_+^j \rangle \right) - \gamma_\parallel \left(1 + \langle \hat{\sigma}_z^j \rangle \right) .
\end{aligned} \tag{2.79}$$

Up to now we have derived a mathematical framework with which we can describe the physical processes which are ongoing in our experiment. In the next chapter we therefore will describe the experimental setup, in particular the cavity and spin ensemble, in more detail.

Die approbierte gedruckte Originalversion dieser Diplomarbeit ist an der TU Wien Bibliothek verfügbar
The approved original version of this thesis is available in print at TU Wien Bibliothek.
TU Bibliothek Your knowledge hub WIEN

TU Bibliothek Your knowledge hub WIEN
Die approbierte gedruckte Originalversion dieser Diplomarbeit ist an der TU Wien Bibliothek verfügbar
The approved original version of this thesis is available in print at TU Wien Bibliothek.

3 Experimental Setup

In this chapter we want to go into more detail and explain the characteristics of our building parts with which we are performing cavity QED experiments: especially the cavity and the spin system we use. Besides that we will briefly explain why we are working at cryogenic temperatures and how our fridge is working. Next, the experimental measurement scheme including IQ mixing is discussed. Finally, the design procedure of the chirp pulse with which we are inverting our spins and the simulation of the system are mentioned.

3.1 Real Cavity

The response function, i.e. the transmission as a function of frequency, of an ideal cavity is a delta distribution, we only see a non-zero response at its resonance frequency. Such a response function will never be observed in our experimental setup. This is because our cavity has unavoidable losses which lead to an additional term in the differential equation which we have neglected so far. Now we take that term for losses into account and further add some external drive since we want to calculate the transmission for a driven cavity. This driven LC circuit can be described with

$$\frac{\mathrm{d}^2 I(t)}{\mathrm{d}t^2} + \frac{R}{L}\frac{\mathrm{d}I(t)}{\mathrm{d}t} + \frac{1}{LC}I(t) = f_0 \mathrm{e}^{-\mathrm{i}\omega t}, \tag{3.1}$$

where $f_0 \mathrm{e}^{-\mathrm{i}\omega t}$ is a periodic driving term. By introducing new variables, $\omega_0^2 = \frac{1}{LC}$ and $\gamma = \frac{R}{2L}$, we get

$$\ddot{I} + 2\gamma\dot{I} + \omega_0^2 I = f_0 \mathrm{e}^{-\mathrm{i}\omega t}, \tag{3.2}$$

where we omit the t dependence, for better readability, as well. For solving this differential equation we make the ansatz $I(t) = A_0 \mathrm{e}^{-\mathrm{i}\omega t}$, i.e., we assume stationarity, the amplitude A_0 can be complex. Inserting that into Eq. (3.2) leads to

$$\left(-\omega^2 - 2\mathrm{i}\omega\gamma + \omega_0^2\right) A_0 = f_0. \tag{3.3}$$

The corresponding intensity can therefore be written as

$$|A_0|^2 = \frac{f_0^2}{\left(\omega_0^2 - \omega^2\right)^2 + 4\omega^2\gamma^2}. \tag{3.4}$$

Die approbierte gedruckte Originalversion dieser Diplomarbeit ist an der TU Wien Bibliothek verfügbar
The approved original version of this thesis is available in print at TU Wien Bibliothek.
TU Bibliothek Your knowledge hub WIEN

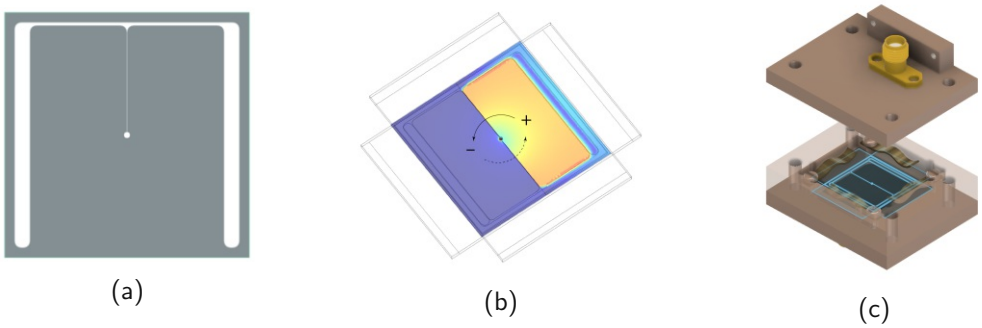

Figure 3.1: In our experiment we use a so-called double chip resonator. It consists of two chips as depicted in (a) whereby the upper chip gets rotated by $180°$ and then put on top of the other. By doing so, one obtains two capacitors between which the charges oscillate as depicted in (b) where the (oscillating) electric field is shown as a heatmap on the right half. Besides that field, the oscillating charges lead to a current which causes a magnetic field. The left half shows a colorplot of the corresponding magnetic field strength which is almost exclusively concentrated in the small hole in the center. Since the magnetic mode volume is pretty small and the B field is proportional to $\frac{1}{\sqrt{V}}$ as can be seen in Eq. (2.15), it couples strongly to the spin ensemble which is placed in that hole. Finally, the two niobium chips which are superconducting at our cryogenic temperatures are put in a copper housing (c).

By dividing $|A_0(\omega)|^2$ by $|A_0(\omega_0)|^2$, and assuming that we are near the resonant frequency, i.e., $|\omega - \omega_0| \ll \omega_0$, we find

$$\frac{|A_0(\omega)|^2}{|A_0(\omega_0)|^2} = \frac{f_0^2}{(\omega_0^2 - \omega^2)^2 + 4\omega^2\gamma^2}\frac{4\omega_0^2\gamma^2}{f_0^2} \approx \frac{4\omega_0^2\gamma^2}{4\omega_0^2(\omega_0 - \omega)^2 + 4\omega^2\gamma^2} \approx \frac{\gamma^2}{(\omega_0 - \omega)^2 + \gamma^2}, \tag{3.5}$$

where we used $\omega_0^2 - \omega^2 = (\omega_0 + \omega)(\omega_0 - \omega) \approx 2\omega_0(\omega_0 - \omega)$ for the second step and assumed $\omega \approx \omega_0$. Please note that we further assume that the damping is small compared to the resonant frequency, i.e., $\gamma \ll \omega_0$. This is done because for large damping the resonance frequency gets shifted. The resulting response function (Eq. (3.5)) is a Lorentzian distribution with γ defining the half width at half maximum (HWHM). With that, we can define the cavity quality factor, $Q = \omega/\Delta\omega = \omega/(2\gamma)$. Roughly speaking, it is the number of oscillation periods a photon survives in the cavity before it is lost through damping processes. In the latter the damping parameter γ will be identified with the cavity loss rate κ. This derivation is based on Ref. [35].

Until now we talked about cavities in general, now we want to get more specific. We use a so-called double chip resonator. The chips are made of niobium, lithographically patterned onto a sapphire substrate, which is superconducting at

Die approbierte gedruckte Originalversion dieser Diplomarbeit ist an der TU Wien Bibliothek verfügbar
The approved original version of this thesis is available in print at TU Wien Bibliothek.
TU Bibliothek Your knowledge hub WIEN

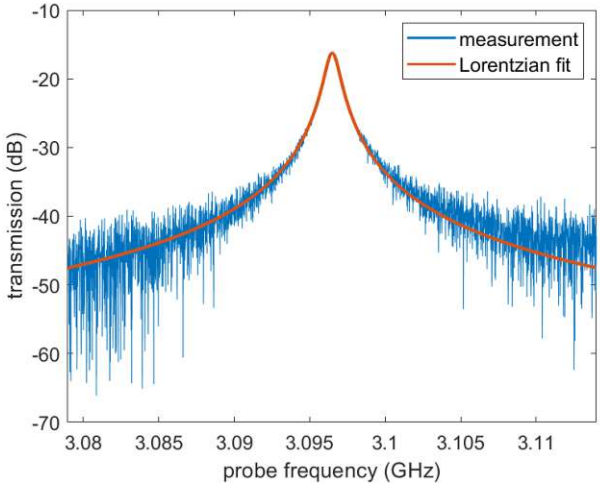

Figure 3.2: A characteristic transmission spectrum of our double-chip resonator used in the experiment. The with a VNA measured S_{21} parameter for different frequencies is shown in blue. The obtained Lorentzian fit (given by Eq. (3.5)) of the data can be seen in red. From that fit we obtain a cavity resonance frequency of $\omega_c = 3.0965 \cdot 2\pi$ GHz, a cavity loss rate of $\kappa = 0.4754 \cdot 2\pi$ MHz and $Q = 3260$.

cryogenic temperatures we work. They have a slit which forces the charges to oscillate between the one and the other side over a specific way. The upper chip gets rotated by 180° and then put on top of the other chip so that the slit of the lower one looks like that shown in Fig. 3.1(a), whereas the slit of the upper one goes from the hole in the middle downwards. These two chips on top of each other make up two capacitors between which the charges oscillate. This causes an electric field as depicted in Fig. 3.1(b). These oscillating charges cause a magnetic field inside the hole in the middle where the spin ensemble is placed. Because of the small volume and since the magnetic field scales with $\frac{1}{\sqrt{V}}$ (as can be seen in Eq. (2.15)), it gets strong and therefore the coupling increases. This makes it possible (although the diamond is quite small and therefore does not contain that many NV centers) to enter the strong coupling regime which is necessary for our experiment. Finally, the double chips are placed in a copper housing as shown in Fig. 3.1(c).

In our experiment, the transmission of such a cavity, i.e. the S_{21} parameter, is measured with a vector network analyzer (VNA). We obtain the transmission curve shown in Fig. 3.2 where one can see the measured data with a Loretzian fit (given by Eq. (3.5)). From the fit we obtain a cavity resonance frequency of $\omega_c = 3.0965 \cdot 2\pi$ GHz and a cavity loss rate of $\kappa = 0.4754 \cdot 2\pi$ MHz from which one can calculate the quality factor Q which in our case is $Q = 3260$. A more detailed explanation about our VNA measurement scheme as well as a setup schematic can

Die approbierte gedruckte Originalversion dieser Diplomarbeit ist an der TU Wien Bibliothek verfügbar
The approved original version of this thesis is available in print at TU Wien Bibliothek.
TU Bibliothek Your knowledge hub WIEN

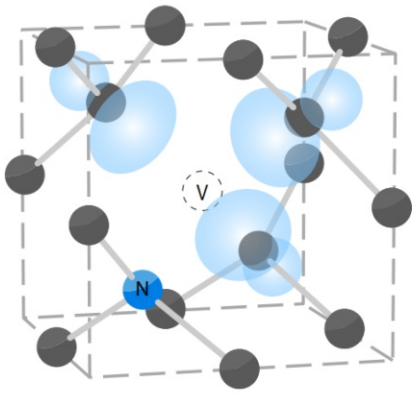

Figure 3.3: A carbon atom is replaced by a nitrogen atom and forms with a vacancy as next neighbor a NV center. Because of the face-centered-cubic structure of the diamond, such a NV center can point in all corners of a tetrahedron which leads to 4 different NV subensembles. This needs to be taken into account when aligning the external magnetic field so that the chosen number of NV subensembles are in resonance. Picture taken from Ref. [36].

be found in Sec. 3.4.

After explaining the cavity we use in our experiment we want to explain the properties of the spin ensemble under test.

3.2 NV Center

The nitrogen-vacancy center (NV center) is one of numerous point defects in diamond. One reason why such a diamond with NV centers is used often in experiments is that it is very stable and robust. Unless it does not get exposed to extremely conditions such as high temperatures or something similar it is (nearly) unbreakable. It consists of a nitrogen atom which replaces one carbon atom. As shown in Fig. 3.3, the nitrogen atom has a vacancy as a next neighbor, this is where the name comes from. Since these centers are embedded in the face-centered-cubic structure of the diamond, the NV centers can point in all corners of a tetrahedron which leads to 4 different subensembles. Furthermore, these NV centers can occur as agglomerates in the carbon structure of the diamond or as over the whole crystal uniformly distributed defects. For our experiment we use uniformly distributed NV centers which can be implemented by irradiating the crystal with electrons or neutrons [38]. We use a neutron irradiated sample for our experiment. Such defects furthermore occur with two different charges: in one case the NV center is uncharged, in the other case the center has a charge of -1 e [37]. If one counts the free electrons one gets in total 5: two unused from the nitrogen atom and three from the carbon atoms which

Die approbierte gedruckte Originalversion dieser Diplomarbeit ist an der TU Wien Bibliothek verfügbar
The approved original version of this thesis is available in print at TU Wien Bibliothek.
TU Bibliothek Your knowledge hub WIEN

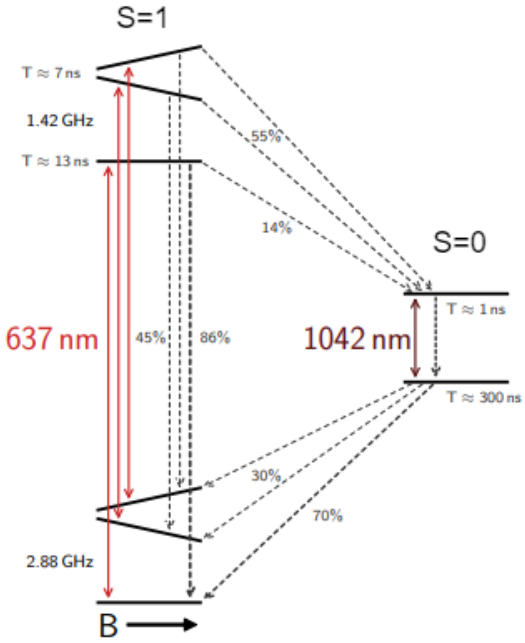

Figure 3.4: The energy scheme of the NV centers clearly shows a ground and excited state which are separated by $637\,\mathrm{nm}$ [37]. Because of a total spin of 1, we have a triplet state in the ground as well as the excited state. The meta stable states on the right hand side can be interpreted as the corresponding singlet states. Due to dipole-dipole interaction the NV centers show a zero field splitting. By applying an external magnetic field the energy levels get shifted by the Zeeman effect and the degeneration vanishes. The transition rates and the corresponding transition probabilities are shown as well. Picture taken from Ref. [34].

surrounds the vacancy. Nevertheless, experimental spin resonance measurements show that the NV center has to have a even number of electrons, since the total spin is $S = 1$ [37]. This problem of different electron numbers is not finally solved yet. One hypothesis is that the additional sixth electron comes from the lattice. In our experiment we are dealing with negatively charged NV centers.

The energy scheme of a NV center is shown in Fig. 3.4 where one can see a ground and an excited state which are separated by $637\,\mathrm{nm}$ [37]. Because of a total spin of $S = 1$, we have an antisymmetric triplet spin state in the ground as well as in the excited state. The singlet states can be seen on the right hand side of the figure and build a meta stable state.

Furthermore, the NV centers show zero field splitting. This splitting arises from the dipole-dipole interaction where one dipole consists of two unpaired electrons.

Die approbierte gedruckte Originalversion dieser Diplomarbeit ist an der TU Wien Bibliothek verfügbar
The approved original version of this thesis is available in print at TU Wien Bibliothek.
TU Bibliothek Your knowledge hub WIEN

Therefore, the dipole-dipole interaction Hamiltonian reads like [39]

$$\hat{H}_D = \hat{\boldsymbol{S}}\hat{\boldsymbol{D}}\hat{\boldsymbol{S}} = D_x\hat{S}_x^2 + D_y\hat{S}_y^2 + D_z\hat{S}_z^2, \tag{3.6}$$

where $\hat{\boldsymbol{D}}$ is a symmetric and traceless matrix (which it has to be when the underlying interaction is of dipole-dipole type [40]) and $\hat{\boldsymbol{S}}$ the total spin, i.e., $\hat{\boldsymbol{S}} = \hat{\boldsymbol{S}}_1 + \hat{\boldsymbol{S}}_2$. We now want to express $D_x\hat{S}_x^2 + D_y\hat{S}_y^2$ as a mean value with some deviation $\hat{\Delta}$,

$$D_x\hat{S}_x^2 + D_y\hat{S}_y^2 = \frac{D_x + D_y}{2}\left(\hat{S}_x^2 + \hat{S}_y^2\right) + \hat{\Delta}. \tag{3.7}$$

Using this equation we get an expression for the deviation, i.e.,

$$\hat{\Delta} = \frac{D_x - D_y}{2}\left(\hat{S}_x^2 - \hat{S}_y^2\right). \tag{3.8}$$

Now we insert these expressions in the original one leading to

$$\hat{H}_D = \frac{D_x + D_y}{2}\left(\hat{S}_x^2 + \hat{S}_y^2\right) + \frac{D_x - D_y}{2}\left(\hat{S}_x^2 - \hat{S}_y^2\right) + D_z\hat{S}_z^2. \tag{3.9}$$

By using $\hat{S}^2 = \hat{S}_x^2 + \hat{S}_y^2 + \hat{S}_z^2$ and using the fact that $\boldsymbol{D}$ is traceless we get

$$\begin{aligned}\hat{H}_D &= -\frac{D_z}{2}\left(\hat{S}^2 - S_z^2\right) + \frac{D_x - D_y}{2}\left(\hat{S}_x^2 - \hat{S}_y^2\right) + D_z\hat{S}_z^2 \\ &= \frac{3D_z}{2}\left(\hat{S}_z^2 - \frac{\hat{S}^2}{3}\right) + \frac{D_x - D_y}{2}\left(\hat{S}_x^2 - \hat{S}_y^2\right).\end{aligned} \tag{3.10}$$

By introducing $D = \frac{3D_z}{2}$ and $E = \frac{D_x - D_y}{2}$ we end up with an equation for the zero field splitting

$$\hat{H}_D = D\left(\hat{S}_z^2 - \frac{\hat{S}^2}{3}\right) + E\left(\hat{S}_x^2 - \hat{S}_y^2\right). \tag{3.11}$$

If we take an external magnetic field into account as well we get

$$\hat{H}_D = D\left(\hat{S}_z^2 - \frac{\hat{S}^2}{3}\right) + E\left(\hat{S}_x^2 - \hat{S}_y^2\right) + \hbar\mu_S\hat{\boldsymbol{B}}_{\text{ext}} \cdot \hat{\boldsymbol{S}} \tag{3.12}$$

for our final NV Hamiltonian. The zero field splitting of the NV centers is $D = 2.88 \cdot 2\pi\,\text{MHz}$ [37, 41], their axial strain is $E = 1 \cdot 2\pi$ to $10 \cdot 2\pi\,\text{MHz}$ and is very sample dependent [34] and the magnetic moment of the spin is $\mu_S = 28\,\text{MHz}\,\text{mT}^{-1}$ [34].

By applying an external magnetic field the degenerate $m_S = \pm 1$ levels get shifted by the Zeeman effect where we choose that external field in such a way that the transition frequency from the $m_s = 0$ to the $m_s = +1$ state matches the cavity

Die approbierte gedruckte Originalversion dieser Diplomarbeit ist an der TU Wien Bibliothek verfügbar
The approved original version of this thesis is available in print at TU Wien Bibliothek.
TU Bibliothek Your knowledge hub WIEN

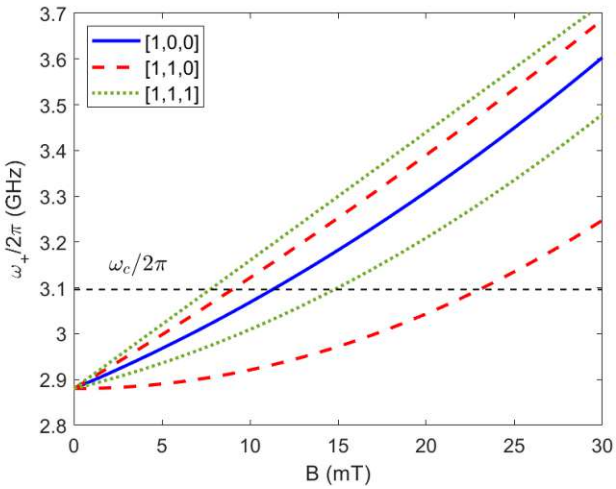

Figure 3.5: Transition frequency of corresponding NV subensembles as a function of external magnetic field strength and for different B field directions. Since the NV centers can point in all 4 directions of a tetraeder, the magnetic field they experience, i.e. the projection of the field onto the NV axis, is only the same for an external field direction of $[1, 0, 0]$. For the direction $[1, 1, 0]$ and $[1, 1, 1]$ $2 + 2$ and $3 + 1$ subensembles are in resonance, respectively.

frequency so that the spin system can be manipulated by the cavity. This is necessary since one cannot change the cavity frequency. Since the NV centers can point in all corners of a tetrahedron, there are 4 different subensembles. Therefore, not only the strength of the external magnetic field is important but also the direction. In Fig. 3.5 the transition frequency between the $m_s = 0$ to the $m_s = 1$ state is plotted as a function of its strength and for different directions. If the magnetic field points in the $[1, 0, 0]$ direction, all 4 subensembles are in resonance, for the direction $[1, 1, 0]$ and $[1, 1, 1]$ $3+1$ and $2+2$ subensembles are in resonance, respectively. For the case the magnetic field points in any other direction, then the transition freuqency of all 4 subensembles is different for the same magnetic field.

Now we are interested in what state the spins are in. This can be calculated with Boltzmann statistics where we have to sum over all possible states. If there are degenerate energy values then these (equivalent) states have to be counted several times (as many times as the multiplicity of the degeneration). For that calculation we assume that we do not have an external magnetic field, which leads us to the following occupation probability of the ith level

$$\frac{\langle n_i \rangle}{\sum n_i} = \frac{1}{Z} g_i \mathrm{e}^{-\frac{\varepsilon_i}{k_B T}}, \tag{3.13}$$

where g_i is the degeneracy of the ith energy level, ε_i the corresponding energy and

Die approbierte gedruckte Originalversion dieser Diplomarbeit ist an der TU Wien Bibliothek verfügbar
The approved original version of this thesis is available in print at TU Wien Bibliothek.
TU Bibliothek Your knowledge hub WIEN

Z is the partition function which is given by

$$Z = \sum_i g_i \mathrm{e}^{-\frac{\varepsilon_i}{k_B T}}. \tag{3.14}$$

With that, it is easy to calculate the probability for the spins being in the ground- or excited state. For the ground state we get

$$P(n_0) = \frac{\mathrm{e}^{-\frac{\varepsilon_\downarrow}{k_B T}}}{\mathrm{e}^{-\frac{\varepsilon_\downarrow}{k_B T}} + 2\mathrm{e}^{-\frac{\varepsilon_\uparrow}{k_B T}}} = \frac{1}{1 + 2\mathrm{e}^{-\frac{\varepsilon_\uparrow - \varepsilon_\downarrow}{k_B T}}} = \frac{1}{1 + 2\mathrm{e}^{-\frac{\hbar\omega_s}{k_B T}}}, \tag{3.15}$$

where $\varepsilon_\downarrow$ and $\varepsilon_\uparrow$ denote the energies of the corresponding levels (down for the ground state and up for the excited state). For the probability of the spins being in the excited state one gets

$$P(n_{-1} + n_{+1}) = \frac{2\mathrm{e}^{-\frac{\varepsilon_\uparrow}{k_B T}}}{\mathrm{e}^{-\frac{\varepsilon_\downarrow}{k_B T}} + 2\mathrm{e}^{-\frac{\varepsilon_\uparrow}{k_B T}}} = \frac{2}{\mathrm{e}^{\frac{\hbar\omega_s}{k_B T}} + 2}. \tag{3.16}$$

As seen in Fig. 3.4, the transition frequency without any external field is $\omega_s = 2.88 \cdot 2\pi\,\mathrm{GHz}$, so for our experiment which is carried out at roughly 30 mK almost all spins (approx 98% after they had enough time to thermalize) are in the ground state. The calculated probabilities of being in the $m_s = 0$ and $m_s = \pm 1$ state as a function of temperature are depicted in Fig. 3.6. At roughly 150 mK the expressions $\hbar\omega_s$ and $k_B T$ have the same magnitude. For temperatures higher than $\approx 10\,\mathrm{K}$ the second expression is roughly 100 times larger which means that the states get occupied with the same probability, for 3 states this gives a probability of $\frac{1}{3}$ per state. Please note that we used the spin frequency without any external field which is slightly less than the cavity resonance frequency of $\omega_c = 3.1 \cdot 2\pi\,\mathrm{GHz}$ (with which the spins are brought in resonance) but since the order is the same, we obtain qualitatively the same result.

Since we know that after waiting a suitable time all spins are in the ground state and by applying such an external field so that the transition frequency to the $m_s = 1$ state matches the cavity frequency, only two of the aforementioned levels play a role in the experiment. The NV center can therefore be understood as an effectively two level system and the equations derived in Ch. 2 hold.

Until now we only take single spins into account and neglect spin-spin interactions. Since, however, we couple to a large spin ensemble in our experiment, we now want to estimate the strength of that interaction. Furthermore, it has to be checked if the interaction strength is small enough so that the treatment of the NV centers as independent two-level systems as done in Ch. 2 is justified. To calculate that strength, one needs to know the distance between two NV centers. With a ^{12}C concentration of $c \approx 1.76 \cdot 10^{29}\ \frac{^{12}\mathrm{C}}{\mathrm{m}^3}$ [16] we get a mean distance of

$$r = \sqrt[3]{\frac{1}{c \cdot 40 \cdot 10^{-6}}} = 5.22\,\mathrm{nm}, \tag{3.17}$$

Die approbierte gedruckte Originalversion dieser Diplomarbeit ist an der TU Wien Bibliothek verfügbar
The approved original version of this thesis is available in print at TU Wien Bibliothek.
TU Bibliothek Your knowledge hub WIEN

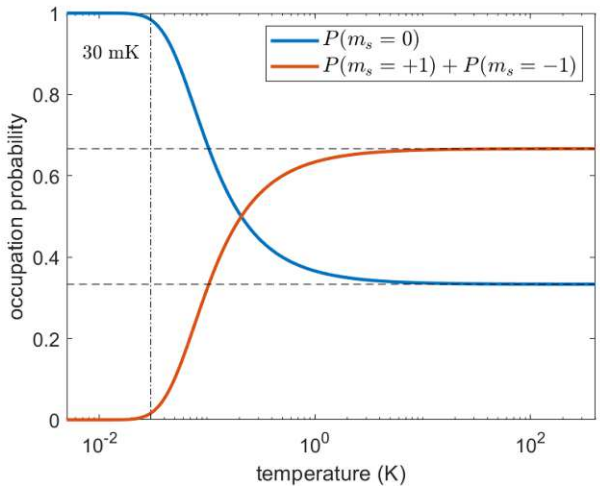

Figure 3.6: The occupation probability of the $m_s = 0$ and $m_s = \pm 1$ state as a function of temperature is shown in blue and red, respectively. At our working temperature of roughly $30\,\mathrm{mK}$ almost all spins (approx 98%) can be found in the ground state after they had enough time to relax. For temperatures higher than $\approx 10\,\mathrm{K}$, the expression $k_B T$ is roughly 100 times larger than $\hbar\omega$ and therefore all states are occupied with the same probability, i.e. $\frac{1}{3}$ per state.

where we assumed a NV center concentration of 40 ppm. The spin-spin interaction strength can then be calculated with [16]

$$\frac{h\mu_0\mu_S^2}{4\pi r^3} \approx 400 \text{ kHz}, \tag{3.18}$$

where μ_0 is the magnetic permeability in vacuum. With Eqs. (3.17) and (3.18), one sees that the interaction strength increases linearly with the concentration of NV centers in diamond. Since the interaction strength for a NV center concentration of 40 ppm is smaller than the cavity linewidth and the inhomogeneous broadened spin ensemble, the spin-spin interaction will be neglected in the following. However, as stated in Sec. 2.6, this spin-spin interaction leads in combination with the spin-bath interaction to loss of coherence with a rate $\gamma_\perp = 1/T_2$ [34].

Based on the above mentioned ^{12}C and NV center concentration, we can roughly estimate how many NV centers are in our sample. For the sample which has the form of a square frustum whereby the length of the base square is $a \approx 200\,\mu\mathrm{m}$, we estimate $\approx 10^{12}$ NV centers.

In the following, we now want to explain how we realize the cryogenic temperatures at which we are working.

Die approbierte gedruckte Originalversion dieser Diplomarbeit ist an der TU Wien Bibliothek verfügbar
The approved original version of this thesis is available in print at TU Wien Bibliothek.
TU Bibliothek Your knowledge hub WIEN

3.3 Dilution Refrigerator

All our experiments are carried out in a cryostat at temperatures of roughly 30 mK which is done because of 2 major reasons. First, as discussed in Sec. 3.2, we know that all our NV centers are in the ground state then. Furthermore, operating at low temperatures allow us to use superconducting resonators which have the advantage of having higher Q values which corresponds to lower damping rates.

Low temperatures are reached with a ^{3}He/^{4}He Dilution Refrigerator from Oxford Instruments (Triton 400 fridge). Such a dilution fridge uses a ^{3}He/^{4}He mixture which undergoes a phase separation when cooled below 870 mK. One obtains a nearly pure ^{3}He phase and a dilute phase with approximately 6.6% ^{3}He [42]. The ^{3}He dissolves from the pure phase through the phase boundary into the dilute phase. Since the process of moving the ^{3}He through the phase boundary is endothermic, heat is removed and the environment (the lowest stage) gets cooled. The flow of ^{3}He is driven by a pressure gradient which is reached by pumping with two turbo pumps (at room temperature). On the way up, the ^{3}He at some point evaporates and gets compressed by the turbo pumps. On the way down, it gets condensed and the upflowing ^{3}He precools the downflowing helium in heat exchangers and finally enters the pure ^{3}He phase, the cycle is completed. With the procedure mentioned, we have a cooling power of roughly 400 µW for a base temperature of 100 mK [34].

For precooling, a pulse tube cooler is used with which a temperature of 2.7 K can be reached [34]. After that, the condensing of the ^{3}He/^{4}He mixture is reached by evaporative cooling of ^{3}He.

Please note that the temperature limit of 30 mK is not due to any physical limitations since the dilute phase contains 6.6% of ^{3}He all the way down to 0 K [42] which means that theoretically 0 K can be reached. The reason why we do not get temperatures lower than that is the introduced heat from the cables going down to the lowest stage with which we are doing our measurements. By heat-anchoring them on every temperature stage one can reduce that introduced heat from the cables but one does not get completely rid of it.

After explaining the working principles of our dilution fridge and the need for such cryogenic temperatures, we want to introduce our experimental measurement methods in the following.

3.4 Experimental Measurement Methods

As the energy of the NV centers depends on the external magnetic field, we have a Helmholtz coil cage with which we can apply a magnetic field of up to 300 Gauss in any direction. Inside that, the cavity containing the NV sample is placed as shown in Fig. 3.7. As can be seen in Sec. 3.2, by changing the direction of the external field, one can choose from 1 to 4 subensembles of NV centers being in resonance

Die approbierte gedruckte Originalversion dieser Diplomarbeit ist an der TU Wien Bibliothek verfügbar
The approved original version of this thesis is available in print at TU Wien Bibliothek.
TU Bibliothek Your knowledge hub WIEN

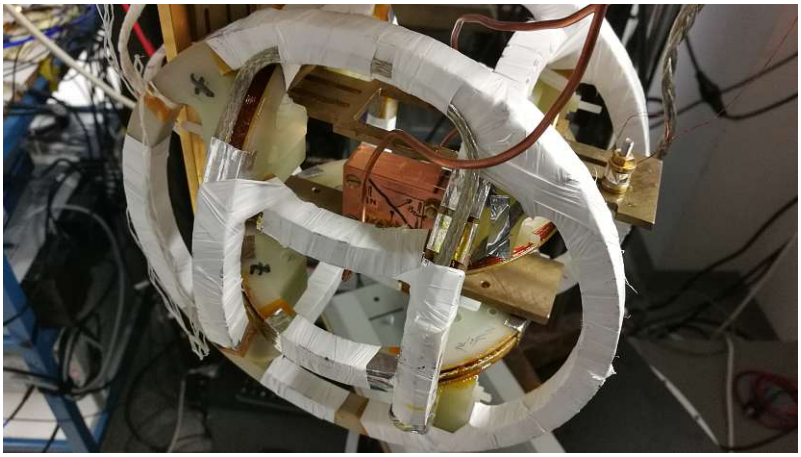

Figure 3.7: To bring the NV subensembles in resonance with our cavity, we place our double chip resonator inside a Helmholtz coil cage with which we can apply magnetic fields up to 300 Gauss in any direction.

with the cavity. Since the collective coupling scales with the number of spins, we can change the coupling by applying a different magnetic field. With semi-rigid SMA cables the vacuum flange at room temperature is connected with the cavity which is placed in the chamber with lowest temperature (approximately 30 mK). To reduce the thermal influence of the cables, they are heat-anchored at every stage as mentioned in Sec. 3.3. To reduce the number of thermal photons (i.e. noise, which therefore leads to a better signal to noise ratio as well) inside the cables and to reduce the thermal occupation number of the cavity mode, we use attenuators which are heat-anchored at every stage as well. By using them on every temperature stage we are able to block the thermal photons coming from the hotter stage.

But how do we know how many NV subensembles are in resonance with the cavity? By changing the magnetic field with the Helmholtz coils and measuring the transmission of the cavity with our VNA, we get the corresponding energy spectrum. A schematic of our experimental setup can be seen in Fig. 3.8(a). By measuring with low power we can assume to be in the linear regime and therefore expect eigenenergies as mentioned in Sec. 2.4. If the measurement power of the VNA is too high then we bleach the spins (for the whole spin ensemble $\sum_j \langle \hat{\sigma}_z^j \rangle = 0$) and one only measures the cavity. As shown in Sec. 2.4, each avoided crossing is caused by a corresponding spin transition. If we get qualitatively the same picture as shown in Fig. 2.7(d) then we know that all 4 subensembles have the same transition frequency and are in resonance with the cavity. Such a measurement result can be seen in Fig. 3.9. When one gets pictures like Figs. 2.7(a) or (b) we know that $1+3$ or $2+2$ spin ensembles are in resonance, respectively. Depending on the direction of the magnetic field, up to 4 avoided crossings are possible.

In addition to the steady state measurement method, we are able to do time

Die approbierte gedruckte Originalversion dieser Diplomarbeit ist an der TU Wien Bibliothek verfügbar
The approved original version of this thesis is available in print at TU Wien Bibliothek.
TU Bibliothek Your knowledge hub WIEN

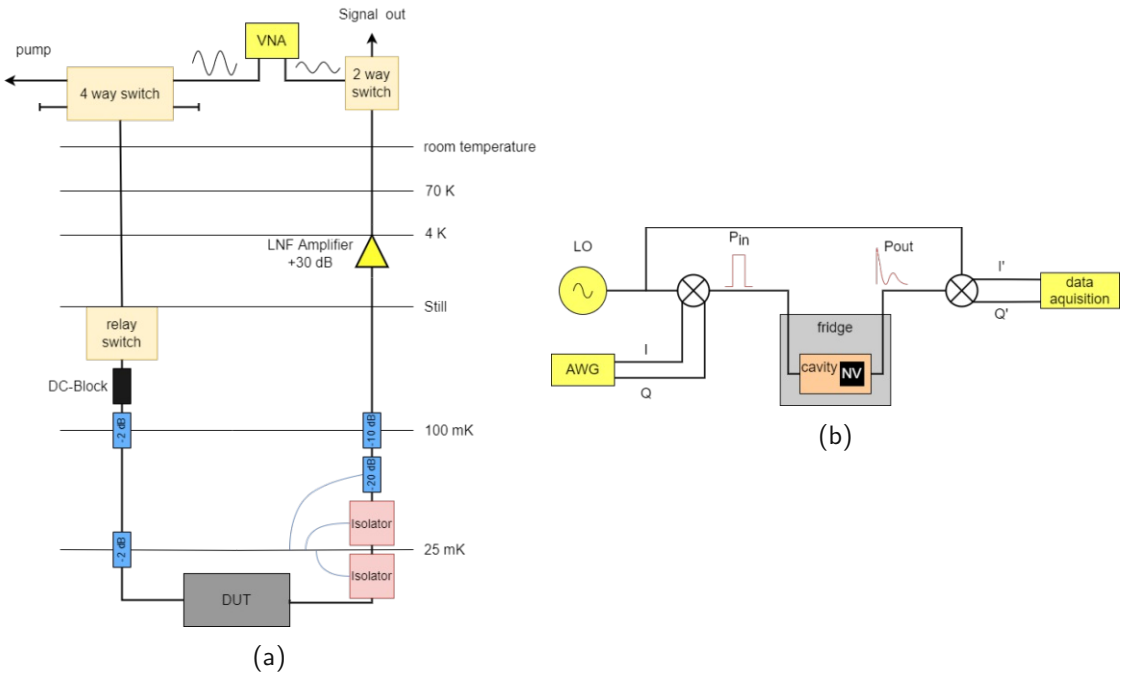

Figure 3.8: The transmission of our cavity for different frequencies, i.e. the S_{21} parameter, is measured with a VNA as depicted in (a). To cool the microwave downline properly, the semi-rigid SMA cables get heat-anchored on every stage. To reduce the number of thermal photons (i.e. noise, which therefore leads to a better signal to noise ratio) inside the cables and reduce the thermal occupation number of the cavity mode, we use attenuators which are heat-anchored at every stage as well. To avoid thermal photons in the upline which are leaking in from the hotter stages, we use a low noise amplifier (LNF) on the $4\,\mathrm{K}$ and isolators on the $25\,\mathrm{mK}$ stage (the blue lines indicate the heat-anchoring). The outcoming signal is fed back into the VNA where the resulting transmission as a function of frequency is shown. With the two switches at room temperature, one can switch between the steady state and time resolved measurement apparatus. The latter one is shown in (b) and consists of a carrier signal with a fixed frequency (in general the cavity resonance frequency) on which we mix our two quadratures I and Q. The carrier signal is generated by a local oscillator (LO), the quadratures by an arbitrary waveform generator (AWG), respectively. The resulting signal gets amplified and is then send into the fridge with the cavity containing the NV centers. With the reference signal of the local oscillator one can decompose the signal coming out of the fridge into the two quadratures again which then can be measured with a data acquisition card placed in the computer.

Die approbierte gedruckte Originalversion dieser Diplomarbeit ist an der TU Wien Bibliothek verfügbar
The approved original version of this thesis is available in print at TU Wien Bibliothek.
TU Bibliothek Your knowledge hub WIEN

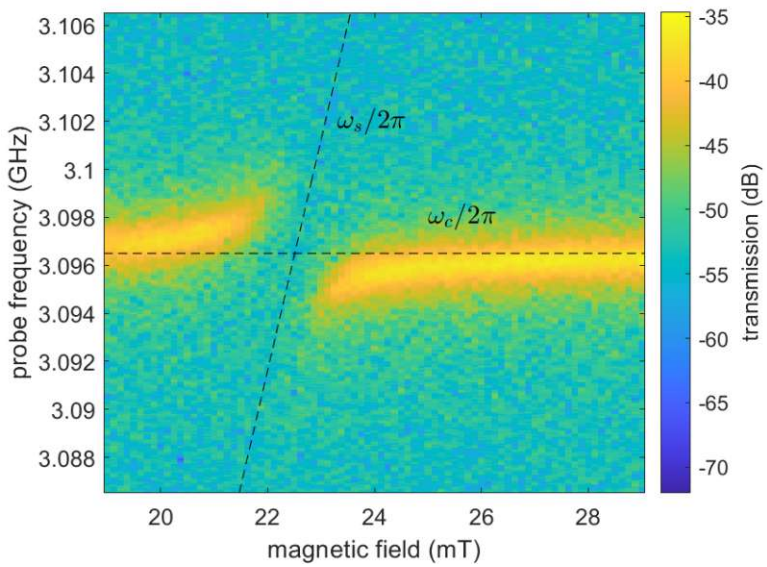

Figure 3.9: By aligning an external field correctly, all 4 NV subensembles are in resonance with the cavity, we get qualitatively the same picture as shown in Fig. 2.7(d) and only see one avoided crossing. This picture is obtained by consecutively ramping to a certain magnetic field and then measuring the transmission of the cavity, i.e. the S_{21} parameter, with the VNA for different frequencies. Please note that one has to measure with low power to be in the linear regime and get qualitatively the same pictures as shown in Sec. 2.4. If the power is too high one bleaches the spin system ($\sum_j \langle \hat{\sigma}_z^j \rangle = 0$) and one only measures the transmission of the cavity. As guide for the eye, the cavity as well as the spin frequency are depicted in black as well.

resolved measurements as depicted in Fig. 3.8(b). Onto a carrier signal with a fixed frequency (which in general is chosen as the resonance frequency of the cavity) we mix two quadratures I and Q. The carrier signal gets generated by a local oscillator (LO), the quadratures by an arbitrary waveform generator (AWG), respectively. The resulting signal gets amplified and is then sent into the fridge with the cavity containing the NV centers. With the reference signal of the local oscillator one can decompose the signal coming out of the fridge into the two quadratures again which then can be measured with a data acquisition card placed in the computer.

After explaining our steady state and time resolved measurement setup, we will explain the quadrature mixing procedure in more detail.

Die approbierte gedruckte Originalversion dieser Diplomarbeit ist an der TU Wien Bibliothek verfügbar
The approved original version of this thesis is available in print at TU Wien Bibliothek.
TU Bibliothek Your knowledge hub WIEN

3.5 Homodyne Measurement and IQ Mixing

For our time resolved measurement, which is depicted in Fig. 3.8(b), we make use of the quadrature amplitude modulation procedure. During this process, one uses two carrier signals which have a phase difference of 90° which get modulated by time dependent components named $I(t)$ and $Q(t)$. So in total our RF signal can be written as

$$s(t) = I(t)\sin(\omega_d t) + Q(t)\sin\left(\omega_d t + \frac{\pi}{2}\right) = I(t)\sin(\omega_d t) + Q(t)\cos(\omega_d t), \tag{3.19}$$

where ω_d is the frequency of the carrier signal (drive frequency) and usually chosen to be the resonance frequency of the cavity. The two quadratures $I(t)$ and $Q(t)$ can be time dependent and are generated with an arbitrary waveform generator.

To demodulate the signal coming out of the fridge, it gets multiplied with a sine and a cosine signal separately, one gets

$$\begin{aligned} s_{\text{out}}(t)\cdot\sin(\omega_d t) &= \tilde{I}(t)\sin(\omega_d t)\sin(\omega_d t) - \tilde{Q}(t)\cos(\omega_d t)\sin(\omega_d t), \\ s_{\text{out}}(t)\cdot\cos(\omega_d t) &= \tilde{I}(t)\sin(\omega_d t)\cos(\omega_d t) + \tilde{Q}(t)\cos(\omega_d t)\cos(\omega_d t), \end{aligned} \tag{3.20}$$

where the tilde denotes that these are the quadratures of the outcoming signal. Using the trigonometric identities $\sin(2\alpha) = 2\sin\alpha\cdot\cos\alpha$ and $\cos(2\alpha) = 2\cos^2\alpha - 1$ (or $\cos(2\alpha) = 1 - 2\sin^2\alpha$, they follow from the angle addition theorems) gives

$$\begin{aligned} s_{\text{out}}(t)\cdot\sin(\omega_d t) &= \frac{\tilde{I}(t)}{2}\left(1-\cos(2\omega_d t)\right) + \frac{\tilde{Q}(t)}{2}\sin(2\omega_d t), \\ s_{\text{out}}(t)\cdot\cos(\omega_d t) &= -\frac{\tilde{I}(t)}{2}\sin(2\omega_d t) + \frac{\tilde{Q}(t)}{2}\left(1+\cos(2\omega_d t)\right). \end{aligned} \tag{3.21}$$

By low pass filtering that signal one gets rid of the faster oscillating terms and one ends up with the decomposed quadratures, i.e.,

$$\begin{aligned} \frac{\tilde{I}(t)}{2} &= s_{\text{out}}(t)\cdot\sin(\omega_d t), \\ \frac{\tilde{Q}(t)}{2} &= s_{\text{out}}(t)\cdot\cos(\omega_d t). \end{aligned} \tag{3.22}$$

If we remove the device under test then $s_{\text{out}}(t) = s(t)$ and one resembles the original quadratures $I(t)$ and $Q(t)$. These two quadratures are mathematically equivalent to external electric and magnetic driving fields. One can therefore do the same derivation as shown in Sec. 2.5 which leads to the following Hamiltonian

$$\hat{H} = \hbar\Delta_c\hat{a}^\dagger\hat{a} + \sum_j \frac{\hbar\Delta_s^j}{2}\hat{\sigma}_z^j + \sum_j \mathrm{i}\hbar g_j\left(\hat{\sigma}_-^j\hat{a}^\dagger - \hat{\sigma}_+^j\hat{a}\right) + \mathrm{i}\hbar I(t)\left(\hat{a}^\dagger - \hat{a}\right) + \hbar Q(t)\left(\hat{a}^\dagger + \hat{a}\right). \tag{3.23}$$

Die approbierte gedruckte Originalversion dieser Diplomarbeit ist an der TU Wien Bibliothek verfügbar
The approved original version of this thesis is available in print at TU Wien Bibliothek.
TU Bibliothek WIEN Your knowledge hub

As a consequence, we get a slightly different first Maxwell-Bloch equation,

$$\langle \dot{\hat{a}} \rangle = -\kappa \langle \hat{a} \rangle - \mathrm{i}\Delta_c \langle \hat{a} \rangle + \sum_j g_j \langle \hat{\sigma}_-^j \rangle + I(t) - \mathrm{i}Q(t), \tag{3.24}$$

the other Maxwell-Bloch equations stay unchanged. By comparing Eq. (3.24) with Eq. (2.79), one sees that the two quadratures correspond to the real and imaginary part of the original drive, i.e., $\eta = I(t) - \mathrm{i}Q(t)$.

After explaining how we can drive our cavity with arbitrary driving pulses, the next question which naturally occurs is how must the pulse look like to manipulate the spins in a certain way. This will be done in the next section.

3.6 Design of OCT Pulse

In our experiment we want to investigate the decay of an inverted spin ensemble. To be able to do so, we now think about what the driving pulse has to look like to invert as many spins as possible. After we choose our external magnetic field in such a way so that the spins are in resonance with the cavity, we know the transition frequency of the spins. A first guess for the pulse would then be a simple rectangular pulse whereby the drive frequency is chosen to be the cavity frequency. This pulse, however, would just invert spins that are in resonance with the cavity (which of course is the largest number of spins) but will not or just slightly affect the spins which are off-resonant due to inhomogeneous broadening. To invert those spins as well we continuously change the frequency of our driving pulse. But is this the pulse which we have to send in our cavity? No, it unfortunately is not. Such a pulse would be ideal only if the spins would get manipulated and not the cavity spin system as depicted in Fig. 3.10. Therefore, we conclude (or postulate) that the complex cavity amplitude $\langle \hat{a} \rangle$ has to look like the pulse mentioned above and from that we deduce how the driving term η has to look like. The starting point for the backward engineering are the aforementioned Maxwell-Bloch equations,

$$\begin{aligned}
\langle \dot{\hat{a}} \rangle &= -\mathrm{i}\Delta_c \langle \hat{a} \rangle + \sum_j g_j \langle \hat{\sigma}_-^j \rangle + \eta - \kappa \langle \hat{a} \rangle , \\
\langle \dot{\hat{\sigma}}_-^j \rangle &= -\mathrm{i}\Delta_s^j \langle \hat{\sigma}_-^j \rangle + g_j \langle \hat{a} \rangle \langle \hat{\sigma}_z^j \rangle - \left(\frac{\gamma_\parallel}{2} + \gamma_\perp \right) \langle \hat{\sigma}_-^j \rangle , \\
\langle \dot{\hat{\sigma}}_z^j \rangle &= -2g_j \left(\langle \hat{a}^\dagger \rangle \langle \hat{\sigma}_-^j \rangle + \langle \hat{a} \rangle \langle \hat{\sigma}_+^j \rangle \right) - \gamma_\parallel \left(1 + \langle \hat{\sigma}_z^j \rangle \right) .
\end{aligned} \tag{3.25}$$

As explained, we want to apply a chirp pulse which, with no loss of generality, should start with a frequency of $\omega_s - \frac{\omega_{\mathrm{span}}}{2}$ and after some fixed time (at the end of the pulse duration) it should have a frequency of $\omega_s + \frac{\omega_{\mathrm{span}}}{2}$. So our pulse should look like

$$\langle \hat{a} \rangle \propto \sin \left(\left[\omega_s + \omega_{\mathrm{span}} \left(\frac{t}{t_{\mathrm{span}}} - \frac{1}{2} \right) \right] t \right) , \tag{3.26}$$

Die approbierte gedruckte Originalversion dieser Diplomarbeit ist an der TU Wien Bibliothek verfügbar
The approved original version of this thesis is available in print at TU Wien Bibliothek.
TU Bibliothek Your knowledge hub WIEN

where the term $\left(\frac{t}{t_{\text{span}}} - \frac{1}{2}\right)$ maps the time $t \in [0, t_{\text{span}}]$ to $\left[-\frac{1}{2}, \frac{1}{2}\right]$ and ensures that the frequency is varied in the aforementioned interval.

By having a look at the system in its rotating frame as suggested in the supplementary material of Ref. [43], one sees that this pulse is suitable for our purpose. In the rotating frame the ith spin is detuned by $\delta_i = \omega_s^i - \omega_c$ where we assumed that the spins are in resonance and therefore the central frequency is equal to the cavity frequency ω_c. When we transform the pulse of Eq. (3.26) into the rotating frame we get

$$\langle \hat{a} \rangle_{\text{rot. frame}} \propto \sin\left[\omega_{\text{span}}\left(\frac{t}{t_{\text{span}}} - \frac{1}{2}\right)t\right]. \tag{3.27}$$

From that equation we see that the ith spin is in resonance when $\delta_i = \omega_{\text{span}}\left(\frac{t}{t_{\text{span}}} - \frac{1}{2}\right)$, i.e., at the time $t = \left(\frac{\delta_i}{\omega_{\text{span}}} + \frac{1}{2}\right)t_{\text{span}}$. By continuously changing this frequency, all spins are in resonance successively and therefore one can invert them well.

Besides the target of inverting the spins as good as possible we have to make sure that the whole system follows the modulation. Therefore, it is necessary to avoid large gradients of the chirp pulse which is achieved by multiplying the pulse with a Gaussian envelope. In the initial non-rotating frame, one gets

$$\langle \hat{a} \rangle \propto \exp\left(\frac{-x^2}{2\sigma^2}\right)\sin\left(\left[\omega_s + \omega_{\text{span}}\left(\frac{t}{t_{\text{span}}} - \frac{1}{2}\right)\right]t\right). \tag{3.28}$$

We choose t_{span} to be the FWHM of the Gaussian envelope, therefore the variance σ^2 can be calculated with $\sigma = t_{\text{span}}/(2 \cdot \sqrt{2\ln(2)})$. Applying the addition theorem for a sine wave we get

$$\begin{aligned}
&\exp\left(\frac{-x^2}{2\sigma^2}\right)\sin\left(\left[\omega_s + \omega_{\text{span}}\left(\frac{t}{t_{\text{span}}} - \frac{1}{2}\right)\right]t\right) \\
&\quad = \exp\left(\frac{-x^2}{2\sigma^2}\right)\cos\left(\omega_{\text{span}}\left(\frac{t}{t_{\text{span}}} - \frac{1}{2}\right)t\right)\sin(\omega_s t) \\
&\quad + \exp\left(\frac{-x^2}{2\sigma^2}\right)\sin\left(\omega_{\text{span}}\left(\frac{t}{t_{\text{span}}} - \frac{1}{2}\right)t\right)\cos(\omega_s t).
\end{aligned} \tag{3.29}$$

By comparing Eq. (3.29) with Eq. (3.19) we see that we can identify the first part with $I(t)$ and the second with $Q(t)$. Please note that, as stated above, these are not the two quadratures of the driving pulse we send into our cavity, we want that our spin ensemble interact with such a pulse. Therefore, as can be seen in Fig. 3.10, we want our cavity amplitude $\langle \hat{a} \rangle$ to look like these quadratures. By making this ansatz, we have a function for our cavity amplitude $\langle \hat{a} \rangle$, i.e., $\langle \hat{a}(t) \rangle = I(t) - \mathrm{i}Q(t)$. But to be able to calculate the cavity drive η from the first Maxwell-Bloch equation, we have to know the $\langle \hat{\sigma}_-^j \rangle$ components. Since the second equation is coupled with

Die approbierte gedruckte Originalversion dieser Diplomarbeit ist an der TU Wien Bibliothek verfügbar
The approved original version of this thesis is available in print at TU Wien Bibliothek.
TU Bibliothek Your knowledge hub WIEN

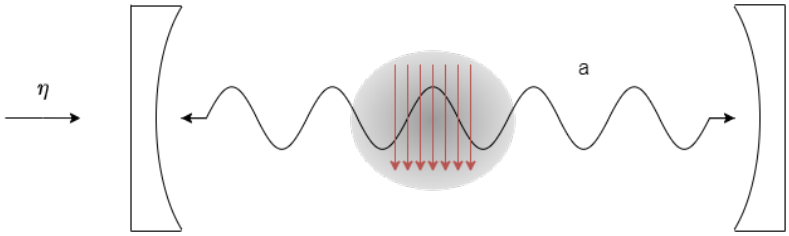

Figure 3.10: To invert the spin ensemble as good as possible, we want that it interacts with our designed pulse. Therefore, we make the ansatz $\langle \hat{a} \rangle = I(t) - \mathrm{i}Q(t)$ from which the corresponding driving pulse η can be calculated from the Maxwell-Bloch equations.

the third equation, we solve the system of differential equations simultaneously and get an expression for the $\langle \hat{\sigma}_-^j \rangle$ values. By plugging that solution into the rearranged first Maxwell-Bloch equation, i.e.,

$$\eta = \langle \dot{\hat{a}} \rangle + \mathrm{i}\Delta_c \langle \hat{a} \rangle + \kappa \langle \hat{a} \rangle - \sum_j g_j \langle \hat{\sigma}_-^j \rangle , \tag{3.30}$$

one is able to calculate the corresponding cavity drive pulse η which real and imaginary parts are the two quadratures $\tilde{I}(t)$ and $\tilde{Q}(t)$ which we are looking for. To be able to calculate that corresponding drive pulse we first, however, have to determine the unknown parameter g_j. Furthermore, we have to think how we can solve the Maxwell-Bloch equations since it is impossible to solve them for every spin. This will be shown in the next section.

3.7 Simulation of the System

As derived in Ch. 2, our open quantum system can be described by the Maxwell-Bloch equations. The parameters used there are (apart from the cavity decay rate κ) unknown.

As mentioned before, the transition frequency of the spins is not the same, it is inhomogeneously broadened. This broadening can be modeled with a q-Gaussian function [18, 19]

$$\rho(\omega) = \left(1 - (1-q)\frac{(\omega - \omega_0)^2}{\delta^2}\right)^{\frac{1}{1-q}} , \tag{3.31}$$

with

$$\delta = \frac{\gamma}{2 \cdot \sqrt{\frac{2^q - 2}{2q - 2}}}, \tag{3.32}$$

Die approbierte gedruckte Originalversion dieser Diplomarbeit ist an der TU Wien Bibliothek verfügbar
The approved original version of this thesis is available in print at TU Wien Bibliothek.
TU Bibliothek Your knowledge hub WIEN

where γ is the full width at half maximum (FWHM).

We further take into account that the NV centers are split by a hyperfine splitting of 2.3 MHz. We end up with a spin distribution which we then can normalize and obtain a probability density function. Besides the unknown parameters, it is clear that we cannot simulate a system with 10^{12} spins because it is unfeasible to solve $2 \cdot 10^{12} + 1$ coupled differential equations. To overcome this issue and still be able to simulate our system correctly, we discretize the probability density function, i.e.,

$$\rho(\omega) = \frac{1}{g_{coll}^2} \sum_{k=1}^{N} g_k^2 \delta(\omega - \omega_k), \tag{3.33}$$

and then calculate the corresponding coupling strengths g_k. To do so, we approximate our probability function with rectangular bars with width $\Delta\omega$ and get

$$\rho(\omega_k)\Delta\omega \approx \int_{\omega_k - \frac{\Delta\omega}{2}}^{\omega_k + \frac{\Delta\omega}{2}} \rho(\omega)\mathrm{d}\omega = \int_{\omega_k - \frac{\Delta\omega}{2}}^{\omega_k + \frac{\Delta\omega}{2}} \frac{1}{g_{coll}^2} \sum_{k=1}^{N} g_k^2 \delta(\omega - \omega_k)\mathrm{d}\omega = \frac{g_k^2}{g_{coll}^2}. \tag{3.34}$$

With $\sum_k g_k^2 = g_{coll}^2$ we obtain

$$\Delta\omega = \frac{1}{\sum_{k=1}^{N} \rho(\omega_k)}, \tag{3.35}$$

and finally we find [34]

$$g_k = g_{coll} \sqrt{\frac{\rho(\omega_k)}{\sum_{k=1}^{N} \rho(\omega_k)}}. \tag{3.36}$$

For that derivation we assumed equally distributed spins where the spins which are closer to the resonant frequency ω_c are coupled stronger. This is mathematically the same as assuming a fixed coupling but the closer we get to the resonant frequency the more spins we find as it is the case in nature. In other words it does not make any difference if we change the number of spins in a given interval and let the coupling be the same or vice versa.

By fitting the cavity amplitude obtained from the Maxwell-Bloch equations to the results obtained with the VNA, the unknown parameters are obtained. Since one cannot measure time resolved with the VNA we take the Maxwell-Bloch equations and have a look on the steady state, i.e.,

$$\begin{aligned}
0 &= -\mathrm{i}\Delta_c \langle \hat{a} \rangle + \sum_j g_j \langle \hat{\sigma}_-^j \rangle + \eta - \kappa \langle \hat{a} \rangle, \\
0 &= -\mathrm{i}\Delta_s^j \langle \hat{\sigma}_-^j \rangle + g_j \langle \hat{a} \rangle \langle \hat{\sigma}_z^j \rangle - \left(\frac{\gamma_\parallel}{2} + \gamma_\perp \right) \langle \hat{\sigma}_-^j \rangle, \\
0 &= -2g_j \left(\langle \hat{a}^\dagger \rangle \langle \hat{\sigma}_-^j \rangle + \langle \hat{a} \rangle \langle \hat{\sigma}_+^j \rangle \right) - \gamma_\parallel \left(1 + \langle \hat{\sigma}_z^j \rangle \right).
\end{aligned} \tag{3.37}$$

Die approbierte gedruckte Originalversion dieser Diplomarbeit ist an der TU Wien Bibliothek verfügbar
The approved original version of this thesis is available in print at TU Wien Bibliothek.
TU Bibliothek WIEN Your knowledge hub

We now want to find an expression for the steady state of the cavity amplitude of a weakly driven cavity. Since we then are in the linear regime, we can apply the Holstein-Primakoff approximation which leads to two coupled harmonic oscillators. Therefore, we assume that all spins are in the ground state, i.e., $\langle \hat{\sigma}_z^j \rangle = -1$ for all j. Then, using the second equation we find

$$\left\langle \hat{\sigma}_-^j \right\rangle = -\frac{g_j \langle \hat{a} \rangle}{\mathrm{i}\Delta_s^j + \left(\frac{\gamma_\parallel}{2} + \gamma_\perp\right)}, \tag{3.38}$$

which when inserted in equation one gives the following expression

$$\langle \hat{a} \rangle = \frac{\eta}{\mathrm{i}\Delta_c + \kappa + \sum_j \frac{g_j^2}{\mathrm{i}\Delta_s^j + \left(\frac{\gamma_\parallel}{2} + \gamma_\perp\right)}}, \tag{3.39}$$

for the cavity amplitude in the steady state.

Please note that with this ansatz for the cavity amplitude we exclude a correct modeling of phenomena like spin bleaching, where the steady state value of $\langle \hat{\sigma}_z^j \rangle$ would differ from -1. Therefore, this ansatz is only valid for a low drive power, i.e., low η values.

This cavity amplitude function can be fitted to the measured cavity amplitude which is shown in Fig. 3.11. From that the unknown parameters are obtained. For now (see Sec. 3.1) we know the cavity parameters κ and ω_c i.e. $\Delta_c = \omega_c - \omega_d$. We furthermore assume that the q value of the distribution is $q = 1.40$ since the sample we use is very similar to that used in Refs. [18, 19] and therefore assume the q value mentioned therein. From fitting we obtain the width of that q-Gaussian distribution ($\gamma = 8.7204 \cdot 2\pi\,\mathrm{MHz}$), the collective coupling g_{coll} ($g_{coll} = 4.3941 \cdot 2\pi\,\mathrm{MHz}$) and a possible overall frequency offset between the spin distribution and the cavity ($\Delta_{sc} = 0\,\mathrm{MHz}$). As can be seen the fit is in quite good agreement. Please note that we do not fit the parameters $\gamma_\parallel = \frac{1}{T_1}$ and $\gamma_\perp = \frac{1}{T_2}$. From Ref. [36] we know that T_1 is in the range of $T_1 \approx 150\,\mathrm{s}$ and therefore its reciprocal value is negligible small. We further know from other measurements we carried out that T_2 is in the range of few hundred ns to tens of µs, we assume $\gamma_\perp = 20 \cdot 2\pi\,\mathrm{kHz}$. However, the value of $\gamma_\perp$ is not too important since the corresponding term of the second Maxwell-Bloch equation is always much smaller than the term which is proportional to Δ_s^j and covers the inhomogeneous broadening of the spin ensemble. The corresponding width of the q-Gaussian with which we model this broadening namely is $\gamma = 8.7204 \cdot 2\pi\,\mathrm{MHz}$ and therefore larger than $\gamma_\perp$.

After explaining our experimental measurement scheme, the design of the optimal spin inversion pulse and how we can simulate the system, we now want to present our experimental results.

Die approbierte gedruckte Originalversion dieser Diplomarbeit ist an der TU Wien Bibliothek verfügbar
The approved original version of this thesis is available in print at TU Wien Bibliothek.
TU Bibliothek Your knowledge hub WIEN

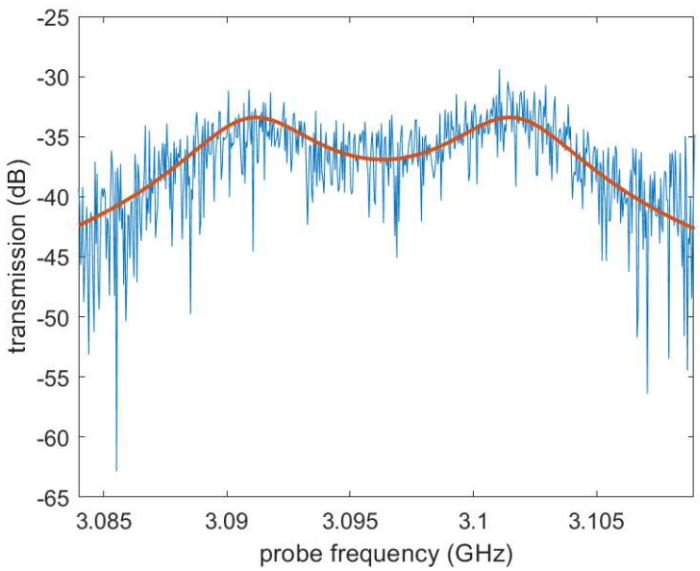

Figure 3.11: By fitting Eq. (3.39) to the measured cavity transmission one gets the parameters with which our experiment can be modeled. The values obtained from this fit are $g_{coll} = 4.3941 \cdot 2\pi\,\mathrm{MHz}$, $\gamma = 8.7204 \cdot 2\pi\,\mathrm{MHz}$ (width of the q-Gaussian) and $\Delta_{sc} = 0\,\mathrm{MHz}$ (a possible overall frequency offset between the spin distribution and the cavity). Please note that we assume that the q value of the distribution is $q = 1.40$ since the sample we use is very similar to that used in Refs. [18, 19] and therefore assume the q value mentioned therein.

Die approbierte gedruckte Originalversion dieser Diplomarbeit ist an der TU Wien Bibliothek verfügbar
The approved original version of this thesis is available in print at TU Wien Bibliothek.
TU Bibliothek Your knowledge hub WIEN

4 Experiment

As mentioned in the previous section, we are investigating an inverted spin ensemble. Since we are working in a cryogenic environment, we can be sure that after waiting some time all spins relax into the ground state no matter in which state they are before. Then we are able to drive our cavity with the aforementioned chirp pulse by which the spins will get inverted. The design and how one can calculate it is mentioned in Sec. 3.6, with the parameters we obtained by fitting the VNA trace (as shown in Sec. 3.7) we are able to calculate it. The central frequency is the cavity frequency, we choose the span to be $20 \cdot 2\pi$ MHz. We calculate 801 data points which lead to a pulse duration of 400 ns since our AWGs sampling rate is 2e9 points per second. The obtained pulse is depicted in Fig. 4.1 where the first quadrature $I(t)$ is shown in blue and the second $Q(t)$ in red, respectively.

Since we do not know how strong the pulse has to be, i.e., what the right amplitude is, we perform an amplitude scan. This is done by mixing the two quadratures onto the carrier signal and then changing the attenuation of it. Afterwards it is send into the fridge with the cavity. The output is then again demodulated and the obtained quadratures get measured with a data acquisition card. After each run we wait until the spins are in the ground state again. When all spins are in the ground state we expect a transmission as shown in Fig. 3.11. However, when the spins are excited the inverted spin ensemble decays superradiantly on the ns timescale which gets stopped due to spin dephasing before all spins are in the ground state again, the transmission therefore looks like that of an empty cavity. From there the spins slowly relax with a rate $\gamma_{\parallel} = 1/T_1$ (which is far slower than before) into the ground state. When (nearly) all excitations are gone we enter the low excitation regime again and observe the aforementioned transmission.

The obtained attenuation scan result is depicted in Fig. 4.2. One can see the cavity drive at the beginning which gets stronger with every scan and after the OCT pulse is over one can distinguish two regions. Either the driving was too weak so (most of) the spins stay in the ground state and therefore the cavity amplitude is (nearly) zero, this happened for attenuations below roughly 11 dB. If the pulse, however, has a certain strength then the spins get driven in direction of the north pole onto the Bloch sphere and decay after some time again. This decay leads to emitted photons which further lead to a non-zero signal. Please note that despite the general convention we define (for the whole thesis) that the south pole of the Bloch sphere is the ground state, the north pole corresponds to the excited state. As can be seen in the figure, the optimal pump attenuations are 0 and 6 dB. After

Die approbierte gedruckte Originalversion dieser Diplomarbeit ist an der TU Wien Bibliothek verfügbar
The approved original version of this thesis is available in print at TU Wien Bibliothek.
TU Bibliothek Your knowledge hub WIEN

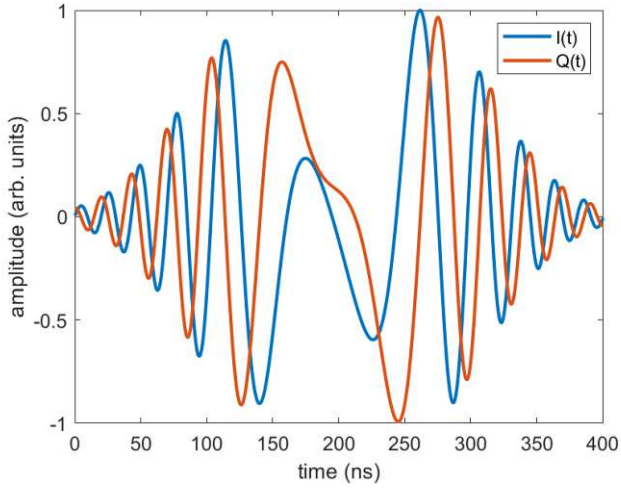

Figure 4.1: The two quadratures of the calculated optimal control pulse as described in Sec. 3.6 are shown in blue ($I(t)$) and red ($Q(t)$), respectively.

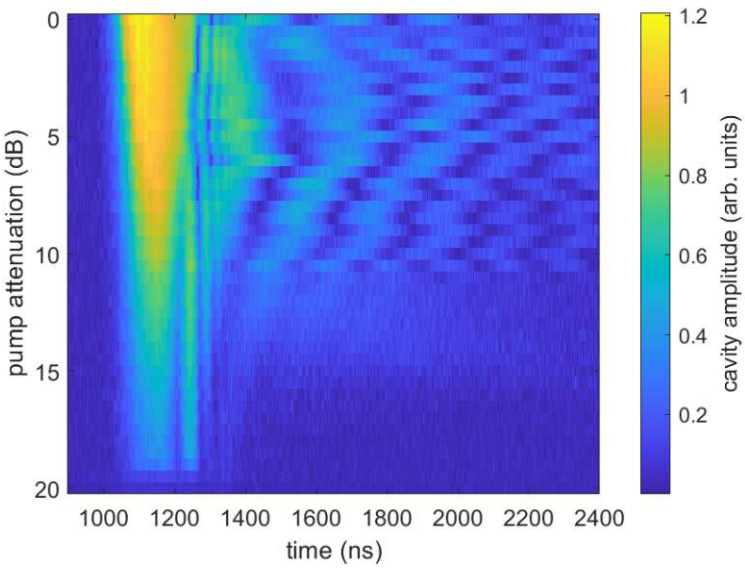

Figure 4.2: In order to find the optimal attenuation of the optimal control pulse we scan its attenuation. The cavity amplitude is shown as a function of attenuation and time. For an attenuation of 0 and 6 dB it takes the longest time until we see photons again from which we can deduce that after such a pulse the spins are inverted the best, as many as possible point to the north pole of the Bloch sphere. We are able to reproduce that picture with numerical simulations from which we have access to the $\langle \hat{\sigma}_z \rangle$ values of the spin system, we get $\sum_j \langle \hat{\sigma}_z^j \rangle = 0.72$.

Die approbierte gedruckte Originalversion dieser Diplomarbeit ist an der TU Wien Bibliothek verfügbar
The approved original version of this thesis is available in print at TU Wien Bibliothek.
TU Bibliothek Your knowledge hub WIEN

applying a pulse with that strength, it takes the longest time until we see photons in the cavity again which means that the spins are stable over a longer time. After such a pulse they are inverted the best and therefore this sequence corresponds to a (best achievable) "π" pulse. If we increase the power even further, we overrotate the spins and therefore they are closer to the equator of the Bloch sphere again which lead to a faster decay. Furthermore, we are able to reproduce that picture with numerical simulations from which we have access to the $\langle\hat{\sigma}_z\rangle$ values of the spin system, we get $\sum_j\langle\hat{\sigma}_z^j\rangle = 0.72$. Before that chirp pulse we used a pulse based on the Fourier coefficients mentioned in Ref. [44] with which we were able to get a spin inversion of roughly $\sum_j\langle\hat{\sigma}_z^j\rangle = 0.65$.

After inverting the spins we now want to stabilize them. This can be done in two different ways which will be explained in the following sections.

4.1 Constant Spin Detuning - Detection of Thermal Microwave Background

In order to stabilize the spins in that inverted position we now change the magnetic field very quickly so that the spins are detuned from the cavity. By doing so, they stay inverted because the spins do not have any mode left in which they can decay. During that, the spins precess and the $\langle\hat{\sigma}_x\rangle$ and $\langle\hat{\sigma}_y\rangle$ values cancel each other to zero as schematically shown in Fig. 4.3. As a consequence, if we wait long enough then there is only a $\langle\hat{\sigma}_z\rangle$ component left.

The fast changing magnetic field is realized with an additional small coil as shown in Fig. 4.4. By applying a current of 1 A a corresponding magnetic field which adds up to the external field caused by the 3 Helmholtz coils is produced. We choose the field of the 3 Helmholtz coils such that all 4 subensembles are in resonance when the small loop and the Helmholtz coils are switched on, i.e., we detune the spins by switching off the small loop instantaneously. This switching can be done in roughly 250 ns by which we can reach a spin detuning of approximately 15 MHz which is enough to prevent the spins from decaying (at least for some time). The corresponding traces of the NV ensembles in resonance (red) and detuned (yellow) can be seen in Fig. 4.5 where for comparison the trace of the empty cavity is depicted in blue as well.

After some time we turn the current on again and by doing so we bring the spins in resonance again. Quite surprisingly, we see a photon burst coming out of the cavity which means that the spins decayed by themselves. This is at a first sight counterintuitive because the idea of detuning the spins was exactly the opposite: due to the spin precision the $\langle\hat{\sigma}_x\rangle$ and $\langle\hat{\sigma}_y\rangle$ component should be zero and only a $\langle\hat{\sigma}_z\rangle$ component should be left and as a consequence they should be stable. However, as

Die approbierte gedruckte Originalversion dieser Diplomarbeit ist an der TU Wien Bibliothek verfügbar
The approved original version of this thesis is available in print at TU Wien Bibliothek.
TU Bibliothek Your knowledge hub WIEN

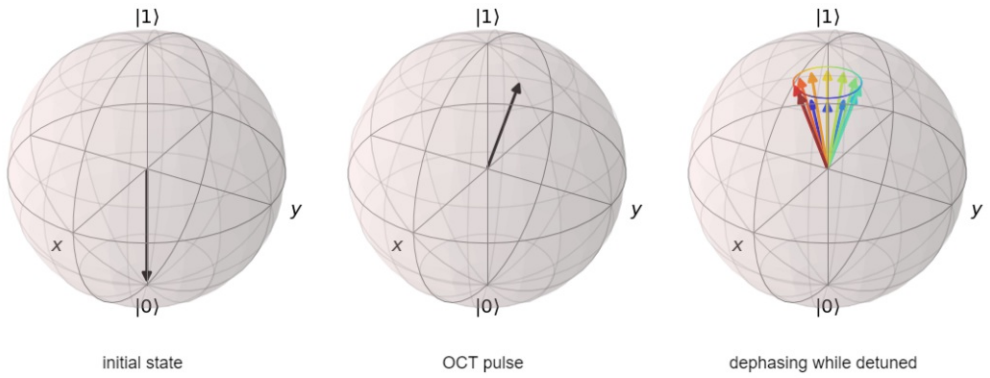

Figure 4.3: After driving the initial spin states with an OCT pulse, they are inverted but still have non-zero $\langle\hat{\sigma}_x\rangle$ and $\langle\hat{\sigma}_y\rangle$ components. To get rid of them, we now instantaneously change the magnetic field by which the spins get detuned from the cavity. By doing so, they do not have a decay channel to decay into any more. During that time the spins precise and after some time the $\langle\hat{\sigma}_x\rangle$ and $\langle\hat{\sigma}_y\rangle$ values cancel each other to zero.

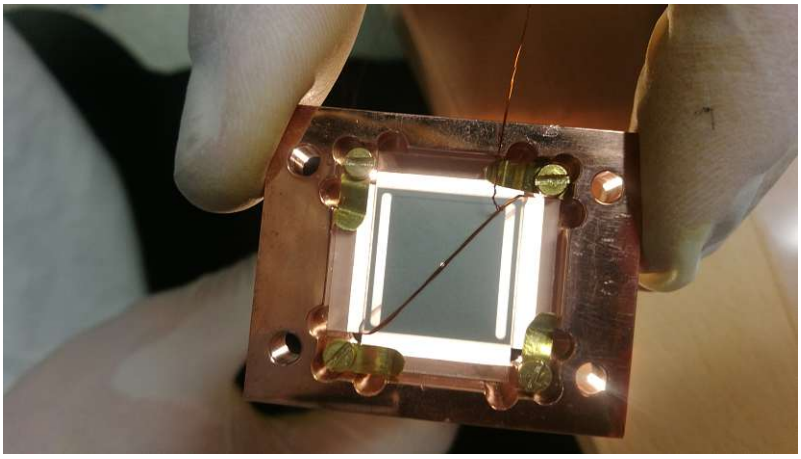

Figure 4.4: Additional small coil with which we can change the magnetic field and as a consequence can detune the spins fast from the cavity.

Die approbierte gedruckte Originalversion dieser Diplomarbeit ist an der TU Wien Bibliothek verfügbar
The approved original version of this thesis is available in print at TU Wien Bibliothek.
TU Bibliothek Your knowledge hub WIEN

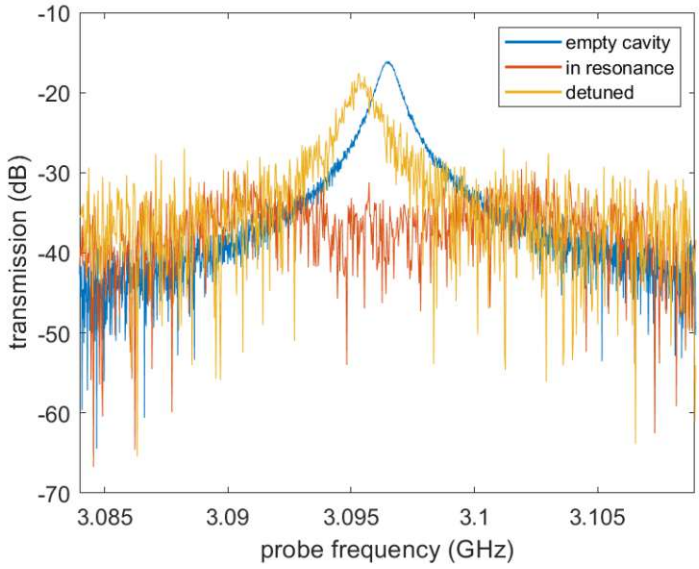

Figure 4.5: Comparison of the transmission of the pure cavity (blue), when all NV centers are in resonance (red) and when the spins are detuned from the cavity (yellow). By switching off the small loop one can detune the spins by roughly 15 MHz.

shown in Ref. [22] in the framework of cavity QED one can define the cooperativity

$$C = \sum_j C_j = \sum_j \frac{g_j^2 \left(\frac{\gamma_\parallel}{2} + \gamma_\perp\right)}{\kappa \left[\left(\frac{\gamma_\parallel}{2} + \gamma_\perp\right)^2 + \Delta_s^{j\,2}\right]}, \tag{4.1}$$

where the total cooperativity C is the sum over the corresponding single spin cooperativities C_j and can be understood as a stability parameter. The parameter Δ_s^j denotes a possible detuning of the jth spin from the cavity. A very similar equation can be found in Ref. [45]. For $C > 1$ the system is inherently instable and stable for values smaller than 1. By plugging in the numbers we obtained in Sec. 3.1 and 3.7, we get a value of roughly 11, i.e., we have an instable system which explains the self decay. Since Δ_s^j denotes the detuning of the spins from the cavity one can, according to Eq. (4.1), reduce the cooperativity by detuning the spins. At some point the cooperativity parameter is smaller than 1 and therefore the system gets stable.

Now there are two questions which naturally occur: when do we have to detune the spins, i.e., at what time after the OCT pulse should we switch off the loop and how long can we stay detuned and still see a photon burst after we tune back. For the first question one would expect a switching between about 200 ns and 400 ns after the start of the pump pulse (which take place at $t = 1000$ ns) because, as can

Die approbierte gedruckte Originalversion dieser Diplomarbeit ist an der TU Wien Bibliothek verfügbar
The approved original version of this thesis is available in print at TU Wien Bibliothek.
TU Bibliothek Your knowledge hub WIEN

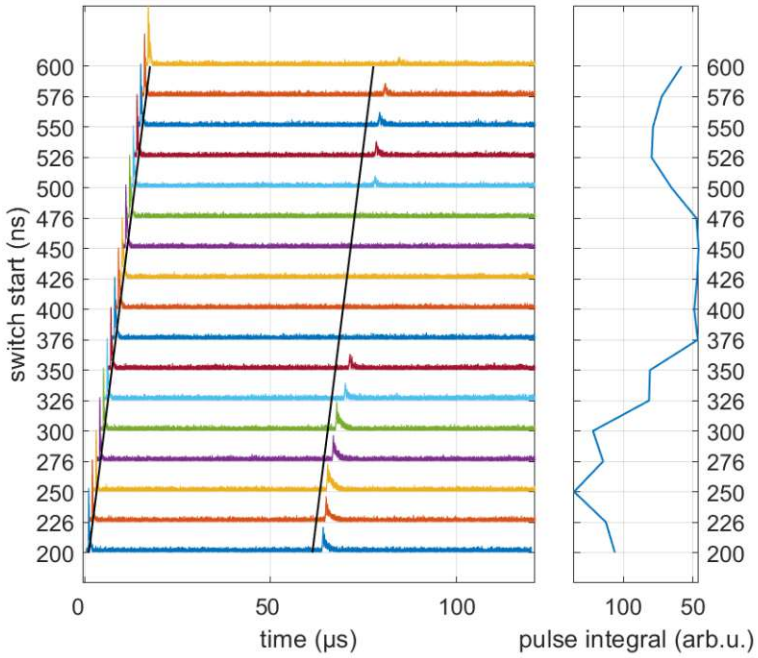

Figure 4.6: The cavity amplitude is shown for different switch start times. Shortly after bringing the spins back in resonance with the cavity (which is depicted as black line) one sees a photon burst coming out. As can be seen from the integral of the amplitude, the burst is the largest for a starting time of $250\,\mathrm{ns}$. Please note that the time on the x axis should be understand as a relative scale since we shift each run a little bit to better compare the obtained results.

be seen in Fig. 4.2, there the number of photons in the cavity is minimal so the whole energy is in the spin system. And in fact, as can be seen in Fig. 4.6, the optimal start time for detuning the spins is 250 ns. For that time the integral of the photon burst coming out of the cavity is maximal and we can deduce that during the time of detuning the number of the inverted spins have to be maximal as well.

A answer for the second question would be that the spins while being detuned cannot decay into the cavity mode and therefore can only decay by relaxation processes going on in the crystal. This process is the aforementioned spin phonon interaction which happens with a rate of $\gamma_{\parallel} = 1/T_1$. Since for our NV centers $T_1 \approx 150\,\mathrm{s}$ we expect the spins to stay inverted for that time scale. But as can be seen in Fig. 4.7, the timescale is very different. We can hold the spins inverted for roughly 30 ms, afterwards we do not see any photon burst coming out of the cavity any more. After these two scans there are two further questions which occur:

Die approbierte gedruckte Originalversion dieser Diplomarbeit ist an der TU Wien Bibliothek verfügbar
The approved original version of this thesis is available in print at TU Wien Bibliothek.
TU Bibliothek Your knowledge hub WIEN

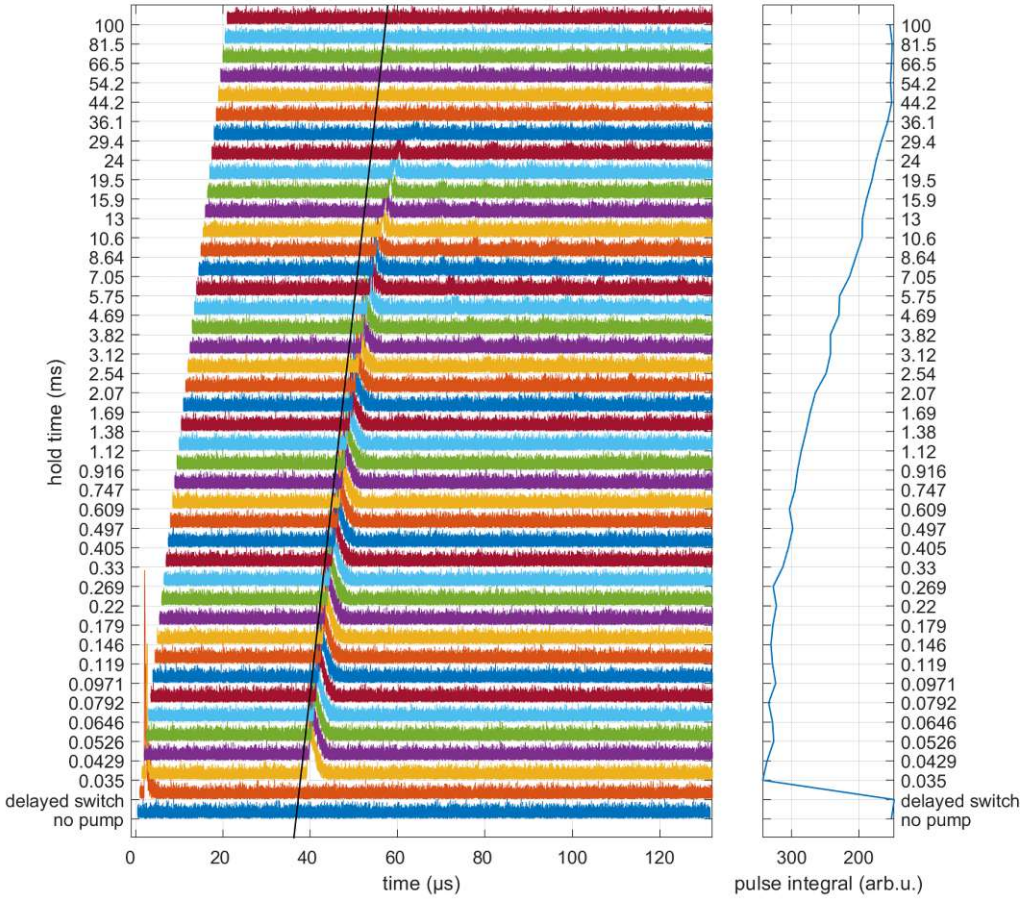

Figure 4.7: Cavity amplitude for different detuning times. After tuning the spins back (shown as black line) we see a photon burst coming out which decreases and then completely vanishes for holding times longer than approximatley $30\,\mathrm{ms}$. One would expect to observe a photon burst coming out for holding times in the range of T_1 since the expected decaying rate during detuning is $\gamma_{\parallel} = 1/T_1$. But as can be seen clearly the decaying happens much faster, the reason for that will be explored in the following. Please note that the time on the x axis should be understand as a relative scale since the time zeros are different for different runs. We further shift each run a little bit to better compare the obtained results.

Die approbierte gedruckte Originalversion dieser Diplomarbeit ist an der TU Wien Bibliothek verfügbar
The approved original version of this thesis is available in print at TU Wien Bibliothek.
TU Bibliothek Your knowledge hub WIEN

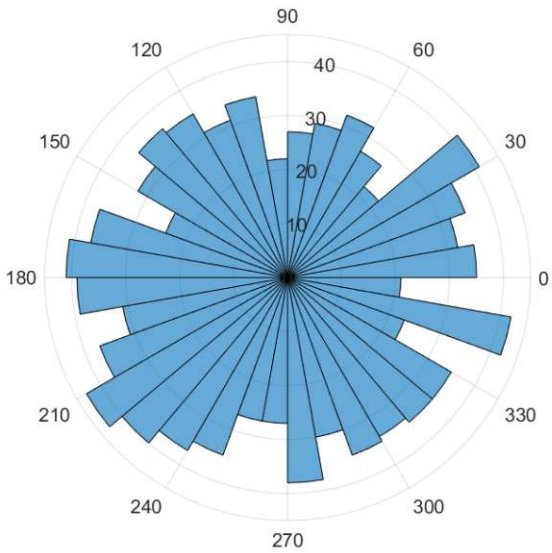

Figure 4.8: Phases between the two quadratures $I(t)$ and $Q(t)$ of the photon burst coming out of the cavity after bringing the spins back in resonance (n = 1181). As can be seen clearly, the phase between the quadratures is random from which we conclude that the decay process is not triggered by external photon sources.

- Are the spins really decaying by themselves or triggered by something, e.g. some noise?
- Why are the hold times so much shorter than expected?

To investigate the decay of the spins, we repeat the measurement several times and have a look at the phase between the two quadratures of the photon burst. Therefore, we choose a fix start time for detuning the spins (250 ns as obtained from the scan before) and fix the hold time as well (we choose it to be 70 µs). To get the phase between the two quadratures we fit the function

$$s(t) = A\mathrm{e}^{-\gamma t}\mathrm{e}^{\mathrm{i}(\omega t+\phi)} \tag{4.2}$$

to the acquired data where we also take into account that the amplitude A of the signal decreases exponentially over time. The obtained phases from 1181 runs between the two quadratures $I(t)$ and $Q(t)$ can be seen in Fig. 4.8 where the phase ϕ is plotted in a polar histogram with 36 bins. As can be clearly seen, the phase between the quadratures is random from which we conclude that the decay process is not triggered by external photon sources.

However, we unfortunately cannot say that it is not triggered by the thermal photon bath. To investigate that and gain better knowledge about the self decay,

Die approbierte gedruckte Originalversion dieser Diplomarbeit ist an der TU Wien Bibliothek verfügbar
The approved original version of this thesis is available in print at TU Wien Bibliothek.
TU Bibliothek Your knowledge hub WIEN

we added a relay switch on the still stage as can be seen in Fig. 3.8(a). This switch allows us to physically separate the microwave downline and as a consequence, no photons get to the lowest stage any more. To avoid thermal photons entering the lowest stage over the upline, we use two isolators, two attenuators and a low noise amplifier as shown in Fig. 3.8(a) as well. By keeping the relay switch open all the time and just close it shortly (for 2 ms) for the spin inversion pulse, one can reduce the cavity mode temperature from roughly 300 K to approximately 1 K which corresponds to a thermal photon number reduction from $\bar{n} \approx 2000$ to $\bar{n} \approx 6$ with

$$\bar{n}(\omega) = \frac{1}{\mathrm{e}^{\hbar\omega/k_B T} - 1}. \tag{4.3}$$

But before doing so, we want to mention an additional observation.

During taking the statistical runs we observed that the time it took the spins to decay after we tuned them back in resonance differs from run to run. The time at which the amplitude maximum coming out of the cavity occurred is shown in Fig. 4.9(a) for the same 1181 runs. As can be clearly seen, the decay is not normal distributed but slightly asymmetric and shifted to the left side. As explained and stated in Ref. [46], the probability that such a superradiant decay of spins happens at a given time can be calculated with

$$P(t_D) = N^2 \Gamma \mathrm{e}^{-N\Gamma t_D} \exp\left[\mathrm{e}^{-N\Gamma t_D}\right], \tag{4.4}$$

where N is the number of spins and Γ the transition matrix element, i.e., the rate with which the spins decay. This decay is caused by quantum fluctuations. The average delay $\langle t_D \rangle$ and the standard deviation Δt_D are given by

$$\langle t_D \rangle = \frac{1}{\Gamma N} \ln(N) \qquad \Delta t_D = \frac{1.3}{\Gamma N}. \tag{4.5}$$

The fit of that function can be seen in Fig. 4.9(a) as well. As stated in Ref. [47], the average delay and the standard deviation with thermal photons $\bar{n}(\omega)$ read like

$$\langle t_D \rangle = \frac{1}{\Gamma N} \ln\left(\frac{N}{1+\bar{n}}\right) \qquad \Delta t_D = \frac{1.3}{\Gamma N} \frac{1}{\sqrt{1+\bar{n}}}. \tag{4.6}$$

with $\bar{n}(\omega) = \frac{1}{\mathrm{e}^{\hbar\omega/k_B T} - 1}$.

This function is a measurement for temperature, the more thermal photons are in the cavity the narrower the distribution gets and the earlier the decay happens. Please note that since we fitted Eq. (4.4) which does not take thermal photons into account we included a time offset as fit parameter as well. This is also necessary, since the switching on of the current through the loop does not happen instantaneously as assumed in Ref. [46] for the derivation of Eq. (4.4) but takes $\approx 5\,\mu$s. We now do the same measurement with open relay and expect to get a broader distribution. And

Die approbierte gedruckte Originalversion dieser Diplomarbeit ist an der TU Wien Bibliothek verfügbar
The approved original version of this thesis is available in print at TU Wien Bibliothek.
TU Bibliothek Your knowledge hub WIEN

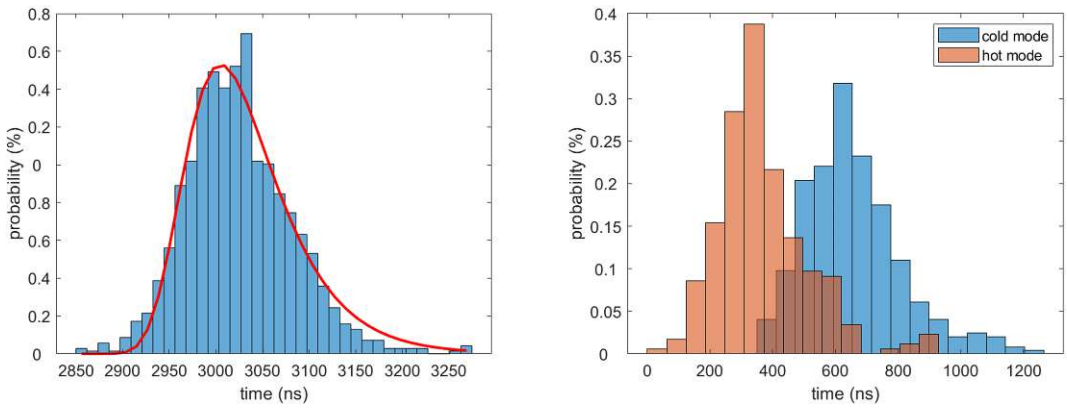

(a) (b)

Figure 4.9: Time it takes the photon burst coming out of the cavity after bringing the inverted spin ensemble back in resonance. In Fig. (a) the obtained results from the spin decay into the hot cavity mode (i.e. closed relay switch) obtained from the same 1181 runs are shown, the fitted probability density function (Eq. (4.4)) is depicted in Fig. (a) in red as well. Since this equation does not take thermal photons into account, we included a time offset as fit parameter as well. In Fig. (b) the statistics obtained with a closed relay (i.e. hotter cavity mode, 279 runs) and an open relay (i.e. colder cavity mode, 397 runs) are shown. One clearly sees that the decay happens earlier the more thermal photons in the cavity are. Unfortunately, we cannot clearly see a difference in their widths but this is due to the less run number. By taking better statistics, a difference in their widths should be getting visible. Please note that the number of runs of the decay into the hotter mode is lower compared to Fig. (a). This is because the other measurement took place with a slightly different setup and therefore is not direct comparable. The histograms are normalized in such a way so that the integral, i.e. the sum of the areas of the bars, is 1.

Die approbierte gedruckte Originalversion dieser Diplomarbeit ist an der TU Wien Bibliothek verfügbar
The approved original version of this thesis is available in print at TU Wien Bibliothek.
TU Bibliothek Your knowledge hub WIEN

indeed, as shown in Fig. 4.9(b), when cutting the connection between the semi-rigid SMA cables in the downline by open the relay, it takes the spin ensemble longer to decay in comparison to the decay into the hotter mode. Please note that because of the lower number of runs (n(hot mode) = 279, n(cold mode) = 397) one cannot clearly see a difference of their widths. By taking better statistics, a difference in their widths should be getting visible. The run number of the decay into the hotter mode is in Fig. 4.9(b) compared to (a) lower as well because we had to take new runs since the other measurement took place with a slightly different setup and therefore is not directly comparable. In other words, one can use this experimental setup to detect microwave photons at low temperatures which is only limited by blackbody radiation. Unfortunately, the relaxation of the spin ensemble between the runs takes a few minutes and therefore it takes quite a while to gather enough data for getting good statistical results. Furthermore, this detector is useful to characterize the thermal microwave background and/or microwave pulses which can trigger the spin decay as well. To can be sure that the spin decay is triggered by the pulse and not due to self decay, one has a quite narrow time window of $\approx 3\,\mu\text{s}$ after tuning the spins back in which one has to send in the pulse.

After we see that our relay switch works we want to investigate if the colder cavity mode leads to a longer hold time. This could be possible since the spin decay gets enhanced by thermal photons. If one does not neglect the Liouvillian terms containing thermal photons as done in Sec. 2.6, the third Maxwell-Bloch equation reads like

$$\langle \dot{\hat{\sigma}}_z^j \rangle = -\gamma_\parallel \left(1 + 2\bar{n}\right) \left\langle \hat{\sigma}_z^j \right\rangle - \gamma_\parallel - 2g_j \left(\left\langle \hat{a}^\dagger \right\rangle \left\langle \hat{\sigma}_-^j \right\rangle + \langle \hat{a} \rangle \left\langle \hat{\sigma}_+^j \right\rangle \right). \tag{4.7}$$

By neglecting the term proportional to g_j (which is justified during the detuning of the spins) one can solve the differential equation and get

$$\left\langle \hat{\sigma}_z^j(t) \right\rangle = \frac{1}{2\bar{n}+1} \left[\mathrm{e}^{-\gamma_\parallel (2\bar{n}+1)t} (2\bar{n} + 2 - 1) \right]. \tag{4.8}$$

Thus, thermal photons lead to an enhanced spin decay.

With our numerical simulations we have seen that this spin decay always happen no matter if the spins are in resonance or detuned. Therefore, by using the relay switch, we might be able to increase the time we can stabilize the spins in its inverted state. For that measurement the relay switch is always open, i.e., the semi-rigid SMA cables in the downline are physically separated and only for sending in the inversion pulse we close the relay switch as short as possible. The shortest time we are able to achieve is a closed time of roughly 2 ms. The results of the hold time scan with the colder cavity mode are shown in Fig. 4.10. Unfortunately, we do not see any difference in comparison to before, after a detuning time of approximately 30 ms we cannot observe a photon burst coming out of the cavity any more. By plugging in numbers in Eq. (4.8) we can calculate the expected decaying rate. Without thermal

Die approbierte gedruckte Originalversion dieser Diplomarbeit ist an der TU Wien Bibliothek verfügbar
The approved original version of this thesis is available in print at TU Wien Bibliothek.
TU Bibliothek Your knowledge hub WIEN

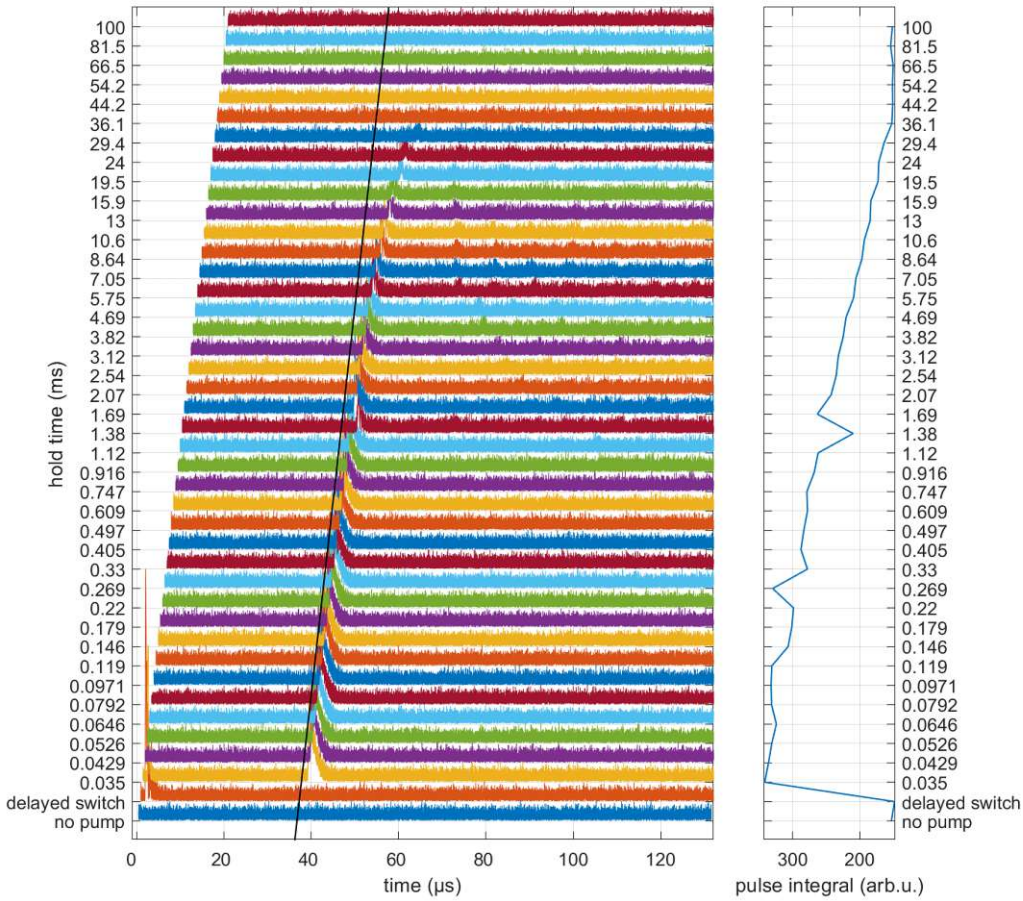

Figure 4.10: Results of the same hold time scan but now with a colder cavity mode in contrast to before. This is realized by letting the relay switch open the whole time (the semi-rigid SMA cables in the downline are physically separated) and just close it as short as possible (for roughly $2\,\mathrm{ms}$) to send in the inversion pulse. However, as can be seen clearly, this colder cavity mode has not led to a longer holding time, the results are comparable to that obtained before (see Fig. 4.7 for comparison).

Die approbierte gedruckte Originalversion dieser Diplomarbeit ist an der TU Wien Bibliothek verfügbar
The approved original version of this thesis is available in print at TU Wien Bibliothek.
TU Bibliothek Your knowledge hub WIEN

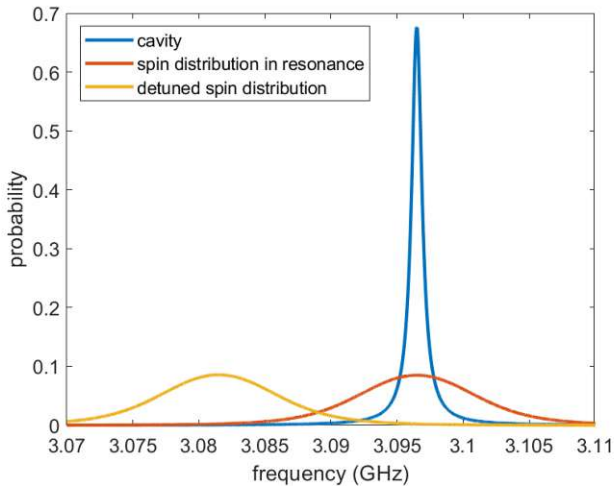

Figure 4.11: The Lorentzian transmission of the cavity as a function of frequency is shown in blue, the corresponding q-Gaussian spin distribution in resonance can be seen in red, the $15\,\mathrm{MHz}$ detuned one is depicted in yellow, respectively. The distributions are normalized in such a way so that the area under the function is 1. For the detuned spin distribution a overlap with the cavity is clearly visible. The parameters we used here are $\kappa = 0.4754 \cdot 2\pi\,\mathrm{MHz}$ for the Lorentzian, $\gamma = 8.7204 \cdot 2\pi\,\mathrm{MHz}$ (width q-Gaussian) and $q = 1.4$ for the q-Gaussian of the spins, respectively.

photons the $\langle \hat{\sigma}_z^j(t) \rangle$ values of the inverted spin ensemble would decrease by a factor of e^{-1} after the time $1/\gamma_{\|} = T_1 \approx 150\,\mathrm{s}$. With thermal photons that time decreases to $1/(\gamma_{\|}(2\bar{n}+1)) = T_1/(2\bar{n}+1)$ which for $\bar{n} = 6$ would lead to $T_{\mathrm{e}^{-1}} \approx 11.5\,\mathrm{s}$ and for $\bar{n} = 2000$ to $T_{\mathrm{e}^{-1}} \approx 0.075\,\mathrm{s}$. Since, however, the spin decay into the hot and cold mode (see Figs. 4.7 and 4.10) is comparable, we conclude, that thermal photons are not the limiting factor in our hold time scans.

Another possible explanation for the decay is that by detuning the spin ensemble by $15\,\mathrm{MHz}$ some of the spins are still in resonance. This can be seen in Fig. 4.11 where the Lorentzian transmission function of the cavity (blue) and the q-Gaussian spin distribution in the resonant (red) as well as for the detuned case (yellow) are shown. The distributions are normalized in a way such that the area under the function is 1. For the detuned spin distribution a non-zero overlap with the cavity is clearly visible. Therefore, these spins can decay although the spin ensemble is detuned and through spin diffusion processes in the crystal the spins can exchange energy. This means in frequency space that the spins can change place in the q-Gaussian spin distribution which subsequently means that after a while inverted spins are again in resonance with the cavity even though the whole spin system is detuned. After roughly $30\,\mathrm{ms}$ the overall $\sum_j \langle \hat{\sigma}_z^j \rangle$ component of the system is 0 and

Die approbierte gedruckte Originalversion dieser Diplomarbeit ist an der TU Wien Bibliothek verfügbar
The approved original version of this thesis is available in print at TU Wien Bibliothek.
TU Bibliothek Your knowledge hub WIEN

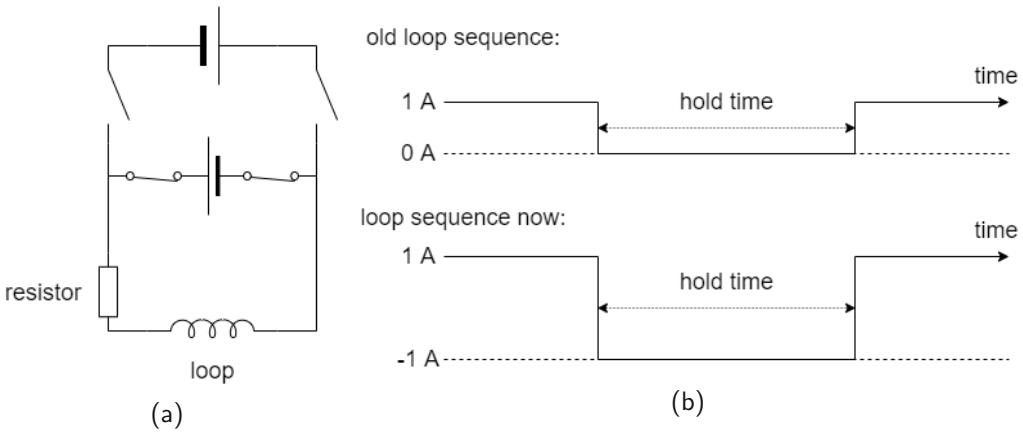

Figure 4.12: To be able to increase the spin detuning, we add a second power supply to the setup as depicted in Fig. (a). We connect that power supply with the opposite polarity compared to the first one by which we are able to increase the spin detuning. By opening the closed switches via a TTL signal we change the current through the loop from 1 to 0 A. After doing so, we close the now open switches (again via a TTL signal) by which we change the current from 0 to −1 A. By measuring the voltage drop over a resistor with an oscilloscope we monitor that current. The new current sequence is shown in Fig. (b), with the new sequence we are able to detune the spins by approximately 30 MHz.

therefore we cannot observe a superradiant decay pulse any more. If our working hypothesis is right we should be able to observe a photon burst for longer hold times if we increase the spin detuning.

To be able to do so, we extend our setup and use a second power supply as shown in Fig. 4.12(a). After opening the closed switches via a TTL signal by which we change the current through the loop from 1 to 0 A we close the open switches (again via a TTL signal) and get a connection to the second power supply with different polarity. By doing so, we change the current from 0 to −1 A and as a consequence detune the spins even further. By measuring the voltage drop over a resistor with an oscilloscope we can monitor the current. In Fig. 4.12(b) the old and new current sequences through the loop are depicted. With the additional power supply and the now possible further spin detuning we again do a hold time scan, the results are shown in Fig. 4.13. Unfortunately, as before, this working hypothesis turns out to be wrong again, as we still are not able to stabilize the spins for times longer than 30 ms. Since this is quite counter intuitive and we expected some changes, even though they can be very small, we now fixed the time the spins stay detuned and vary the detuning amplitude, i.e., the negative current value. The obtained results are depicted in Fig. 4.14. As before, we see no difference in the photon burst, no

Die approbierte gedruckte Originalversion dieser Diplomarbeit ist an der TU Wien Bibliothek verfügbar
The approved original version of this thesis is available in print at TU Wien Bibliothek.
TU Bibliothek Your knowledge hub WIEN

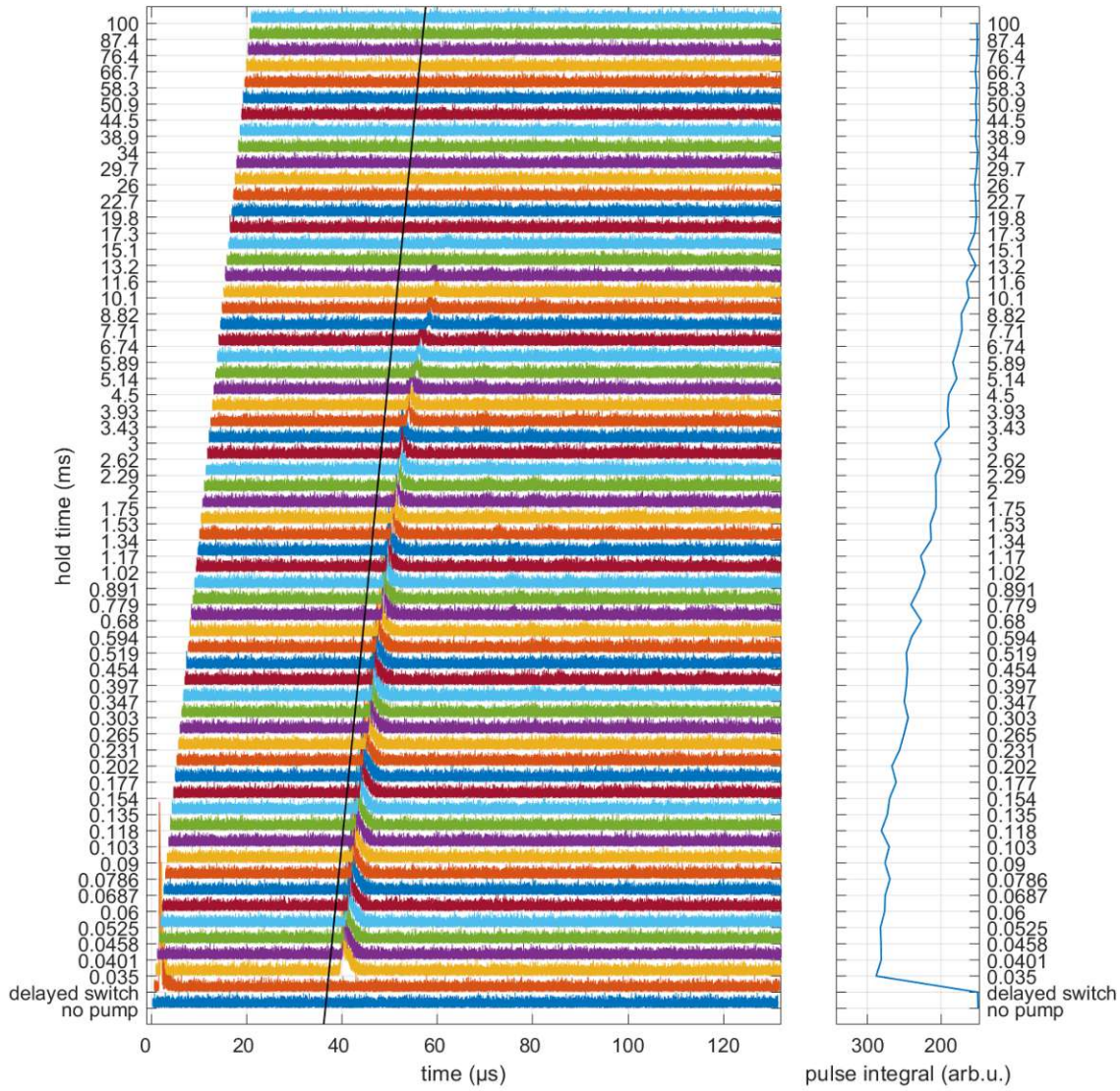

Figure 4.13: For that hold time scan we use the new setup with the corresponding new current sequence. By doing so, we are able to detune the spins by $30\,\mathrm{MHz}$. Unfortunately, the hold time does not change, the results we obtain are comparable to the one shown in Figs. 4.7 and 4.10.

Die approbierte gedruckte Originalversion dieser Diplomarbeit ist an der TU Wien Bibliothek verfügbar
The approved original version of this thesis is available in print at TU Wien Bibliothek.

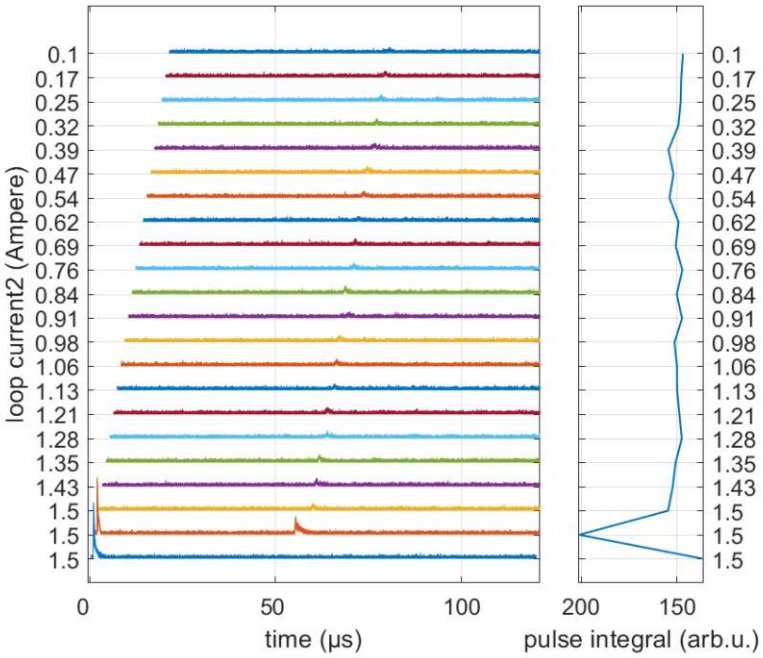

Figure 4.14: To further investigate the spin detuning we did a scan of the detuning. Therefore, we change the current of the second power supply, i.e., changed the absolute value of the negative current. As clearly visible, the photon burst coming out of the cavity is always the same, it makes no difference if we detune the spins by 15 or 30 MHz. Please note that for the first run we do not detune the spins at all, for the second one the holding time is shorter and therefore these runs are not comparable. Please note further that the time offset was introduced to be able to better compare the runs and is arbitrary.

matter how far the spins are detuned. Please note that for the first run we do not detune the spins at all, for the second one the holding time is shorter. That is why the photon burst of the second run is larger, these runs are therefore not comparable.

After we experimentally tried everything to increase the holding time and still are unable to do so, we try to explain that enhanced decay by solid state physics effects. And in fact, we now have a beautiful working hypothesis which is also mentioned in Ref. [48]. Some of the NV centers in our crystal are not as stable as the others. With stable we mean that they have, because of their environment in the host crystal, a (much) shorter T_1 time. Due to spin-spin interaction these "bad" NV centers are somehow an additional decay channel for the inverted spin ensemble and therefore shortens the lifetime of every inverted spin. This can be seen in computer simulations and in Fig. 3(b) in Ref. [48]. Since this is a spin relaxation process caused by the

Die approbierte gedruckte Originalversion dieser Diplomarbeit ist an der TU Wien Bibliothek verfügbar
The approved original version of this thesis is available in print at TU Wien Bibliothek.
TU Bibliothek Your knowledge hub WIEN

solid state structure of the crystal itself, it is very hard to experimentally overcome that issue and with the current setup not possible. Therefore, detuning the spins cannot prevent the spins from decaying as well.

Now we want to return to the self decay of the spins again. As stated before, the inverted spin ensemble is useful to characterize the thermal microwave background and/or microwave pulses which can trigger the spin decay as well. Then one has to has the right timing to be sure that the decay is triggered by the pulse and not due to self decay. Therefore, one has a time window of a few µs after tuning the spins back which is not quite what a detector is supposed to do. Nevertheless, we have another idea to overcome this timing issue and detect the pulse over a longer time range. This will be presented in the following.

4.2 Periodic Spin Detuning - Detection of Short Microwave Pulses

Besides the possibility of detuning the whole spin ensemble we can apply a sinusoidal pulse by which the inverted spin ensemble gets stabilized as well. By doing so, the NV centers are repeatably detuned and brought back in resonance. This is based on the idea mentioned in the supplementary information of Ref. [49]. Since we do not know how such a stabilization pulse has to look like, we start with numerical simulations. Mathematically, we can describe the detuning as

$$\begin{aligned}
\langle \dot{\hat{a}} \rangle &= -\mathrm{i}\Delta_c \langle \hat{a} \rangle + \sum_j g_j \left\langle \hat{\sigma}_-^j \right\rangle + \eta - \kappa \langle \hat{a} \rangle \,, \\
\langle \dot{\hat{\sigma}}_-^j \rangle &= -\mathrm{i} \left(\Delta_s^j + \delta(t) \right) \left\langle \hat{\sigma}_-^j \right\rangle + g_j \langle \hat{a} \rangle \left\langle \hat{\sigma}_z^j \right\rangle - \left(\frac{\gamma_\parallel}{2} + \gamma_\perp \right) \left\langle \hat{\sigma}_-^j \right\rangle \,, \\
\langle \dot{\hat{\sigma}}_z^j \rangle &= -2 g_j \left(\left\langle \hat{a}^\dagger \right\rangle \left\langle \hat{\sigma}_-^j \right\rangle + \langle \hat{a} \rangle \left\langle \hat{\sigma}_+^j \right\rangle \right) - \gamma_\parallel \left(1 + \left\langle \hat{\sigma}_z^j \right\rangle \right) \,,
\end{aligned} \tag{4.9}$$

where the new introduced term $\delta(t)$ denotes the periodically detuning of the spins. Since we want to stabilize an inverted spin system which can be experimentally realized using the aforementioned OCT pulse, we start with such an inverted ensemble and simulate the temporal evolution of the spins. Thus, the initial values are $\langle \hat{\sigma}_z^j(0) \rangle = 0.5172$, $\langle \hat{\sigma}_-^j(0) \rangle = -0.0062 - 0.0023\mathrm{i}$ and $\langle \hat{a}(0) \rangle = 0.6779$. This corresponds to a spin tilting angle (angle between spin ensemble and vertical) of $\alpha = \arctan\left(\frac{|\langle \hat{\sigma}_-^j(0) \rangle|}{\langle \hat{\sigma}_z^j(0) \rangle} \right) = 0.0128\,\mathrm{rad} = 0.7325°$. We assume nonzero $\langle \hat{\sigma}_-^j(0) \rangle$ and $\langle \hat{a}(0) \rangle$ values since we cannot model quantum fluctuations with the Maxwell-Bloch equations. In contrast to the experiment, where the cavity amplitude as well as the $\langle \hat{\sigma}_-^j \rangle$ components decay exponentially and get sufficiently small when waiting long enough, i.e., the values are (nearly) zero, we numerically need nonzero values to simulate the quantum fluctuations and to evaluate if the stabilization procedure

Die approbierte gedruckte Originalversion dieser Diplomarbeit ist an der TU Wien Bibliothek verfügbar
The approved original version of this thesis is available in print at TU Wien Bibliothek.
TU Bibliothek Your knowledge hub WIEN

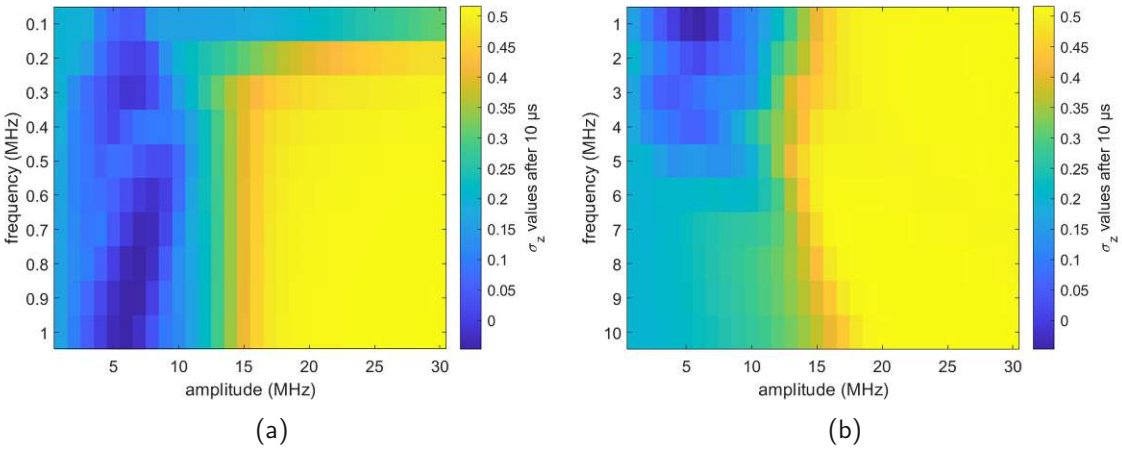

Figure 4.15: Final (after $10\,\mu s$) $\sum_j \langle \hat{\sigma}_z^j \rangle$ values for sinusoidal stabilization pulses with different amplitudes and frequencies. That pulses periodically detune the NV centers and bring them back in resonance again. In (a) the results for pulses with frequencies between 0.1 and $1\,\mathrm{MHz}$ are shown whereas in (b) we choose them to be between 1 and $10\,\mathrm{MHz}$. As can be seen clearly, the frequency does not have a big influence. As long as the frequency is higher than approximately $0.4 \cdot 2\pi\,\mathrm{MHz}$ and the amplitude higher than roughly $18\,\mathrm{MHz}$ the spins do not (significantly) decay any more.

works. Please note that we obtained these starting values by numerically inverting the spin ensemble with the OCT pulse we used before (which is based on the Fourier coefficients mentioned in Ref. [44]) and then by detuning the spins at the right time by $15\,\mathrm{MHz}$ for $0.75\,\mu s$. The further parameters we used are $q = 1.14$ and $\gamma = 7.4 \cdot 2\pi\,\mathrm{MHz}$ which defines our q-Gaussian spin distribution, the collective coupling is $g_{coll} = 4.3 \cdot 2\pi\,\mathrm{MHz}$ and we choose our dephasing parameter to be $\frac{\gamma_\parallel}{2} + \gamma_\perp = 0.5 \cdot 2\pi\,\mathrm{MHz}$. The cavity parameters used are $\omega_c = 3123.57 \cdot 2\pi\,\mathrm{MHz}$ and $\kappa = 0.616\,35 \cdot 2\pi\,\mathrm{MHz}$, the overall frequency offset between the spin distribution and the cavity is $\Delta_{sc} = 0.128\,75 \cdot 2\pi\,\mathrm{MHz}$.

As said before, we first start with an amplitude frequency scan of the stabilization pulse. Therefore, we simulate the temporal evolution of our system for $10\,\mu s$ and observe the change of the $\langle \hat{\sigma}_z^j \rangle$ components over that time. The numerical solutions are shown in Fig. 4.15 where the final $\sum_j \langle \hat{\sigma}_z^j \rangle$ values (after $10\,\mu s$) are shown for different pulse amplitudes and frequencies. Quite surprisingly, one sees that the frequency does not have a big influence, as long as the frequency is higher than approximately $0.4 \cdot 2\pi\,\mathrm{MHz}$ and the amplitude higher than roughly $18\,\mathrm{MHz}$ the spins do not significantly decay any more. As can be seen in Fig. 4.16 where we apply a pulse with $\omega = 0.5 \cdot 2\pi\,\mathrm{MHz}$ and an amplitude of $18\,\mathrm{MHz}$ most of the inversion can be kept in the system although some of the spins decay.

Die approbierte gedruckte Originalversion dieser Diplomarbeit ist an der TU Wien Bibliothek verfügbar
The approved original version of this thesis is available in print at TU Wien Bibliothek.
TU Bibliothek Your knowledge hub WIEN

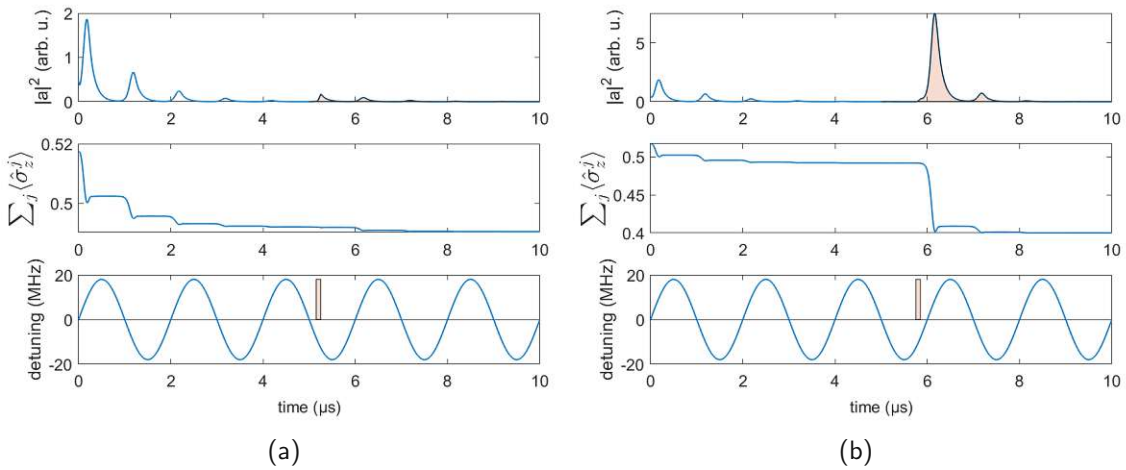

Figure 4.16: In our numerical simulation, the $100\,\mathrm{ns}$ long probe pulse with an amplitude of 5 is send in at different times. When we send in the pulse at (a) $5.15\,\mu\mathrm{s}$ which is right after the spins got detuned from the cavity (as shown in the lowest plots) only a few spins decay since most of them do not have any decay channel. The situation changes when one sends in the pulse shortly before the spins are in resonance, for example at (b) $5.75\,\mu\mathrm{s}$. Then all spins are in resonance and can decay perfectly. The integral of the cavity intensity which will be used in the following is shown as red area in the uppermost plots as well.

After we see that the stabilization of the inverted spin ensemble is possible with such a sinusoidal pulse we now want to trigger the spin decay by sending in a probe pulse. By doing so, two questions immediately occur: at what time should we send in the probe pulse and how strong should it be?

To answer that we again do numerical simulations where the probe pulse in the Maxwell-Bloch equations is denoted by η. For all following simulations we assume a stabilization pulse $\delta(t)$ with a frequency of $\omega = 0.5 \cdot 2\pi\,\mathrm{MHz}$ and an amplitude of $18\,\mathrm{MHz}$. We choose our probe pulse to be $100\,\mathrm{ns}$ long and since we have a sinusoidal stabilization pulse with a period of $2\,\mu\mathrm{s}$, we do a start time scan over one half period, i.e. we choose a start time of that probe pulse between 5 and $6\,\mu\mathrm{s}$. The concept of the numerical simulation is shown in Fig. 4.16 where we send in the probe pulse with amplitude 5 at $5.15\,\mu\mathrm{s}$ and $5.75\,\mu\mathrm{s}$ as shown as red rectangle in the lowest plots, respectively. As can be clearly seen, the earlier probe pulse leads to a small spin decay and as a consequence only few photons in the cavity whereas the second pulse leads to a significant spin decay and photon intensity in the cavity mode. The timing of the probe pulse with respect to the stabilization pulse is crucial. In the first case the probe pulse was sent in right after the spins got detuned from the cavity and therefore one can nearly completely prevent the spins from decaying since they have

Die approbierte gedruckte Originalversion dieser Diplomarbeit ist an der TU Wien Bibliothek verfügbar
The approved original version of this thesis is available in print at TU Wien Bibliothek.
TU Bibliothek Your knowledge hub WIEN

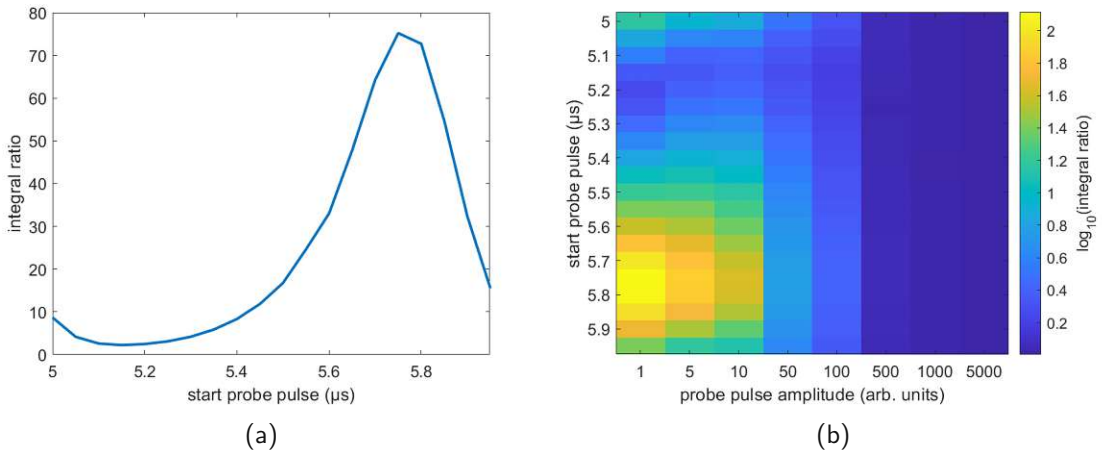

Figure 4.17: To quantify how good the spin decay can be triggered by such a probe pulse, we compare the calculated integral of the intensity after the spin decay and compare it with the one one would obtain with an empty cavity. In (a) this gain factor is shown for a $100\,\mathrm{ns}$ probe pulse with an amplitude of 5 as a function of different start times. As stated before, the intensity is the largest if one sends in the pulse right before the spins are in resonance, one gets a gain factor of roughly 75. Even for suboptimal timings between stabilization and probe pulse the amplification is not below 3. In Fig. (b) the gain factor is shown for different probe pulse amplitudes, one clearly sees that the amplification is the best for the weakest pulses. Please note that $\log_{10}$(integral ratio) is plotted, the initial $\langle\hat{\sigma}_z^j\rangle$ values are $\langle\hat{\sigma}_z^j(0)\rangle = 0.5172$.

no free decay channel. In the second case the timing is optimal, the probe pulse was sent in right before the spins were in resonance. Shortly after the spins are triggered they are in resonance with the cavity and can therefore decay easily.

We furthermore do a scan of the strength of the probe pulse. To be able to qualitatively say how good the triggering of the spin decay works, we calculate the integral of the cavity intensity (as depicted in Fig. 4.16 in the uppermost plots) which is proportional to the number of photons and compare it with the integral one would obtain without any spins, i.e., with an empty cavity. The ratio of these two values is the gain of the probe pulse coming from the inverted spin ensemble. This ratio, i.e. gain of a 100 ns probe pulse with amplitude 5, is depicted as function of different start times in Fig. 4.17(a). As said before, the intensity in the cavity is the largest when sending the probe pulse in right before the spins are in resonance for which we get a gain factor of roughly 75. When sending the probe pulse in right after the spins got detuned the gain factor is the lowest, but we still get an amplification of our probe pulse. In Fig. 4.17(b) we compare the results obtained with different probe pulse amplitudes. One clearly sees that the lower the amplitude

Die approbierte gedruckte Originalversion dieser Diplomarbeit ist an der TU Wien Bibliothek verfügbar
The approved original version of this thesis is available in print at TU Wien Bibliothek.
TU Bibliothek Your knowledge hub WIEN

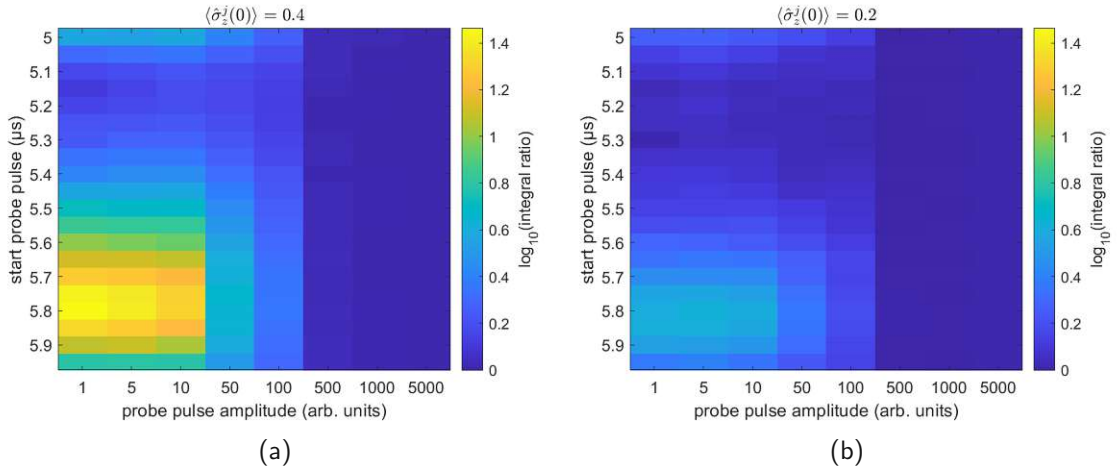

Figure 4.18: Gain factor of a 100 ns probe pulse as a function of its start time and amplitude. Now the initial $\langle\hat{\sigma}_z^j\rangle$ values are (a) 0.4 and (b) 0.2, respectively. One obtains qualitatively the same picture as before but due to the fact that less spins are inverted the amplification of the pulse is reduced. To be able to compare these results with the one obtained before, we furthermore fix the initial tilting angle of the spin system (as before $\alpha = 0.7325°$) and change the initial values for $\langle\hat{\sigma}_-^j\rangle$ correspondingly. Please note that $\log_{10}$(integral ratio) is plotted.

the higher the gain factor. Please note that $\log_{10}$(integral ratio) is plotted.

Besides that we do the same numerical simulations with a 50 ns and a 200 ns long probe pulse where we again scan the starting time as well as the amplitude of the pulse. We get qualitatively the same results as shown in Fig. 4.17(b).

More interesting is the question how different initial $\langle\hat{\sigma}_z^j\rangle$ values change the amplification factor of the probe pulse. The obtained results for initial $\langle\hat{\sigma}_z^j\rangle$ values of 0.4 and 0.2 are shown in Figs. 4.18(a) and (b), respectively. To be able to compare these results with the one obtained before, we furthermore fix the initial tilting angle of the spin system (as before $\alpha = 0.7325°$) and change the initial values for $\langle\hat{\sigma}_-^j\rangle$ correspondingly. One sees again a maximum of the amplification factor when sending in a weak probe pulse right before the spins are in resonance with the cavity. But since less spins are inverted the gain factor is reduced. Since the inversion is the most difficult part of the experiment, we plot the gain factor as function of initial $\sum_j\langle\hat{\sigma}_z^j\rangle$ components for a 100 ns probe pulse which starts at 5.75 µs and has an amplitude of 5. The numerical results are depicted in Fig. 4.19 where one sees that the amplification increases exponentially with the $\sum_j\langle\hat{\sigma}_z^j\rangle$ component. This is not only true for that specific pulse but is true in general: the better the inversion of the spin system the higher the amplification factor. Therefore, the most important part of the experiment is the inversion of the spin ensemble with a suitable OCT pulse

Die approbierte gedruckte Originalversion dieser Diplomarbeit ist an der TU Wien Bibliothek verfügbar
The approved original version of this thesis is available in print at TU Wien Bibliothek.
TU Bibliothek Your knowledge hub WIEN

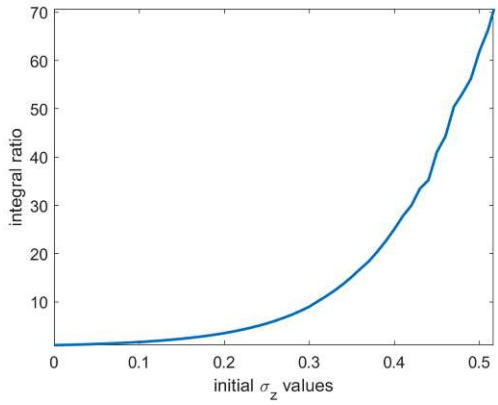

Figure 4.19: Function of the amplification of a 100 ns probe pulse which starts at 5.75 µs and has an amplitude of 5. Since the amplification increases exponentially with the $\langle \hat{\sigma}_z^j \rangle$ components (which is true in general and not only for this specific probe pulse), the most important part of the experiment is to ensure that as many as possible spins are inverted and are then hold in that position.

followed by a detuning of the NV centers by 15 MHz achieved by the additional small coil. After waiting a suitable long time where the cavity amplitude and the $\langle \hat{\sigma}_-^j \rangle$ components decrease exponentially one can tune the spins back and then apply the aforementioned $\delta(t)$ pulse during which the spins stay inverted. After doing so, a probe pulse, which is sent in at any arbitrary time can trigger a decay and therefore gets amplified as well.

To get rid of the timing problem between the stabilization and probe pulse, one can just increase the frequency of the stabilization pulse. For the next simulation, we choose a frequency of $\omega = 10 \cdot 2\pi$ MHz and an amplitude of 18 MHz. To be able to compare the results with the one obtained before, we apply again a 100 ns probe pulse and scan the start time as well as its amplitude. The results are shown in Fig. 4.20. Since the period of the stabilization pulse is 100 ns and therefore as long as the probe pulse, the timing of the pulse has nearly no influence. Furthermore, the decay of the inverted spin ensemble is different than before, the spins are decaying slower. This is because now they are in resonance with the cavity only for short amount of times and, therefore, have only short time to decay before they get detuned and do not have a decay channel any more. Because of that the maximum amplification factor is now roughly 10 and less than before. Please note again that $\log_{10}$(integral ratio) is plotted. Since it is nearly impossible to detune the spins with such a high frequency which is due to technical reasons we did not investigate that pulse further and stick to that one with a lower frequency.

Please note that we get quite the same results as shown in Fig. 4.15(a) when doing the same simulations with smaller initial spin tilting angle. We still need a

Die approbierte gedruckte Originalversion dieser Diplomarbeit ist an der TU Wien Bibliothek verfügbar
The approved original version of this thesis is available in print at TU Wien Bibliothek.
TU Bibliothek Your knowledge hub WIEN

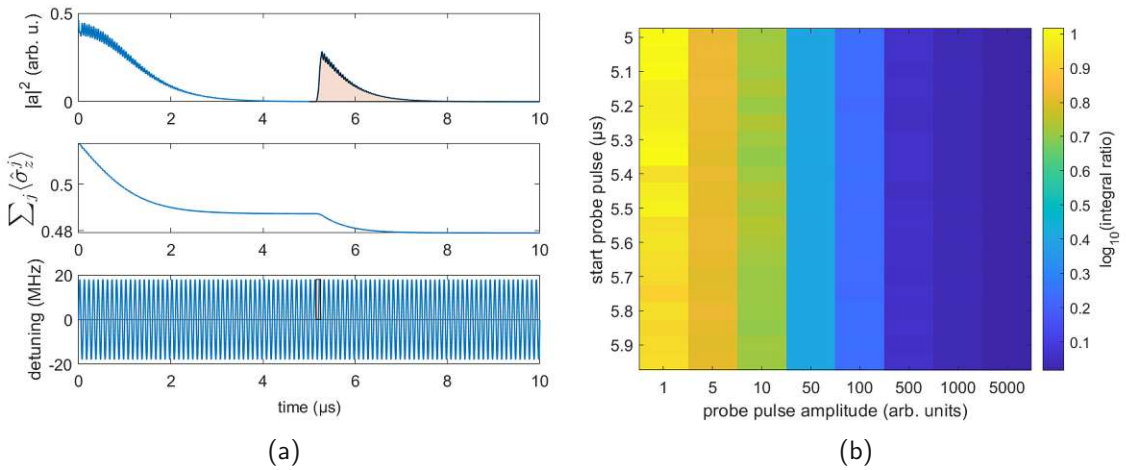

Figure 4.20: By stabilizing the spin ensemble with a pulse with a frequency of $\omega = 10 \cdot 2\pi\,\mathrm{MHz}$ and an amplitude of $18\,\mathrm{MHz}$, one gets rid of the timing problem between the stabilization and probe pulse. As can be seen in Fig. (b) where we again scan the start time as well as the amplitude of a $100\,\mathrm{ns}$ long probe pulse, the start time has nearly no influence. This is because the period of the stabilization pulse is as long as the probe pulse. Furthermore, because the spins are only a short time in resonance before they get detuned again the decay of the spins happens much slower (a) which gets triggered by a pulse send in at $5.15\,\mu\mathrm{s}$ with amplitude 5. Because of that the maximal amplification factor is now roughly 10 and less than before. Please note again that $\log_{10}$(integral ratio) is plotted.

pulse with $\omega \approx 0.4 \cdot 2\pi\,\mathrm{MHz}$ and an amplitude of $\approx 18\,\mathrm{MHz}$. Since the spin tilting angle is quite large, we conclude that our stabilization mechanism is quite powerful. As shown in the figures of that section, up to now we simulate the behavior of the spins over a time range of $10\,\mu\mathrm{s}$. To see how good our stabilization procedure works, we extend the time and simulate the behavior of the spins over a time range of $500\,\mu\mathrm{s}$. With the mentioned stabilization pulse, the spins can be kept inverted for that time. Simulating the evolution over a longer time range is numerically quite costly and therefore takes time. However, we think that we can in principle stabilize our inverted spin ensemble for some ms with that method, it should only be limited by the shortened spin lifetime caused by the "bad" NV centers. As long as we do not warm up our fridge (too much) with this method, we are very optimistic to be able to experimentally implement this stabilizing mechanism. Please note, that we do not know what probe pulse amplitude should we send in to reproduce the presented results. This, however, can be easily solved by scanning the probe pulse amplitude we experimentally use until we get the same integral ratios presented here.

To sum up, by this periodical detuning one gets a meta stable spin state which

Die approbierte gedruckte Originalversion dieser Diplomarbeit ist an der TU Wien Bibliothek verfügbar
The approved original version of this thesis is available in print at TU Wien Bibliothek.
TU Bibliothek Your knowledge hub WIEN

means that they do not decay by themselves but one can easily trigger it. However, compared to the spin decay triggered with the same pulse right after switching the spins back after constantly detuning them, the photon burst coming out during the periodical detuning is smaller than before. Therefore, one can choose if one wants to have a detector where the spin decay can be triggered within a few µs long time window but causing a larger photon burst or where it can be triggered over longer time ranges (some ms, the limiting factor here are the "bad" NV centers as well) but causing a smaller burst.

Die approbierte gedruckte Originalversion dieser Diplomarbeit ist an der TU Wien Bibliothek verfügbar
The approved original version of this thesis is available in print at TU Wien Bibliothek.
TU Bibliothek Your knowledge hub WIEN

5 Conclusion and Outlook

Quite recently, superradiant emission from NV^- colour centres in diamond was observed for the first time [24]. Building up on these findings, we asked us whether it is possible to prevent the inverted spin ensemble from decaying immediately, which, as a consequence, would lead to a delayed photon burst coming out of the cavity. We further wondered if we can improve the inversion pulse mentioned in Ref. [44] so that it better fits to the parameter describing our spin ensemble.

In this thesis we present a new chirped pulse which leads to an improved inversion of the ensemble, we reach a inversion of approximately $\sum_j \langle \hat{\sigma}_z^j \rangle = 0.75$. Furthermore, by detuning the spin ensemble at the right time very fast from the cavity we are able to hold them inverted for roughly 30 ms. As presented, this limitation of the holding time is not due to technical reasons but rather caused by some "bad" NV centers which have a much shorter T_1 time. Over spin-spin interaction these centers lead to an enhanced decay of the whole ensemble, no matter whether the spins are in resonance with the cavity or not. Additionally, one cannot overcome the self decay of the spins after bringing them back in resonance since our system is inherently unstable. This, however, gives the possibility to measure the mode temperature of the cavity which is proportional to the time it takes the spins to decay after they are brought back in resonance. Of course the spin decay can be triggered by short pulses as well but for doing so one has a time window of a few µs.

We furthermore present a possibility to overcome that timing issue and detect microwave pulses over a longer time range. This can be done by stabilizing the spin ensemble with a sinusoidal periodic detuning which would lead to a meta stable state and therefore the spins would decay after they get triggered but not by themselves. Because of that the amplification of the triggering pulse would be not as high as before but the advantage of this method would be that one can detect pulses over a longer timescale. Our insights regarding the periodical detuning are until now based on numerical simulations.

Based on our so far obtained results, the next steps to be done are to investigate how weak a possible trigger pulse in that few µs long time window can be to trigger the spin decay. Until now, due to experimental reasons, we only were able to show that one can trigger the decay with a pulse but we were not able to specify its properties. Secondly, the concept of stabilizing the inverted spins by periodically detuning them has to be proven experimentally. We once tried to realize the periodic current modulation with a laser diode driver. However, by switching it on and off at the begin and end of the corresponding sequence some current spikes occurred

Die approbierte gedruckte Originalversion dieser Diplomarbeit ist an der TU Wien Bibliothek verfügbar
The approved original version of this thesis is available in print at TU Wien Bibliothek.
TU Bibliothek Your knowledge hub WIEN

which have broken our small loop. Since we think we know how to overcome this technical issues we are optimistic to verify the theoretical predictions soon.

Die approbierte gedruckte Originalversion dieser Diplomarbeit ist an der TU Wien Bibliothek verfügbar
The approved original version of this thesis is available in print at TU Wien Bibliothek.
TU WIEN Bibliothek Your knowledge hub

A Cavity QED Calculations

A.1 Quantization of Electromagnetic Field - Evaluate Integral

Here we want to evaluate the integral of Eq. (2.18), i.e.,

$$\begin{aligned}\int_0^L \sin\left(\frac{n\pi}{L}z\right)\sin\left(\frac{m\pi}{L}z\right)\mathrm{d}z \\ = \frac{1}{2}\int_0^L \cos\left(\frac{(n-m)\pi}{L}z\right)\mathrm{d}z - \frac{1}{2}\int_0^L \cos\left(\frac{(n+m)\pi}{L}z\right)\mathrm{d}z,\end{aligned} \tag{A.1}$$

where we use $\sin(x)\sin(y) = \frac{1}{2}\left[\cos(x-y) - \cos(x+y)\right]$ with n and m being integer numbers. Now we have to distinguish between two different cases: namely the ones where $n = m$ and $n \neq m$. First, we assume $n = m$ and get

$$\frac{1}{2}\int_0^L \cos(0)\,\mathrm{d}x - \frac{1}{2}\int_0^L \cos\left(\frac{2n\pi}{L}x\right)\mathrm{d}x = \frac{L}{2} - \frac{L}{4n\pi}\sin\left(\frac{2n\pi}{L}x\right)\Big|_0^L = \frac{L}{2}. \tag{A.2}$$

If $n \neq m$ we end up with

$$\begin{aligned}&\frac{1}{2}\int_0^L \cos\left(\frac{(n-m)\pi}{L}x\right)\mathrm{d}x - \frac{1}{2}\int_0^L \cos\left(\frac{(n+m)\pi}{L}x\right)\mathrm{d}x \\ &= \frac{L}{2\pi(n-m)}\sin\left(\frac{(n-m)\pi}{L}x\right)\Big|_0^L - \frac{L}{2\pi(n+m)}\sin\left(\frac{(n+m)\pi}{L}x\right)\Big|_0^L = 0.\end{aligned} \tag{A.3}$$

By combining the results of Eqs. (A.2) and (A.3), one can write the result of Eq. (A.1) as

$$\int_0^L \sin(kx)\sin(k'x)\,\mathrm{d}x = \int_0^L \sin\left(\frac{n\pi}{L}x\right)\sin\left(\frac{m\pi}{L}x\right)\mathrm{d}x = \frac{L}{2}\delta_{nm} = \frac{L}{2}\delta_{kk'}. \tag{A.4}$$

A.2 Unitary Operator Transformation

In that section we want to calculate the unitary transformation of an operator. This will be needed for changing between Schrödinger and Interaction picture and for the transformation of the driven Tavis-Cummings Hamiltonian. The starting point is

$$\hat{a}_I = \hat{U}^\dagger \hat{a}\hat{U}, \tag{A.5}$$

Die approbierte gedruckte Originalversion dieser Diplomarbeit ist an der TU Wien Bibliothek verfügbar
The approved original version of this thesis is available in print at TU Wien Bibliothek.
TU Bibliothek Your knowledge hub WIEN

where the subscript I denotes the Interaction picture. The unitary transformation is given by

$$\hat{U} = \mathrm{e}^{-\mathrm{i}\omega\hat{a}^\dagger\hat{a}t}. \tag{A.6}$$

Now we want to rewrite the expression $\hat{a}\hat{U}$. Therefore, we write the exponential as a serial expansion and rewrite the term $\hat{a}\hat{a}^\dagger\hat{a}$ using the commutator $[\hat{a}, \hat{a}^\dagger] = 1$, i.e., $\hat{a}\hat{a}^\dagger = \hat{a}^\dagger\hat{a} + 1$. We get

$$\begin{aligned}
\hat{a}\hat{U} &= \hat{a}\left(1 - \mathrm{i}\omega\hat{a}^\dagger\hat{a}t - \frac{\omega^2}{2}\hat{a}^\dagger\hat{a}\hat{a}^\dagger\hat{a}t + \ldots\right) \\
&= \hat{a} - \mathrm{i}\omega\left(\hat{a}^\dagger\hat{a} + 1\right)\hat{a}t - \frac{\omega^2}{2}\left(\hat{a}^\dagger\hat{a} + 1\right)\left(\hat{a}^\dagger\hat{a} + 1\right)\hat{a}t + \ldots \\
&= \left(1 - \mathrm{i}\omega\left(\hat{a}^\dagger\hat{a} + 1\right)t - \frac{\omega^2}{2}\left(\hat{a}^\dagger\hat{a} + 1\right)^2 t\right)\hat{a} = \mathrm{e}^{-\mathrm{i}\omega\left(\hat{a}^\dagger\hat{a}+1\right)t}\hat{a} = \hat{U}\hat{a}\mathrm{e}^{-\mathrm{i}\omega t}.
\end{aligned} \tag{A.7}$$

So in total the annihilation operator in the Interaction picture can be written as

$$\hat{a}_I = \hat{U}^\dagger\hat{a}\hat{U} = \hat{a}\mathrm{e}^{-\mathrm{i}\omega t}. \tag{A.8}$$

By taking the conjugate transpose of the above equation we get the transformation rule for the creation operator, i.e.,

$$\hat{a}_I^\dagger = \left(\hat{U}^\dagger\hat{a}\hat{U}\right)^\dagger = \hat{U}^\dagger\hat{a}^\dagger\hat{U} = \hat{a}^\dagger\mathrm{e}^{\mathrm{i}\omega t}. \tag{A.9}$$

The situation is similar if we transform the $\hat{\sigma}_z$ operator with the unitary transformation

$$\hat{U} = \mathrm{e}^{-\frac{\mathrm{i}\omega}{2}\hat{\sigma}_z t}. \tag{A.10}$$

Doing the same steps as before and using $[\hat{\sigma}_z, \hat{\sigma}_-] = -2\hat{\sigma}_-$, i.e., $\hat{\sigma}_-\hat{\sigma}_z = \hat{\sigma}_z\hat{\sigma}_- + 2\hat{\sigma}_-$ then gives

$$\begin{aligned}
\hat{\sigma}_-\hat{U} &= \hat{\sigma}_-\left(1 - \frac{\mathrm{i}\omega}{2}\hat{\sigma}_z t - \frac{\omega^2}{4}\hat{\sigma}_z\hat{\sigma}_z t + \ldots\right) \\
&= \hat{\sigma}_- - \frac{\mathrm{i}\omega}{2}\left(\hat{\sigma}_z + 2\right)\hat{\sigma}_- t - \frac{\omega^2}{4}\left(\hat{\sigma}_z + 2\right)^2\hat{\sigma}_- t + \ldots \\
&= \left(1 - \frac{\mathrm{i}\omega}{2}\left(\hat{\sigma}_z + 2\right)t - \frac{\omega^2}{4}\left(\hat{\sigma}_z + 2\right)^2 t + \ldots\right)\hat{\sigma}_- = \mathrm{e}^{-\mathrm{i}\frac{\omega}{2}(\hat{\sigma}_z+2)t}\hat{\sigma}_- = \hat{U}\hat{\sigma}_-\mathrm{e}^{-\mathrm{i}\omega t}.
\end{aligned} \tag{A.11}$$

In total we now get

$$\hat{\sigma}_{-,I} = \hat{U}^\dagger\hat{\sigma}_-\hat{U} = \hat{\sigma}_-\mathrm{e}^{-\mathrm{i}\omega t}. \tag{A.12}$$

If we conjugate transpose that equation we get again the result for the spin raising operator in the Interaction picture

$$\hat{\sigma}_{+,I} = \left(\hat{U}^\dagger\hat{\sigma}_-\hat{U}\right)^\dagger = \hat{U}^\dagger\hat{\sigma}_-^\dagger\hat{U} = \hat{U}^\dagger\hat{\sigma}_+\hat{U} = \hat{\sigma}_+\mathrm{e}^{\mathrm{i}\omega t}, \tag{A.13}$$

where we used the fact that $\hat{\sigma}_-^\dagger = \hat{\sigma}_+$.

Die approbierte gedruckte Originalversion dieser Diplomarbeit ist an der TU Wien Bibliothek verfügbar
The approved original version of this thesis is available in print at TU Wien Bibliothek.
TU Bibliothek Your knowledge hub WIEN

A.3 Calculating Eigenenergies and Eigenvectors of the Jaynes-Cummings Hamiltonian

To begin with, we write the Jaynes-Cummings Hamiltonian

$$\hat{H}_{\mathrm{JC}} = \hbar\omega_c \hat{a}^\dagger \hat{a} + \frac{\hbar\omega_s}{2}\hat{\sigma}_z + \mathrm{i}\hbar g\left(\hat{\sigma}_- \hat{a}^\dagger - \hat{\sigma}_+ \hat{a}\right), \tag{A.14}$$

in matrix form

$$\hat{H} = \begin{array}{cc} |g, n+1\rangle & |e, n\rangle \\ \end{array} \begin{pmatrix} \hbar\omega_c(n+1) - \frac{1}{2}\hbar\omega_s & \mathrm{i}\hbar g\sqrt{n+1} \\ -\mathrm{i}\hbar g\sqrt{n+1} & \hbar\omega_c n + \frac{1}{2}\hbar\omega_s \end{pmatrix}. \tag{A.15}$$

Since the Hilbert space of the system can be written as $\hat{H}_{\mathrm{cavity}} \otimes \hat{H}_{\mathrm{spin}}$, we choose the vectors $|g, n+1\rangle$ and $|e, n\rangle$ as basis vectors. The spin is either in the ground (g) or excited (e) state, the number of photons in the cavity is denoted by n and $n+1$, respectively.

The eigenvalues λ of a matrix are solutions of $\det(\hat{H} - \lambda \cdot \mathbb{1}) = 0$, we obtain

$$\begin{aligned} 0 &= \left(\hbar\omega_c(n+1) - \frac{1}{2}\hbar\omega_s - \lambda\right) \cdot \left(\hbar\omega_c n + \frac{1}{2}\hbar\omega_s - \lambda\right) \\ &\quad - \left(\mathrm{i}\hbar g\sqrt{n+1}\right) \cdot \left(-\mathrm{i}\hbar g\sqrt{n+1}\right) \\ &= \lambda^2 - \lambda\hbar\omega_c\left(2n+1\right) + \hbar^2\omega_c^2 n\left(n+1\right) - \frac{1}{4}\hbar^2\omega_s^2 + \frac{1}{2}\hbar^2\omega_c\omega_s - \hbar^2 g^2\left(n+1\right). \end{aligned} \tag{A.16}$$

Solving the quadratic equation leads to the following eigenvalues

$$\begin{aligned} \lambda_\pm &= \frac{1}{2} \cdot \Big[\hbar\omega_c(2n+1) \\ &\qquad \pm\sqrt{\hbar^2\omega_c^2(2n+1)^2 - 4\hbar^2\omega_c^2 n(n+1) + \hbar^2\omega_s^2 - 2\hbar^2\omega_c\omega_s + 4\hbar^2 g^2(n+1)}\Big] \\ &= \hbar\omega_c\left(n + \frac{1}{2}\right) \pm \frac{1}{2}\sqrt{4\hbar^2 g^2(n+1) + \hbar^2(\omega_c - \omega_s)^2} \\ &= \hbar\omega_c\left(n + \frac{1}{2}\right) \pm \frac{1}{2}\hbar\sqrt{\Omega_n^2 + \delta^2}, \end{aligned} \tag{A.17}$$

with $\Omega_n = 2g\sqrt{n+1}$ and $\delta = \omega_c - \omega_s$. After calculating the eigenvalues we want to calculate the eigenvectors. Therefore, we have to solve $\hat{H}\,|\phi\rangle = \lambda\,|\phi\rangle$. To start with, we calculate the corresponding eigenvector to λ_+, i.e., we solve the equation $(\hat{H} - \lambda_+ \cdot \mathbb{1})\,|\phi\rangle = 0$. Additionally, we decompose the eigenvector into $|\phi\rangle = \alpha\,|g, n+1\rangle + \beta\,|e, n\rangle$ which gives

$$\begin{pmatrix} -\frac{\hbar}{2}\sqrt{\Omega_n^2 + \delta^2} + \frac{1}{2}\delta\hbar & \frac{\mathrm{i}\hbar\Omega_n}{2} \\ -\frac{\mathrm{i}\hbar\Omega_n}{2} & -\frac{\hbar}{2}\sqrt{\Omega_n^2 + \delta^2} - \frac{1}{2}\delta\hbar \end{pmatrix} \cdot \begin{pmatrix} |g, n+1\rangle \\ |e, n\rangle \end{pmatrix} = 0. \tag{A.18}$$

Die approbierte gedruckte Originalversion dieser Diplomarbeit ist an der TU Wien Bibliothek verfügbar
The approved original version of this thesis is available in print at TU Wien Bibliothek.
TU Bibliothek Your knowledge hub WIEN

By explicitly writing down the first line one gets

$$\begin{aligned}|e,n\rangle &= -\frac{2}{\mathrm{i}\hbar\Omega_n}\cdot\left(-\frac{\hbar}{2}\sqrt{\Omega_n^2+\delta^2}+\frac{1}{2}\delta\hbar\right)|g,n+1\rangle \\ &= \mathrm{i}\left(-\frac{\sqrt{\Omega_n^2+\delta^2}}{\Omega_n}+\frac{\delta}{\Omega_n}\right)|g,n+1\rangle = \mathrm{i}\frac{-\sqrt{\frac{\Omega_n^2}{\delta^2}+1}+1}{\frac{\Omega_n}{\delta}}|g,n+1\rangle\,.\end{aligned} \tag{A.19}$$

Now we substitute $\tan(2\theta)=\frac{\Omega_n}{\delta}$ which gives

$$\begin{aligned}|e,n\rangle &= \mathrm{i}\frac{-\sqrt{\tan^2(2\theta)+1}+1}{\tan(2\theta)}|g,n+1\rangle = \mathrm{i}\frac{-\sqrt{\frac{1}{\cos^2(2\theta)}}+1}{\tan(2\theta)}|g,n+1\rangle \\ &= \mathrm{i}\frac{-1+\cos(2\theta)}{\cos(2\theta)\tan(2\theta)}|g,n+1\rangle\,,\end{aligned} \tag{A.20}$$

where we used the trigonometric identity $1+\tan^2(x)=\frac{1}{\cos^2(x)}$. By using $\cos(2x)=\frac{1-\tan^2(x)}{1+\tan^2(x)}$ and $\tan(2x)=\frac{2\tan(x)}{1-\tan^2(x)}$ we get

$$\begin{aligned}|e,n\rangle &= \mathrm{i}\frac{-1+\frac{1-\tan^2(\theta)}{1+\tan^2(\theta)}}{\frac{1-\tan^2(\theta)}{1+\tan^2(\theta)}\frac{2\tan(\theta)}{1-\tan^2(\theta)}}|g,n+1\rangle = \mathrm{i}\frac{-1-\tan^2(\theta)+1-tan^2(\theta)}{2\tan(\theta)}|g,n+1\rangle \\ &= -\mathrm{i}\tan(\theta)|g,n+1\rangle\,,\end{aligned} \tag{A.21}$$

which leads to the following eigenvector

$$|n,+\rangle = \sin(\theta)|g,n+1\rangle + \mathrm{i}\cos(\theta)|e,n\rangle\,. \tag{A.22}$$

Now we calculate the eigenvector to λ_-, the starting point therefore is

$$\begin{pmatrix}\frac{\hbar}{2}\sqrt{\Omega_n^2+\delta^2}+\frac{1}{2}\delta\hbar & \frac{\mathrm{i}\hbar\Omega_n}{2} \\ -\frac{\mathrm{i}\hbar\Omega_n}{2} & \frac{\hbar}{2}\sqrt{\Omega_n^2+\delta^2}-\frac{1}{2}\delta\hbar\end{pmatrix}\cdot\begin{pmatrix}|g,n+1\rangle \\ |e,n\rangle\end{pmatrix}=0. \tag{A.23}$$

The calculation is the same as before, only the sign of the square root changes from minus to plus. We end up with

$$|e,n\rangle = \frac{\mathrm{i}}{\tan(\theta)}|g,n+1\rangle\,, \tag{A.24}$$

which leads to the following eigenvector

$$|n,-\rangle = \cos(\theta)|g,n+1\rangle - \mathrm{i}\sin(\theta)|e,n\rangle\,. \tag{A.25}$$

Die approbierte gedruckte Originalversion dieser Diplomarbeit ist an der TU Wien Bibliothek verfügbar
The approved original version of this thesis is available in print at TU Wien Bibliothek.
TU Bibliothek WIEN Your knowledge hub

Now we want to calculate the eigenenergies and eigenvalues for the Jaynes-Cummings Hamiltonian written in a different form, i.e.,

$$\hat{H}_{\mathrm{JC}} = \hbar\omega_c \hat{a}^\dagger \hat{a} + \frac{\hbar\omega_s}{2}\hat{\sigma}_z + \hbar g \left(\hat{\sigma}_- \hat{a}^\dagger + \hat{\sigma}_+ \hat{a}\right), \tag{A.26}$$

which written in matrix form gives

$$\hat{H} = \begin{array}{c} \begin{array}{cc} |g, n+1\rangle & |e, n\rangle \end{array} \\ \begin{pmatrix} \hbar\omega_c(n+1) - \frac{1}{2}\hbar\omega_s & \hbar g\sqrt{n+1} \\ \hbar g\sqrt{n+1} & \hbar\omega_c n + \frac{1}{2}\hbar\omega_s \end{pmatrix} \end{array}. \tag{A.27}$$

This matrix leads to the same characteristic polynomial as written in Eq. (A.16) and therefore gives exactly the same eigenvalues as before (and as written in Eq. (A.17)). To obtain the eigenvectors, we do the same steps as before and obtain the following relation

$$|e, n\rangle = -\frac{2}{\hbar\Omega_n} \cdot \left(-\frac{\hbar}{2}\sqrt{\Omega_n^2 + \delta^2} + \frac{1}{2}\delta\hbar\right) |g, n+1\rangle, \tag{A.28}$$

where, when we compare Eq. (A.28) with Eq. (A.19), a factor of $-\mathrm{i}$ is missing. Therefore, we divide the before obtained result (Eq. (A.21)) by that factor which leads to

$$|e, n\rangle = \tan(\theta)\, |g, n+1\rangle, \tag{A.29}$$

and therefore

$$|n, +\rangle = \sin(\theta)\, |g, n+1\rangle + \cos(\theta)\, |e, n\rangle \tag{A.30}$$

is the first eigenvector. The other eigenvector is obtained in the same way, we again get a missing factor of $-\mathrm{i}$. By dividing Eq. (A.24) by that factor we get

$$|e, n\rangle = -\frac{1}{\tan(\theta)}\, |g, n+1\rangle, \tag{A.31}$$

which leads to

$$|n, -\rangle = \cos(\theta)\, |g, n+1\rangle - \sin(\theta)\, |e, n\rangle, \tag{A.32}$$

for the second eigenvector.

A.4 Unitary Transformation of driven Tavis-Cummings Hamiltonian

We now want to do a unitary transformation so that we get rid of the time dependence of the driven Tavis-Cummings Hamiltonian. This is equivalent to transform the Hamiltonian into the rotating frame, i.e., we want to transfer it into that system

Die approbierte gedruckte Originalversion dieser Diplomarbeit ist an der TU Wien Bibliothek verfügbar
The approved original version of this thesis is available in print at TU Wien Bibliothek.
TU Bibliothek Your knowledge hub WIEN

which rotates with the spins. Therefore, we first have to derive the transformation rule. Starting point is the Schrödinger equation

$$\frac{\mathrm{d}}{\mathrm{d}t}|\tilde{\psi}\rangle = -\frac{\mathrm{i}}{\hbar}\tilde{\hat{H}}. \tag{A.33}$$

The left hand side can be expressed as

$$\begin{aligned}\frac{\mathrm{d}}{\mathrm{d}t}\left(\hat{U}^\dagger|\psi\rangle\right) &= \frac{\mathrm{d}}{\mathrm{d}t}\left(\hat{U}^\dagger\right)\hat{U}\hat{U}^\dagger|\psi\rangle + \hat{U}^\dagger\frac{\mathrm{d}}{\mathrm{d}t}|\psi\rangle = \frac{\mathrm{d}}{\mathrm{d}t}\left(\hat{U}^\dagger\right)\hat{U}\hat{U}^\dagger|\psi\rangle \\ &+ \hat{U}^\dagger\left(-\frac{\mathrm{i}}{\hbar}\right)\hat{H}\hat{U}\hat{U}^\dagger|\psi\rangle = -\frac{\mathrm{i}}{\hbar}\left(\mathrm{i}\hbar\frac{\mathrm{d}}{\mathrm{d}t}\left(\hat{U}^\dagger\right)\hat{U} + \hat{U}^\dagger\hat{H}\hat{U}\right)\left|\tilde{\psi}\right\rangle,\end{aligned} \tag{A.34}$$

where we use $|\tilde{\psi}\rangle = \hat{U}^\dagger|\psi\rangle$ and $\hat{U}\hat{U}^\dagger$ can be inserted arbitrarily since that is equal to $\mathbb{1}$. By comparing Eq. (A.33) with Eq. (A.34) one sees that

$$\tilde{\hat{H}} = \mathrm{i}\hbar\frac{\mathrm{d}}{\mathrm{d}t}\left(\hat{U}^\dagger\right)\hat{U} + \hat{U}^\dagger\hat{H}\hat{U}. \tag{A.35}$$

Finally, we use the unitarity of $\hat{U}$, i.e., $\hat{U}^\dagger\hat{U} = \mathbb{1}$ and calculate the time derivative, i.e.,

$$\frac{\mathrm{d}}{\mathrm{d}t}\left(\hat{U}^\dagger\right)\hat{U} + \hat{U}^\dagger\frac{\mathrm{d}}{\mathrm{d}t}\left(\hat{U}\right) = 0, \tag{A.36}$$

with which one can rewrite Eq. (A.35). One ends up with

$$\tilde{\hat{H}} = \hat{U}^\dagger\hat{H}\hat{U} - \mathrm{i}\hbar\hat{U}^\dagger\dot{\hat{U}}. \tag{A.37}$$

With that said, it is clear how to transform the Tavis Cummmings Hamiltonian into the rotating frame. we start with

$$\hat{H} = \hbar\omega_c\hat{a}^\dagger\hat{a} + \sum_j\frac{\hbar\omega_s^j}{2}\hat{\sigma}_z^j + \sum_j\mathrm{i}\hbar g_j\left(\hat{\sigma}_-^j\hat{a}^\dagger - \hat{\sigma}_+^j\hat{a}\right) + \mathrm{i}\hbar\eta\left(\hat{a}^\dagger\mathrm{e}^{-\mathrm{i}\omega_d t} - \hat{a}\mathrm{e}^{\mathrm{i}\omega_d t}\right), \tag{A.38}$$

and transform it according to $\tilde{\hat{H}} = \hat{U}^\dagger\hat{H}\hat{U} - \mathrm{i}\hbar\hat{U}^\dagger\dot{\hat{U}}$ with $\hat{U}$ being

$$\hat{U} = \mathrm{e}^{-\mathrm{i}\omega_d t\left(\hat{a}^\dagger\hat{a} + \sum_i\frac{\hat{\sigma}_z^i}{2}\right)} = \mathrm{e}^{-\mathrm{i}\omega_d\hat{a}^\dagger\hat{a}t}\mathrm{e}^{-\mathrm{i}\omega_d\sum_i\frac{\hat{\sigma}_z^i}{2}t} = \hat{U}_a\hat{U}_\sigma. \tag{A.39}$$

First, we have a look on $\hat{U}^\dagger\hat{H}\hat{U}$. For doing that calculation we use the serial expression of the exponential function $\mathrm{e}^x = 1 + x + \frac{x^2}{2} + \ldots$. By doing so, one can easily see that $[\hat{a}^\dagger\hat{a}, \hat{U}] = 0$ since $[\hat{a}^\dagger\hat{a}, \hat{a}^\dagger\hat{a}] = 0$ and therefore the first term of the Hamiltonian does not change. The same holds for the second term which commutes with the $\hat{\sigma}_z$ operator of the exponential. Please note that because the operators $\hat{a}$ and $\hat{\sigma}$ act in different Hilbert spaces they trivially commute with the exponential

Die approbierte gedruckte Originalversion dieser Diplomarbeit ist an der TU Wien Bibliothek verfügbar
The approved original version of this thesis is available in print at TU Wien Bibliothek.
TU Bibliothek Your knowledge hub WIEN

of the other operator, i.e., $\hat{a}$ commutes with $\hat{U}_\sigma$ and $\hat{\sigma}$ commutes with $\hat{U}_a$. For the third term we get

$$\begin{aligned}\hat{U}^\dagger \sum_j \mathrm{i}\hbar g_j \left(\hat{\sigma}_-^j \hat{a}^\dagger - \hat{\sigma}_+^j \hat{a}\right) \hat{U} &= \sum_j \mathrm{i}\hbar g_j \left(\hat{U}^\dagger \hat{\sigma}_-^j \hat{U}\hat{U}^\dagger \hat{a}^\dagger \hat{U} - \hat{U}^\dagger \hat{\sigma}_+^j \hat{U}\hat{U}^\dagger \hat{a}\hat{U}\right) \\ &= \sum_j \mathrm{i}\hbar g_j \left(\hat{U}_\sigma^\dagger \hat{\sigma}_-^j \hat{U}_\sigma \hat{U}_a^\dagger \hat{a}^\dagger \hat{U}_a - \hat{U}_\sigma^\dagger \hat{\sigma}_+^j \hat{U}_\sigma \hat{U}_a^\dagger \hat{a}\hat{U}_a\right),\end{aligned} \tag{A.40}$$

where we inserted $\hat{U}\hat{U}^\dagger = \mathbb{1}$ and use the fact that $\hat{a}$ and $\hat{\sigma}$ act in different Hilbert spaces and therefore commute with the unitary transformation operators containing the other operators. Now we have a sum over the different $\hat{\sigma}_i$ operators in $\hat{U}_\sigma$ and $\hat{U}_\sigma^\dagger$ as well as in Eq. (A.40). Now we use the fact that for $i \neq j$ the operators commute, only for $i = j$ they do not. By using the in Sec. A.2 derived transformation relation, we get

$$\sum_{i=j} \mathrm{i}\hbar g_j \left(\hat{\sigma}_-^j \mathrm{e}^{-\mathrm{i}\omega_d t} \hat{a}^\dagger \mathrm{e}^{\mathrm{i}\omega_d t} - \hat{\sigma}_+^j \mathrm{e}^{\mathrm{i}\omega_d t} \hat{a} \mathrm{e}^{-\mathrm{i}\omega_d t}\right) = \sum_j \mathrm{i}\hbar g_j \left(\hat{\sigma}_-^j \hat{a}^\dagger - \hat{\sigma}_+^j \hat{a}\right), \tag{A.41}$$

which means that the third term of the Hamiltonian stays unchanged as well. Now we transform the last term which gives

$$\begin{aligned}\hat{U}^\dagger \mathrm{i}\hbar\eta \left(\hat{a}^\dagger \mathrm{e}^{-\mathrm{i}\omega_d t} - \hat{a}\mathrm{e}^{\mathrm{i}\omega_d t}\right) \hat{U} &= \mathrm{i}\hbar\eta \left(\hat{U}_a^\dagger \hat{a}^\dagger \hat{U}_a \mathrm{e}^{-\mathrm{i}\omega_d t} - \hat{U}_a^\dagger \hat{a}\hat{U}_a \mathrm{e}^{\mathrm{i}\omega_d t}\right) \\ &= \mathrm{i}\hbar\eta \left(\hat{a}^\dagger \mathrm{e}^{\mathrm{i}\omega_d t}\mathrm{e}^{-\mathrm{i}\omega_d t} - \hat{a}\mathrm{e}^{-\mathrm{i}\omega_d t}\mathrm{e}^{\mathrm{i}\omega_d t}\right) = \mathrm{i}\hbar\eta \left(\hat{a}^\dagger - \hat{a}\right),\end{aligned} \tag{A.42}$$

where we again use the fact that $\hat{a}$ commutes with $\hat{U}_\sigma$. By inserting the before derived transformation relation we see that the exponential factors cancel each other. We reached our first goal and got rid of the time dependency of the driving term. Last but not least we have to calculate the term $-\mathrm{i}\hbar\hat{U}^\dagger\dot{\hat{U}}$. The time derivative leads to

$$\dot{\hat{U}} = -\mathrm{i}\omega_d \left(\hat{a}^\dagger \hat{a} + \sum_i \frac{\hat{\sigma}_z^i}{2}\right) \hat{U}, \tag{A.43}$$

the last term therefore finally gives

$$-\mathrm{i}\hbar\hat{U}^\dagger\dot{\hat{U}} = -\hbar\omega_d \left(\hat{a}^\dagger \hat{a} + \sum_i \frac{\hat{\sigma}_z^i}{2}\right). \tag{A.44}$$

Putting all parts together we end up with the transformed and now time independent Tavis-Cummings Hamiltonian

$$\hat{H} = \hbar\Delta_c \hat{a}^\dagger \hat{a} + \sum_j \frac{\hbar\Delta_s^j}{2} \hat{\sigma}_z^i + \sum_j \mathrm{i}\hbar g_j \left(\hat{\sigma}_-^j \hat{a}^\dagger - \hat{\sigma}_+^j \hat{a}\right) + \mathrm{i}\hbar\eta \left(\hat{a}^\dagger - \hat{a}\right), \tag{A.45}$$

where $\Delta_j^{(i)} = \omega_j^{(i)} - \omega_d$ denote the corresponding detunings from the drive frequency.

Die approbierte gedruckte Originalversion dieser Diplomarbeit ist an der TU Wien Bibliothek verfügbar
The approved original version of this thesis is available in print at TU Wien Bibliothek.
TU Bibliothek Your knowledge hub WIEN

A.5 Derivation of the Lindblad Master Equation

Now we want to derive equations of motion for our system operators which are coupled to a bath. The starting point of the derivation is the von Neumann equation

$$\frac{\mathrm{d}\hat{\rho}_{\mathrm{tot}}}{\mathrm{d}t} = -\frac{\mathrm{i}}{\hbar}\left[\hat{H}_{\mathrm{tot}}, \hat{\rho}_{\mathrm{tot}}\right], \tag{A.46}$$

where $\hat{H}_{\mathrm{tot}} = \hat{H}_S + \hat{H}_B + \hat{H}_{\mathrm{int}}$ is the Hamiltonian of the total system which consists of a system, a bath and an interaction part. We now want to find an expression for the density matrix of the system and want therefore to trace out the components of the bath. This can be done more easily in the Interaction picture, the unitary transformation of an operator reads like $\tilde{\hat{O}} = \hat{U}_0^\dagger \hat{O} \hat{U}_0$ with $\hat{U}_0 = \mathrm{e}^{-\mathrm{i}(\hat{H}_S + \hat{H}_B)t}$. After the transformation, the von Neumann equation reads

$$\frac{\mathrm{d}\tilde{\hat{\rho}}_{\mathrm{tot}}}{\mathrm{d}t} = -\frac{\mathrm{i}}{\hbar}\left[\tilde{\hat{H}}_{\mathrm{int}}, \tilde{\hat{\rho}}_{\mathrm{tot}}\right]. \tag{A.47}$$

After integrating this equation, one gets

$$\tilde{\hat{\rho}}_{\mathrm{tot}}(t) = \tilde{\hat{\rho}}_{\mathrm{tot}}(0) - \frac{\mathrm{i}}{\hbar}\int_0^t \mathrm{d}t' \left[\tilde{\hat{H}}_{\mathrm{int}}(t'), \tilde{\hat{\rho}}_{\mathrm{tot}}(t')\right], \tag{A.48}$$

where we now for clarification added the time dependence. Substituting this expression back into the von Neumann equation yields

$$\frac{\mathrm{d}\tilde{\hat{\rho}}_{\mathrm{tot}}}{\mathrm{d}t} = -\frac{\mathrm{i}}{\hbar}\left[\tilde{\hat{H}}_{\mathrm{int}}(t), \tilde{\hat{\rho}}_{\mathrm{tot}}(0)\right] - \frac{1}{\hbar^2}\int_0^t \mathrm{d}t' \left[\tilde{\hat{H}}_{\mathrm{int}}(t), \left[\tilde{\hat{H}}_{\mathrm{int}}(t'), \tilde{\hat{\rho}}_{\mathrm{tot}}(t')\right]\right]. \tag{A.49}$$

By now, we did not make any assumptions. This is no longer the case, we now assume that the interaction starts at time $t = 0$ and that there are no correlations between the bath and the system at that time. Following that assumptions, the initial density matrix is factorizable, i.e., $\tilde{\hat{\rho}}_{\mathrm{tot}}(0) = \tilde{\hat{\rho}}_S(0) \otimes \tilde{\hat{\rho}}_B(0)$. Now we are able to trace out the unwanted components, i.e., the bath components to get the density matrix of the system:

$$\begin{aligned}\mathrm{Tr_B}\left\{\frac{\mathrm{d}\tilde{\hat{\rho}}_{\mathrm{tot}}}{\mathrm{d}t}\right\} = &-\frac{\mathrm{i}}{\hbar}\mathrm{Tr_B}\left\{\left[\tilde{\hat{H}}_{\mathrm{int}}(t), \tilde{\hat{\rho}}_S(0)\tilde{\hat{\rho}}_B(0)\right]\right\} \\ &- \frac{1}{\hbar^2}\int_0^t \mathrm{d}t'\ \mathrm{Tr_B}\left\{\left[\tilde{\hat{H}}_{\mathrm{int}}(t), \left[\tilde{\hat{H}}_{\mathrm{int}}(t'), \tilde{\hat{\rho}}_{\mathrm{tot}}(t')\right]\right]\right\}.\end{aligned} \tag{A.50}$$

The first term on the right hand side of the equation is usually zero. If that is not the case, we can redefine the Interaction and the System Hamiltonian to obtain that result. Therefore, we omit the first term without loss of generality. To be able to

Die approbierte gedruckte Originalversion dieser Diplomarbeit ist an der TU Wien Bibliothek verfügbar
The approved original version of this thesis is available in print at TU Wien Bibliothek.
TU Bibliothek Your knowledge hub WIEN

solve the remaining equation, one has to know the complete dynamics of the density matrix of the whole system. When we state that the bath is big and the coupling is rather small, the bath eigenvectors stay (nearly) the same and therefore one can make the assumption that $\tilde{\hat{\rho}}_{\text{tot}}(t) = \tilde{\hat{\rho}}_S(t) \otimes \tilde{\hat{\rho}}_B(0)$ which leads to

$$\mathrm{Tr_B}\left\{\frac{\mathrm{d}\tilde{\hat{\rho}}_{\text{tot}}}{\mathrm{d}t}\right\} = -\frac{1}{\hbar^2}\int_0^t \mathrm{d}t'\ \mathrm{Tr_B}\left\{\left[\tilde{\hat{H}}_{\text{int}}(t), \left[\tilde{\hat{H}}_{\text{int}}(t'), \tilde{\hat{\rho}}_S(t')\tilde{\hat{\rho}}_B(0)\right]\right]\right\}. \tag{A.51}$$

This equation is very difficult to solve. Therefore, we make a last approximation. We assume that the density matrix depends only on its current state and not on its past values. This assumption is valid under fast bath dynamics wherein correlations (in the bath) are lost extremely quickly. We end up with

$$\mathrm{Tr_B}\left\{\frac{\mathrm{d}\tilde{\hat{\rho}}_{\text{tot}}}{\mathrm{d}t}\right\} = -\frac{1}{\hbar^2}\int_0^t \mathrm{d}t'\ \mathrm{Tr_B}\left\{\left[\tilde{\hat{H}}_{\text{int}}(t), \left[\tilde{\hat{H}}_{\text{int}}(t'), \tilde{\hat{\rho}}_S(t)\tilde{\hat{\rho}}_B(0)\right]\right]\right\}. \tag{A.52}$$

We now assume that the interaction Hamiltonian is of the following form

$$\tilde{\hat{H}}_{\text{int}}(t) = \hbar\left(\hat{S}(t)\hat{B}^\dagger(t) + \hat{S}^\dagger(t)\hat{B}(t)\right), \tag{A.53}$$

where $\hat{S}^\dagger$ and $\hat{S}$ are the creation and annihilation operators acting in the system, $\hat{B}^\dagger$ and $\hat{B}$ are acting in the bath, respectively. Let us now calculate the double commutator

$$\begin{aligned}
&\left[\tilde{\hat{H}}_{\text{int}}(t), \left[\tilde{\hat{H}}_{\text{int}}(t'), \tilde{\hat{\rho}}_S(t)\tilde{\hat{\rho}}_B(0)\right]\right] \\
&= \hbar^2\left[\hat{S}(t)\hat{B}^\dagger(t) + \hat{S}^\dagger(t)\hat{B}(t), \left[\hat{S}(t')\hat{B}^\dagger(t') + \hat{S}^\dagger(t')\hat{B}(t'), \tilde{\hat{\rho}}_S(t)\tilde{\hat{\rho}}_B(0)\right]\right] \\
&= \Big[\hat{S}(t)\hat{B}^\dagger(t) + \hat{S}^\dagger(t)\hat{B}(t),\ \Big\{\hat{S}(t')\hat{B}^\dagger(t')\tilde{\hat{\rho}}_S(t)\tilde{\hat{\rho}}_B(0) + \hat{S}^\dagger(t')\hat{B}(t')\tilde{\hat{\rho}}_S(t)\tilde{\hat{\rho}}_B(0) \\
&-\tilde{\hat{\rho}}_S(t)\tilde{\hat{\rho}}_B(0)\hat{S}(t')\hat{B}^\dagger(t') - \tilde{\hat{\rho}}_S(t)\tilde{\hat{\rho}}_B(0)\hat{S}^\dagger(t')\hat{B}(t')\Big\}\Big],
\end{aligned} \tag{A.54}$$

where we for convenience set $\hbar = 1$ (which is fine because $\hbar$ drops out when we finally insert the result in Eq. (A.52)). Now we use $[[\hat{A} + \hat{B}], \hat{C}] = [\hat{A}, \hat{C}] + [\hat{B}, \hat{C}]$ and get for the first term

$$\begin{aligned}
[\hat{A}, \hat{C}] =& \hat{S}(t)\hat{B}^\dagger(t)\left[\hat{S}(t')\hat{B}^\dagger(t') + \hat{S}^\dagger(t')\hat{B}(t')\right]\tilde{\hat{\rho}}_S(t)\tilde{\hat{\rho}}_B(0) \\
&-\hat{S}(t)\hat{B}^\dagger(t)\tilde{\hat{\rho}}_S(t)\tilde{\hat{\rho}}_B(0)\left[\hat{S}(t')\hat{B}^\dagger(t') + \hat{S}^\dagger(t')\hat{B}(t')\right] \\
&-\left[\hat{S}(t')\hat{B}^\dagger(t') + \hat{S}^\dagger(t')\hat{B}(t')\right]\tilde{\hat{\rho}}_S(t)\tilde{\hat{\rho}}_B(0)\hat{S}(t)\hat{B}^\dagger(t) \\
&+\tilde{\hat{\rho}}_S(t)\tilde{\hat{\rho}}_B(0)\left[\hat{S}(t')\hat{B}^\dagger(t') + \hat{S}^\dagger(t')\hat{B}(t')\right]\hat{S}(t)\hat{B}^\dagger(t),
\end{aligned} \tag{A.55}$$

Die approbierte gedruckte Originalversion dieser Diplomarbeit ist an der TU Wien Bibliothek verfügbar
The approved original version of this thesis is available in print at TU Wien Bibliothek.
TU Bibliothek Your knowledge hub WIEN

and for the second term

$$
\begin{aligned}
[\hat{B},\hat{C}] =& \hat{S}^\dagger(t)\hat{B}(t)\left[\hat{S}(t')\hat{B}^\dagger(t')+\hat{S}^\dagger(t')\hat{B}(t')\right]\tilde{\hat{\rho}}_S(t)\tilde{\hat{\rho}}_B(0)\\
&-\hat{S}^\dagger(t)\hat{B}(t)\tilde{\hat{\rho}}_S(t)\tilde{\hat{\rho}}_B(0)\left[\hat{S}(t')\hat{B}^\dagger(t')+\hat{S}^\dagger(t')\hat{B}(t')\right]\\
&-\left[\hat{S}(t')\hat{B}^\dagger(t')+\hat{S}^\dagger(t')\hat{B}(t')\right]\tilde{\hat{\rho}}_S(t)\tilde{\hat{\rho}}_B(0)\hat{S}^\dagger(t)\hat{B}(t)\\
&+\tilde{\hat{\rho}}_S(t)\tilde{\hat{\rho}}_B(0)\left[\hat{S}(t')\hat{B}^\dagger(t')+\hat{S}^\dagger(t')\hat{B}(t')\right]\hat{S}^\dagger(t)\hat{B}(t).
\end{aligned}
\tag{A.56}
$$

Now we can sort the different terms in groups of $\hat{S}$ and $\hat{B}$ operators. this is allowed since they commute, i.e., $[\hat{S},\hat{B}]=0$ because they act in different Hilbert spaces. After doing so, we can take the trace over the bath as well. For that we use the fact that the trace only affects the components of the bath and not the system, i.e., $\mathrm{Tr_B}\left(\hat{S}\hat{B}\hat{\rho}_B(0)\right)=\hat{S}\mathrm{Tr_B}\left(\hat{B}\hat{\rho}_B(0)\right)$. We further use the fact that some of the traces equals to zero, to be more specific traces like $\mathrm{Tr_B}\left[\hat{B}(t)\hat{B}(t')\hat{\rho}_B(0)\right]=\mathrm{Tr_B}\left[\hat{B}^\dagger(t)\hat{B}^\dagger(t')\hat{\rho}_B(0)\right]=0$. Applying all these steps to the expressions above lead to

$$
\begin{aligned}
\mathrm{Tr_B}[\hat{A},\hat{C}] =& \hat{S}(t)\hat{S}^\dagger(t')\tilde{\hat{\rho}}_S(t)\mathrm{Tr_B}\left[\hat{B}^\dagger(t)\hat{B}(t')\tilde{\hat{\rho}}_B(0)\right]\\
&-\hat{S}(t)\tilde{\hat{\rho}}_S(t)\hat{S}^\dagger(t')\mathrm{Tr_B}\left[\hat{B}^\dagger(t)\tilde{\hat{\rho}}_B(0)\hat{B}(t')\right]\\
&-\hat{S}^\dagger(t')\tilde{\hat{\rho}}_S(t)\hat{S}(t)\mathrm{Tr_B}\left[\hat{B}(t')\tilde{\hat{\rho}}_B(0)\hat{B}^\dagger(t)\right]\\
&+\tilde{\hat{\rho}}_S(t)\hat{S}^\dagger(t')\hat{S}(t)\mathrm{Tr_B}\left[\tilde{\hat{\rho}}_B(0)\hat{B}(t')\hat{B}^\dagger(t)\right]
\end{aligned}
\tag{A.57}
$$

for the first and

$$
\begin{aligned}
\mathrm{Tr_B}[\hat{B},\hat{C}] =& \hat{S}^\dagger(t)\hat{S}(t')\tilde{\hat{\rho}}_S(t)\mathrm{Tr_B}\left[\hat{B}(t)\hat{B}^\dagger(t')\tilde{\hat{\rho}}_B(0)\right]\\
&-\hat{S}^\dagger(t)\tilde{\hat{\rho}}_S(t)\hat{S}(t')\mathrm{Tr_B}\left[\hat{B}(t)\tilde{\hat{\rho}}_B(0)\hat{B}^\dagger(t')\right]\\
&-\hat{S}(t')\tilde{\hat{\rho}}_S(t)\hat{S}^\dagger(t)\mathrm{Tr_B}\left[\hat{B}^\dagger(t')\tilde{\hat{\rho}}_B(0)\hat{B}(t)\right]\\
&+\tilde{\hat{\rho}}_S(t)\hat{S}(t')\hat{S}^\dagger(t)\mathrm{Tr_B}\left[\tilde{\hat{\rho}}_B(0)\hat{B}^\dagger(t')\hat{B}(t)\right]
\end{aligned}
\tag{A.58}
$$

Die approbierte gedruckte Originalversion dieser Diplomarbeit ist an der TU Wien Bibliothek verfügbar
The approved original version of this thesis is available in print at TU Wien Bibliothek.
TU Bibliothek Your knowledge hub WIEN

for the second term. Using the cyclic property of traces, i.e., $\mathrm{Tr}\left[\hat{A}\hat{B}\hat{C}\right] = \mathrm{Tr}\left[\hat{C}\hat{A}\hat{B}\right]$ $= \mathrm{Tr}\left[\hat{B}\hat{C}\hat{A}\right]$ and adding both terms yields

$$\begin{aligned}\mathrm{Tr_B}[\hat{A},\hat{C}] + \mathrm{Tr_B}[\hat{B},\hat{C}] = &\left[\hat{S}(t)\hat{S}^\dagger(t')\tilde{\hat{\rho}}_S(t) - \hat{S}^\dagger(t')\tilde{\hat{\rho}}_S(t)\hat{S}(t)\right]\mathrm{Tr_B}\left[\hat{B}^\dagger(t)\hat{B}(t')\tilde{\hat{\rho}}_B(0)\right]\\ &+\left[\tilde{\hat{\rho}}_S(t)\hat{S}^\dagger(t')\hat{S}(t) - \hat{S}(t)\tilde{\hat{\rho}}_S(t)\hat{S}^\dagger(t')\right]\mathrm{Tr_B}\left[\hat{B}(t')\hat{B}^\dagger(t)\tilde{\hat{\rho}}_B(0)\right]\\ &+\left[\hat{S}^\dagger(t)\hat{S}(t')\tilde{\hat{\rho}}_S(t) - \hat{S}(t')\tilde{\hat{\rho}}_S(t)\hat{S}^\dagger(t)\right]\mathrm{Tr_B}\left[\hat{B}(t)\hat{B}^\dagger(t')\tilde{\hat{\rho}}_B(0)\right]\\ &+\left[\tilde{\hat{\rho}}_S(t)\hat{S}(t')\hat{S}^\dagger(t) - \hat{S}^\dagger(t)\tilde{\hat{\rho}}_S(t)\hat{S}(t')\right]\mathrm{Tr_B}\left[\hat{B}^\dagger(t')\hat{B}(t)\tilde{\hat{\rho}}_B(0)\right].\end{aligned} \tag{A.59}$$

Now its time to evaluate these traces. We assume that the bath is bosonic, i.e., $\hat{H}_B = \hbar\sum_k \omega_k \hat{a}_k^\dagger \hat{a}_k$. By doing so, we can make the ansatz $\hat{B} = \sum_k g_k^* \hat{a}_k$ where g_k are complex coefficients representing coupling constants [50] and which is written in the Schrödinger picture. To insert this expression into the correlation functions we transform it into the Interaction picture which yields

$$\hat{B}(t) = \sum_k g_k^* \hat{a}_k \mathrm{e}^{-\mathrm{i}\omega_k t}. \tag{A.60}$$

We further assume that the bath is in thermal equilibrium, the density matrix therefore reads

$$\hat{\rho}_B(0) = \prod_j \frac{1}{Z_j}\mathrm{e}^{-\hbar\omega_j \hat{a}_j^\dagger \hat{a}_j/k_B T} = \prod_j \mathrm{e}^{-\hbar\omega_j \hat{a}_j^\dagger \hat{a}_j/k_B T}\left(1 - \mathrm{e}^{-\hbar\omega_j/k_B T}\right), \tag{A.61}$$

where the partition functions Z_j can be obtained via

$$Z_j = \mathrm{Tr}\left[\mathrm{e}^{-\hbar\omega_j \hat{a}_j^\dagger \hat{a}_j/k_B T}\right] = \sum_{n=0}^{\infty}\mathrm{e}^{-\hbar\omega_j n/k_B T} = \frac{1}{1-\mathrm{e}^{-\hbar\omega_j/k_B T}}. \tag{A.62}$$

Using that expressions, the evaluation of the traces give

$$\begin{aligned}\mathrm{Tr_B}\left[\hat{B}^\dagger(t)\hat{B}(t')\tilde{\hat{\rho}}_B(0)\right] &= \sum_{j,k} g_j g_k^* \mathrm{e}^{\mathrm{i}\omega_j t}\mathrm{e}^{-\mathrm{i}\omega_k t'}\mathrm{Tr_B}\left[\hat{a}_j^\dagger \hat{a}_k \tilde{\hat{\rho}}_B(0)\right]\\ &= \sum_k |g_k|^2 \mathrm{e}^{\mathrm{i}\omega_k(t-t')}\bar{n}(\omega_k, T),\end{aligned} \tag{A.63}$$

and

$$\begin{aligned}&\mathrm{Tr_B}\left[\hat{B}(t)\hat{B}^\dagger(t')\tilde{\hat{\rho}}_B(0)\right] = \sum_{j,k} g_j^* g_k \mathrm{e}^{-\mathrm{i}\omega_j t}\mathrm{e}^{\mathrm{i}\omega_k t'}\mathrm{Tr_B}\left[\hat{a}_k \hat{a}_j^\dagger \tilde{\hat{\rho}}_B(0)\right]\\ &= \sum_{j,k} g_j^* g_k \mathrm{e}^{-\mathrm{i}\omega_j t}\mathrm{e}^{\mathrm{i}\omega_k t'}\mathrm{Tr_B}\left[(\hat{a}_j^\dagger \hat{a}_k + 1)\tilde{\hat{\rho}}_B(0)\right] = \sum_k |g_k|^2 \mathrm{e}^{-\mathrm{i}\omega_k(t-t')}\left[\bar{n}(\omega_k, T) + 1\right],\end{aligned} \tag{A.64}$$

Die approbierte gedruckte Originalversion dieser Diplomarbeit ist an der TU Wien Bibliothek verfügbar
The approved original version of this thesis is available in print at TU Wien Bibliothek.
TU Bibliothek Your knowledge hub WIEN

where we used $[\hat{a}, \hat{a}^\dagger] = 1$ in the last step and $\bar{n}(\omega_k, T)$ is defined by

$$\bar{n}(\omega_k, T) = \mathrm{Tr_B}\left[\hat{a}^\dagger \hat{a} \tilde{\hat{\rho}}_B(0)\right] = \frac{\mathrm{e}^{-\hbar\omega_k/k_B T}}{1 - \mathrm{e}^{-\hbar\omega_k/k_B T}}. \tag{A.65}$$

This result is obtained by

$$\begin{aligned} Tr(\hat{a}_k^\dagger \hat{a}_k \mathrm{e}^{-\hbar\omega_k \hat{a}_k^\dagger \hat{a}_k \beta}) &= \sum_{n=0}^{\infty} n \mathrm{e}^{-\hbar\omega_k n\beta} = \mathrm{e}^{-\hbar\omega_k\beta} \partial_{\hbar\omega_k\beta} \sum_{n=0}^{\infty} \mathrm{e}^{-\hbar\omega_k n\beta} \\ &= \mathrm{e}^{-\hbar\omega_k\beta} \partial_{\hbar\omega_k\beta} \frac{1}{1 - \mathrm{e}^{-\hbar\omega_k\beta}} = \frac{\mathrm{e}^{-\hbar\omega_k\beta}}{(1 - \mathrm{e}^{-\hbar\omega_k\beta})^2}, \end{aligned} \tag{A.66}$$

where we use $\beta = 1/k_B T$. This gives, when multiplied with the ignored bracket $(1 - \exp(...))$ of Eq. (A.61), the desired result. With the calculation shown above it is clear as well that the before mentioned relations hold

$$\begin{aligned} \mathrm{Tr_B}\left[\hat{B}(t)\hat{B}(t')\tilde{\hat{\rho}}_B(0)\right] &= \sum_{j,k} g_j^* g_k^* \mathrm{e}^{-\mathrm{i}\omega_j t} \mathrm{e}^{-\mathrm{i}\omega_k t'} \mathrm{Tr_B}\left[\hat{a}_j \hat{a}_k \tilde{\hat{\rho}}_B(0)\right] = 0, \\ \mathrm{Tr_B}\left[\hat{B}(t)^\dagger \hat{B}^\dagger(t')\tilde{\hat{\rho}}_B(0)\right] &= \sum_{j,k} g_j g_k \mathrm{e}^{\mathrm{i}\omega_j t} \mathrm{e}^{\mathrm{i}\omega_k t'} \mathrm{Tr_B}\left[\hat{a}_j^\dagger \hat{a}_k^\dagger \tilde{\hat{\rho}}_B(0)\right] = 0. \end{aligned} \tag{A.67}$$

Furthermore, we want to mention that some of the traces can be expressed with another one by complex conjugating them:

$$\begin{aligned} \left(\mathrm{Tr_B}\left[\hat{B}^\dagger(t)\hat{B}(t')\tilde{\hat{\rho}}_B(0)\right]^T\right)^* &= \left\langle [\hat{B}^\dagger(t)\hat{B}(t')]^T \right\rangle^* \\ &= \left\langle \hat{B}^\dagger(t')\hat{B}(t) \right\rangle = \mathrm{Tr_B}\left[\hat{B}^\dagger(t')\hat{B}(t)\tilde{\hat{\rho}}_B(0)\right], \end{aligned} \tag{A.68}$$

where we can take the transpose of these matrices since the trace stays unaffected.

To make things clearer, we want to get rid of the time dependency of the system operators. Therefore, we assume that the system is bosonic as well, i.e, $\hat{H}_S = \hbar\omega_0 \hat{S}^\dagger \hat{S}$, with which we can transform the system operators. As done before, we can write

$$\hat{S}(t) = \hat{S}\mathrm{e}^{-\mathrm{i}\omega_0 t}, \tag{A.69}$$

which is obtained by transforming the time-independent operator $\hat{S}$ into the Interaction picture. If we take the complex conjugate of that equation we find an expression for the creation operator.

Finally, by using Eqs. (A.69), (A.68), (A.64), (A.63), (A.59) and inserting them

Die approbierte gedruckte Originalversion dieser Diplomarbeit ist an der TU Wien Bibliothek verfügbar
The approved original version of this thesis is available in print at TU Wien Bibliothek.
TU Bibliothek Your knowledge hub WIEN

into Eq. (A.52) one ends up with

$$\begin{aligned}\frac{\mathrm{d}\tilde{\hat{\rho}}_S}{\mathrm{d}t} = &-\int_0^t \mathrm{d}t' \left[\hat{S}\hat{S}^\dagger\tilde{\hat{\rho}}_S(t) - \hat{S}^\dagger\tilde{\hat{\rho}}_S(t)\hat{S}\right] \mathrm{e}^{-\mathrm{i}\omega_0(t-t')} \sum_k |g_k|^2 \mathrm{e}^{\mathrm{i}\omega_k(t-t')}\bar{n}(\omega_k, T) \\ &+ \left[\tilde{\hat{\rho}}_S(t)\hat{S}^\dagger\hat{S} - \hat{S}\tilde{\hat{\rho}}_S(t)\hat{S}^\dagger\right] \mathrm{e}^{-\mathrm{i}\omega_0(t-t')} \sum_k |g_k|^2 \mathrm{e}^{\mathrm{i}\omega_k(t-t')} \left[\bar{n}(\omega_k, T) + 1\right] \\ &+ \left[\hat{S}^\dagger\hat{S}\tilde{\hat{\rho}}_S(t) - \hat{S}\tilde{\hat{\rho}}_S(t)\hat{S}^\dagger\right] \mathrm{e}^{\mathrm{i}\omega_0(t-t')} \sum_k |g_k|^2 \mathrm{e}^{-\mathrm{i}\omega_k(t-t')} \left[\bar{n}(\omega_k, T) + 1\right] \\ &+ \left[\tilde{\hat{\rho}}_S(t)\hat{S}\hat{S}^\dagger - \hat{S}^\dagger\tilde{\hat{\rho}}_S(t)\hat{S}\right] \mathrm{e}^{\mathrm{i}\omega_0(t-t')} \sum_k |g_k|^2 \mathrm{e}^{-\mathrm{i}\omega_k(t-t')}\bar{n}(\omega_k, T),\end{aligned} \tag{A.70}$$

where $\hbar$ drops out when we insert Eq. (A.54) into Eq. (A.52). Now we change from discrete frequency values to continuous ones. The sum sign therefore changes to an integral and we have to multiply with the density of states $J(\omega)$, i.e.,

$$\sum_k |g_k|^2 \mathrm{e}^{\mathrm{i}\omega_k(t-t')}\bar{n}(\omega_k, T) \to \int_0^\infty \mathrm{d}\omega J(\omega)|g(\omega)|^2 \mathrm{e}^{\mathrm{i}\omega(t-t')}\bar{n}(\omega, T). \tag{A.71}$$

Additionally, we make the following substitution for the time $t - t' = \tau$ which lead to integrals of the form

$$\frac{\mathrm{d}\tilde{\hat{\rho}}_S}{\mathrm{d}t} = -\left[\hat{S}\hat{S}^\dagger\tilde{\hat{\rho}}_S(t) - \hat{S}^\dagger\tilde{\hat{\rho}}_S(t)\hat{S}\right] \int_0^t \mathrm{d}\tau \mathrm{e}^{-\mathrm{i}\omega_0\tau} \int_0^\infty \mathrm{d}\omega J(\omega)|g(\omega)|^2 \mathrm{e}^{\mathrm{i}\omega\tau}\bar{n}(\omega, T) + \cdots . \tag{A.72}$$

Now we introduce some constants

$$\alpha = \int_0^t \mathrm{d}\tau \int_0^\infty \mathrm{d}\omega J(\omega)|g(\omega)|^2 \mathrm{e}^{-\mathrm{i}(\omega-\omega_0)\tau}, \tag{A.73}$$

$$\beta = \int_0^t \mathrm{d}\tau \int_0^\infty \mathrm{d}\omega J(\omega)|g(\omega)|^2 \mathrm{e}^{-\mathrm{i}(\omega-\omega_0)\tau}\bar{n}(\omega, T), \tag{A.74}$$

which after inserting them into Eq. (A.70) leads to

$$\begin{aligned}\frac{\mathrm{d}\tilde{\hat{\rho}}_S}{\mathrm{d}t} = &-\left[\hat{S}\hat{S}^\dagger\tilde{\hat{\rho}}_S(t) - \hat{S}^\dagger\tilde{\hat{\rho}}_S(t)\hat{S}\right]\beta^* - \left[\tilde{\hat{\rho}}_S(t)\hat{S}^\dagger\hat{S} - \hat{S}\tilde{\hat{\rho}}_S(t)\hat{S}^\dagger\right](\alpha^* + \beta^*) \\ &- \left[\hat{S}^\dagger\hat{S}\tilde{\hat{\rho}}_S(t) - \hat{S}\tilde{\hat{\rho}}_S(t)\hat{S}^\dagger\right](\alpha + \beta) - \left[\tilde{\hat{\rho}}_S(t)\hat{S}\hat{S}^\dagger - \hat{S}^\dagger\tilde{\hat{\rho}}_S(t)\hat{S}\right]\beta.\end{aligned} \tag{A.75}$$

By rearranging the terms one obtains

$$\begin{aligned}\frac{\mathrm{d}\tilde{\hat{\rho}}_S}{\mathrm{d}t} = &\left[\hat{S}\tilde{\hat{\rho}}_S(t)\hat{S}^\dagger - \hat{S}^\dagger\hat{S}\tilde{\hat{\rho}}_S(t)\right]\alpha + \left[\hat{S}\tilde{\hat{\rho}}_S(t)\hat{S}^\dagger - \hat{S}^\dagger\hat{S}\tilde{\hat{\rho}}_S(t) + \hat{S}^\dagger\tilde{\hat{\rho}}_S(t)\hat{S} - \tilde{\hat{\rho}}_S(t)\hat{S}\hat{S}^\dagger\right]\beta \\ &+ \left[\hat{S}\tilde{\hat{\rho}}_S(t)\hat{S}^\dagger - \tilde{\hat{\rho}}_S(t)\hat{S}^\dagger\hat{S}\right]\alpha^* + \left[\hat{S}\tilde{\hat{\rho}}_S(t)\hat{S}^\dagger - \tilde{\hat{\rho}}_S(t)\hat{S}^\dagger\hat{S} + \hat{S}^\dagger\tilde{\hat{\rho}}_S(t)\hat{S} - \hat{S}\hat{S}^\dagger\tilde{\hat{\rho}}_S(t)\right]\beta^*.\end{aligned} \tag{A.76}$$

Die approbierte gedruckte Originalversion dieser Diplomarbeit ist an der TU Wien Bibliothek verfügbar
The approved original version of this thesis is available in print at TU Wien Bibliothek.
TU Bibliothek Your knowledge hub WIEN

Now we extend the upper bound of the time integral to infinity and use $\lim_{t\to\infty}\int_0^t \mathrm{d}\tau \mathrm{e}^{-\mathrm{i}(\omega-\omega_0)\tau} = \pi\delta(\omega-\omega_0) + \mathrm{i}\frac{P}{\omega_0-\omega}$. This is done because the function which we are integrating decrease (quite) fast with t, therefore we do not change the result (much). This is known as the Markov approximation. Our coefficients now read like

$$\alpha = \pi J(\omega_0)|g(\omega_0)|^2 + \mathrm{i}\Delta, \tag{A.77}$$

$$\beta = \pi J(\omega_0)|g(\omega_0)|^2\bar{n}(\omega_0) + \mathrm{i}\Delta', \tag{A.78}$$

and Eq. (A.76) changes to

$$\begin{aligned}\frac{\mathrm{d}\tilde{\hat{\rho}}_S}{\mathrm{d}t} &= \left[2\hat{S}\tilde{\hat{\rho}}_S(t)\hat{S}^\dagger - \hat{S}^\dagger\hat{S}\tilde{\hat{\rho}}_S(t) - \tilde{\hat{\rho}}_S(t)\hat{S}^\dagger\hat{S}\right]\frac{\gamma}{2} \\ &+ \left[\hat{S}\tilde{\hat{\rho}}_S(t)\hat{S}^\dagger - \hat{S}^\dagger\hat{S}\tilde{\hat{\rho}}_S(t) - \hat{S}\tilde{\hat{\rho}}_S(t)\hat{S}^\dagger + \tilde{\hat{\rho}}_S(t)\hat{S}^\dagger\hat{S}\right]\mathrm{i}\Delta \\ &+ \left[2\hat{S}\tilde{\hat{\rho}}_S(t)\hat{S}^\dagger + 2\hat{S}^\dagger\tilde{\hat{\rho}}_S(t)\hat{S} - \hat{S}^\dagger\hat{S}\tilde{\hat{\rho}}_S(t) - \tilde{\hat{\rho}}_S(t)\hat{S}\hat{S}^\dagger - \tilde{\hat{\rho}}_S(t)\hat{S}^\dagger\hat{S} - \hat{S}\hat{S}^\dagger\tilde{\hat{\rho}}_S(t)\right]\frac{\gamma\bar{n}}{2} \\ &+ \Big[\hat{S}\tilde{\hat{\rho}}_S(t)\hat{S}^\dagger - \hat{S}^\dagger\hat{S}\tilde{\hat{\rho}}_S(t) + \hat{S}^\dagger\tilde{\hat{\rho}}_S(t)\hat{S} - \tilde{\hat{\rho}}_S(t)\hat{S}\hat{S}^\dagger \\ &\quad -\hat{S}\tilde{\hat{\rho}}_S(t)\hat{S}^\dagger + \tilde{\hat{\rho}}_S(t)\hat{S}^\dagger\hat{S} - \hat{S}^\dagger\tilde{\hat{\rho}}_S(t)\hat{S} + \hat{S}\hat{S}^\dagger\tilde{\hat{\rho}}_S(t)\Big]\mathrm{i}\Delta',\end{aligned} \tag{A.79}$$

where $\gamma = 2\pi J(\omega_0)|g(\omega_0)|^2$ and $\bar{n} = \bar{n}(\omega_0)$. Now we use the commutator relation $[\hat{S}, \hat{S}^\dagger] = 1$ with which one can rewrite $\tilde{\hat{\rho}}_S(t)\hat{S}^\dagger\hat{S} = \tilde{\hat{\rho}}_S(t)(\hat{S}\hat{S}^\dagger - 1)$ and $\hat{S}\hat{S}^\dagger\tilde{\hat{\rho}}_S(t) = (\hat{S}^\dagger\hat{S} + 1)\tilde{\hat{\rho}}_S(t)$. Inserting this in the above equation leads to the final expression

$$\begin{aligned}\frac{\mathrm{d}\tilde{\hat{\rho}}_S}{\mathrm{d}t} &= \left[2\hat{S}\tilde{\hat{\rho}}_S(t)\hat{S}^\dagger - \hat{S}^\dagger\hat{S}\tilde{\hat{\rho}}_S(t) - \tilde{\hat{\rho}}_S(t)\hat{S}^\dagger\hat{S}\right]\frac{\gamma}{2} - \mathrm{i}\Delta\left[\hat{S}^\dagger\hat{S}, \tilde{\hat{\rho}}_S(t)\right] \\ &\quad + \gamma\bar{n}\left[\hat{S}\tilde{\hat{\rho}}_S(t)\hat{S}^\dagger + \hat{S}^\dagger\tilde{\hat{\rho}}_S(t)\hat{S} - \hat{S}^\dagger\hat{S}\tilde{\hat{\rho}}_S(t) - \tilde{\hat{\rho}}_S(t)\hat{S}\hat{S}^\dagger\right].\end{aligned} \tag{A.80}$$

Until now the density operator is in the Interaction picture. In the following, we want to transform the operator back into the Schrödinger picture. Therefore we use

$$\tilde{\hat{\rho}}_S(t) = \hat{U}^\dagger\hat{\rho}_S(t)\hat{U}, \tag{A.81}$$

where $\hat{U}$ is given by $\exp(-\frac{\mathrm{i}}{\hbar}\hat{H}_S t)$ and $\tilde{\hat{\rho}}(t)$ denotes the density operator in the Interaction, $\hat{\rho}(t)$ in the Schrödinger picture, respectively. Please note that the subscript S means that the density operator describes the system dynamics and does not stand for the Schrödinger picture. Since we want to find an expression for $\mathrm{d}\tilde{\hat{\rho}}_S(t)/\mathrm{d}t$ we calculate the time derivative and get

$$\frac{\mathrm{d}\tilde{\hat{\rho}}_S}{\mathrm{d}t} = \frac{\mathrm{i}}{\hbar}\hat{H}_S\tilde{\hat{\rho}}_S(t) - \tilde{\hat{\rho}}_S(t)\frac{\mathrm{i}}{\hbar}\hat{H}_S + \hat{U}^\dagger\dot{\hat{\rho}}_S(t)\hat{U}. \tag{A.82}$$

Die approbierte gedruckte Originalversion dieser Diplomarbeit ist an der TU Wien Bibliothek verfügbar
The approved original version of this thesis is available in print at TU Wien Bibliothek.
TU Bibliothek WIEN Your knowledge hub

Multiplication with $\hat{U}$ from the left and $\hat{U}^\dagger$ from the right side (note that $[\hat{U}, \hat{H}_S] = 0$]) gives

$$\hat{U}\frac{\mathrm{d}\tilde{\hat{\rho}}_S}{\mathrm{d}t}\hat{U}^\dagger = \frac{\mathrm{i}}{\hbar}\hat{H}_S\hat{\rho}_S(t) - \hat{\rho}_S(t)\frac{\mathrm{i}}{\hbar}\hat{H}_S + \dot{\hat{\rho}}_S(t). \tag{A.83}$$

Rearranging the terms lead to the final expression for the density matrix in the Schrödinger picture

$$\frac{\mathrm{d}\hat{\rho}_S}{\mathrm{d}t} = -\frac{\mathrm{i}}{\hbar}\left[\hat{H}_S, \hat{\rho}_S(t)\right] + \hat{U}\frac{\mathrm{d}}{\mathrm{d}t}\tilde{\hat{\rho}}_S(t)\hat{U}^\dagger. \tag{A.84}$$

To calculate the final result we use $\hat{U} = \exp(-\mathrm{i}\omega_0\hat{S}^\dagger\hat{S}t)$. Let us begin with transforming the commutator of Eq. (A.80) into the Schrödinger picture, i.e.,

$$\begin{aligned}\hat{U}\left(-\mathrm{i}\Delta\left[\hat{S}^\dagger\hat{S}, \tilde{\hat{\rho}}_S(t)\right]\right)\hat{U}^\dagger &= -\mathrm{i}\Delta\hat{U}\hat{S}^\dagger\hat{S}\hat{U}^\dagger\hat{\rho}_S(t)\hat{U}\hat{U}^\dagger + \mathrm{i}\Delta\hat{U}\hat{U}^\dagger\hat{\rho}_S(t)\hat{U}\hat{S}^\dagger\hat{S}\hat{U}^\dagger \\ &= -\mathrm{i}\Delta\hat{U}\hat{S}^\dagger\hat{U}^\dagger\hat{U}\hat{S}\hat{U}^\dagger\hat{\rho}_S(t) + \mathrm{i}\Delta\hat{\rho}_S(t)\hat{U}\hat{S}^\dagger\hat{U}^\dagger\hat{U}\hat{S}\hat{U}^\dagger = -\mathrm{i}\Delta\left[\hat{S}^\dagger\hat{S}, \hat{\rho}_S(t)\right],\end{aligned} \tag{A.85}$$

where we at first used Eq. (A.81), then introduced a one and finally made use of the fact that the creation and annihilation operators transform similarly but with complex conjugated exponent which cancel each other. Doing exact the same calculation for every term leads to our final equation

$$\begin{aligned}\frac{\mathrm{d}\hat{\rho}_S}{\mathrm{d}t} =& -\mathrm{i}\omega_0'\left[\hat{S}^\dagger\hat{S}, \hat{\rho}_S(t)\right] + \frac{\gamma}{2}\left[2\hat{S}\hat{\rho}_S(t)\hat{S}^\dagger - \hat{S}^\dagger\hat{S}\hat{\rho}_S(t) - \hat{\rho}_S(t)\hat{S}^\dagger\hat{S}\right] \\ &+ \gamma\bar{n}\left[\hat{S}\hat{\rho}_S(t)\hat{S}^\dagger + \hat{S}^\dagger\hat{\rho}_S(t)\hat{S} - \hat{S}^\dagger\hat{S}\hat{\rho}_S(t) - \hat{\rho}_S(t)\hat{S}\hat{S}^\dagger\right],\end{aligned} \tag{A.86}$$

where we have taken the additional commutator coming from the transformation into account. The new frequency is given by $\omega_0' = \omega_0 + \Delta$ and is called Lamb shift.

Until now we have taken into account coupling between a single system and a single bath. This can get arbitrary complicated. In our experiment, for example, the cavity is coupled to one bath and the NV centers to two different baths. For every coupling between a system and a bath the calculation looks as presented above but the dimension of the density matrix increases and we have more operators. To cover all that couplings to different baths, one has to sum over the corresponding operators. By doing so, we end up with

$$\begin{aligned}\frac{\mathrm{d}\hat{\rho}_S}{\mathrm{d}t} =& -\frac{\mathrm{i}}{\hbar}\left[\hat{H}_S, \hat{\rho}_S(t)\right] + \sum_j \gamma_j\left[\hat{L}_j\hat{\rho}_S(t)\hat{L}_j^\dagger - \frac{1}{2}\left\{\hat{L}_j^\dagger\hat{L}_j, \hat{\rho}_S(t)\right\}\right] \\ &+ \sum_j 2\gamma_j\bar{n}\left[\hat{L}_j\hat{\rho}_S(t)\hat{L}_j^\dagger + \hat{L}_j^\dagger\hat{\rho}_S(t)\hat{L}_j - \hat{L}_j^\dagger\hat{L}_j\hat{\rho}_S(t) - \hat{\rho}_S(t)\hat{L}_j\hat{L}_j^\dagger\right],\end{aligned} \tag{A.87}$$

which is a so-called master equation in Lindblad form or Lindbladian with the Lindblad operators $\hat{L}_j$. These operators couple to the environment with the rate γ_j. Please note that we neglected the Lamb shift here because it is usually small. The derivation shown in this section is based on Refs. [33, 50, 51].

Die approbierte gedruckte Originalversion dieser Diplomarbeit ist an der TU Wien Bibliothek verfügbar
The approved original version of this thesis is available in print at TU Wien Bibliothek.
TU Bibliothek Your knowledge hub WIEN

A.6 Derivation of the Maxwell-Bloch Equations

The starting point for the derivation is the Lindblad master equation, i.e.,

$$\begin{aligned}\frac{\mathrm{d}\hat{\rho}}{\mathrm{d}t} &= -\frac{\mathrm{i}}{\hbar}[\hat{H},\hat{\rho}] + \hat{\mathcal{L}}\hat{\rho} = -\frac{\mathrm{i}}{\hbar}[\hat{H},\hat{\rho}] + \kappa(2\hat{a}\hat{\rho}\hat{a}^\dagger - \hat{a}^\dagger\hat{a}\hat{\rho} - \hat{\rho}\hat{a}^\dagger\hat{a}) \\ &+ \frac{\gamma_\parallel}{2}\sum_j \left(2\hat{\sigma}_-^j\hat{\rho}\hat{\sigma}_+^j - \hat{\sigma}_+^j\hat{\sigma}_-^j\hat{\rho} - \hat{\rho}\hat{\sigma}_+^j\hat{\sigma}_-^j\right) + \frac{\gamma_\perp}{2}\sum_j\left(\hat{\sigma}_z^j\hat{\rho}\hat{\sigma}_z^j - \hat{\rho}\right),\end{aligned} \tag{A.88}$$

where we neglected the terms which include thermal photons. By using $\mathrm{Tr}[\hat{O}\hat{\rho}] = \langle\hat{O}\rangle$ and $\mathrm{Tr}[\hat{O}\dot{\hat{\rho}}] = \frac{\mathrm{d}}{\mathrm{d}t}\langle\hat{O}\rangle$ (the exchange is allowed since the trace is a linear operator) we now want to calculate the corresponding equations of motion, i.e., the expectation values of the operators. We start with evaluating the equation of motion for the operator $\hat{a}$, i.e.,

$$\begin{aligned}\mathrm{Tr}\left(\dot{\hat{\rho}}\hat{a}\right) &= -\frac{\mathrm{i}}{\hbar}\mathrm{Tr}\left([\hat{H},\hat{\rho}]\hat{a}\right) + \kappa\mathrm{Tr}\left([2\hat{a}\hat{\rho}\hat{a}^\dagger - \hat{a}^\dagger\hat{a}\hat{\rho} - \hat{\rho}\hat{a}^\dagger\hat{a}]\hat{a}\right) \\ &+ \frac{\gamma_\parallel}{2}\sum_j \mathrm{Tr}\left([2\hat{\sigma}_-^j\hat{\rho}\hat{\sigma}_+^j - \hat{\sigma}_+^j\hat{\sigma}_-^j\hat{\rho} - \hat{\rho}\hat{\sigma}_+^j\hat{\sigma}_-^j]\hat{a}\right) + \frac{\gamma_\perp}{2}\sum_j \mathrm{Tr}\left([\hat{\sigma}_z^j\hat{\rho}\hat{\sigma}_z^j - \hat{\rho}]\hat{a}\right).\end{aligned} \tag{A.89}$$

The terms proportional to $\gamma_\parallel$ and $\gamma_\perp$ are equal to zero which one can see when using the cyclic properties of the trace and the fact that the operator $\hat{a}$ commutes with all Pauli spin operators $\hat{\sigma}_i$. Inserting the corresponding terms for the driven Tavis-Cummings Hamiltonian (Eq. (2.74)) leads to

$$\begin{aligned}\langle\dot{\hat{a}}\rangle &= -\mathrm{i}\Delta_c\mathrm{Tr}\left([\hat{a}^\dagger\hat{a},\hat{\rho}]\hat{a}\right) - \mathrm{i}\sum_j\frac{\Delta_s^j}{2}\mathrm{Tr}\left([\hat{\sigma}_z^j,\hat{\rho}]\hat{a}\right) + \sum_j g_j\mathrm{Tr}\left([\hat{\sigma}_-^j\hat{a}^\dagger - \hat{\sigma}_+^j\hat{a},\hat{\rho}]\hat{a}\right) \\ &+ \eta\mathrm{Tr}\left([\hat{a}^\dagger - \hat{a},\hat{\rho}]\hat{a}\right) + \kappa\mathrm{Tr}\left([2\hat{a}\hat{\rho}\hat{a}^\dagger - \hat{a}^\dagger\hat{a}\hat{\rho} - \hat{\rho}\hat{a}^\dagger\hat{a}]\hat{a}\right),\end{aligned} \tag{A.90}$$

where the second term is zero because of the aforementioned reasons as well. By evaluating the commutators we get

$$\begin{aligned}\langle\dot{\hat{a}}\rangle &= -\mathrm{i}\Delta_c\mathrm{Tr}\left(\hat{a}^\dagger\hat{a}\hat{\rho}\hat{a} - \hat{\rho}\hat{a}^\dagger\hat{a}\hat{a}\right) \\ &+ \sum_j g_j\left[\mathrm{Tr}\left(\hat{\sigma}_-^j\hat{a}^\dagger\hat{\rho}\hat{a} - \hat{\rho}\hat{\sigma}_-^j\hat{a}^\dagger\hat{a}\right) - \mathrm{Tr}\left(\hat{\sigma}_+^j\hat{a}\hat{\rho}\hat{a} - \hat{\rho}\hat{\sigma}_+^j\hat{a}\hat{a}\right)\right] \\ &+ \eta\mathrm{Tr}\left(\hat{a}^\dagger\hat{\rho}\hat{a} - \hat{\rho}\hat{a}^\dagger\hat{a}\right) - \eta\mathrm{Tr}\left(\hat{a}\hat{\rho}\hat{a} - \hat{\rho}\hat{a}\hat{a}\right) + \kappa\mathrm{Tr}\left(2\hat{a}\hat{\rho}\hat{a}^\dagger\hat{a} - \hat{a}^\dagger\hat{a}\hat{\rho}\hat{a} - \hat{\rho}\hat{a}^\dagger\hat{a}\hat{a}\right),\end{aligned} \tag{A.91}$$

Die approbierte gedruckte Originalversion dieser Diplomarbeit ist an der TU Wien Bibliothek verfügbar
The approved original version of this thesis is available in print at TU Wien Bibliothek.
TU Bibliothek WIEN Your knowledge hub

where one sees that two terms are zero again. Using the cyclic properties of the trace leads to

$$\begin{aligned}\langle\dot{\hat{a}}\rangle &= -\,\mathrm{i}\Delta_c\mathrm{Tr}\left(\hat{a}\hat{a}^\dagger\hat{a}\hat{\rho}-\hat{a}^\dagger\hat{a}\hat{a}\hat{\rho}\right)+\sum_j g_j\mathrm{Tr}\left(\hat{a}\hat{a}^\dagger\hat{\sigma}_-^j\hat{\rho}-\hat{a}^\dagger\hat{a}\hat{\sigma}_-^j\hat{\rho}\right)\\ &\quad+\eta\mathrm{Tr}\left(\hat{a}\hat{a}^\dagger\hat{\rho}-\hat{a}^\dagger\hat{a}\hat{\rho}\right)+\kappa\mathrm{Tr}\left(2\hat{a}^\dagger\hat{a}\hat{a}\hat{\rho}-\hat{a}\hat{a}^\dagger\hat{a}\hat{\rho}-\hat{a}^\dagger\hat{a}\hat{a}\hat{\rho}\right)\\ &= -\,\mathrm{i}\Delta_c\mathrm{Tr}\left(\left[\hat{a},\hat{a}^\dagger\right]\hat{a}\hat{\rho}\right)+\sum_j g_j\mathrm{Tr}\left(\left[\hat{a},\hat{a}^\dagger\right]\hat{\sigma}_-^j\hat{\rho}\right)+\eta\mathrm{Tr}\left(\left[\hat{a},\hat{a}^\dagger\right]\hat{\rho}\right)\\ &\quad+\kappa\mathrm{Tr}\left(-\left[\hat{a},\hat{a}^\dagger\right]\hat{a}\hat{\rho}\right)\\ &= -\,\mathrm{i}\Delta_c\langle\hat{a}\rangle+\sum_j g_j\langle\hat{\sigma}_-^j\rangle+\eta-\kappa\langle\hat{a}\rangle.\end{aligned} \tag{A.92}$$

Now we want to derive the equation of motion for the operator $\hat{\sigma}_-^j$. We again start with

$$\begin{aligned}\mathrm{Tr}\left(\dot{\hat{\rho}}\hat{\sigma}_-^j\right) &= -\frac{\mathrm{i}}{\hbar}\mathrm{Tr}\left([\hat{H},\hat{\rho}]\hat{\sigma}_-^j\right)+\kappa\mathrm{Tr}\left([2\hat{a}\hat{\rho}\hat{a}^\dagger-\hat{a}^\dagger\hat{a}\hat{\rho}-\hat{\rho}\hat{a}^\dagger\hat{a}]\hat{\sigma}_-^j\right)\\ &+\frac{\gamma_\parallel}{2}\sum_k\mathrm{Tr}\left([2\hat{\sigma}_-^k\hat{\rho}\hat{\sigma}_+^k-\hat{\sigma}_+^k\hat{\sigma}_-^k\hat{\rho}-\hat{\rho}\hat{\sigma}_+^k\hat{\sigma}_-^k]\hat{\sigma}_-^j\right)+\frac{\gamma_\perp}{2}\sum_k\mathrm{Tr}\left([\hat{\sigma}_z^k\hat{\rho}\hat{\sigma}_z^k-\hat{\rho}]\hat{\sigma}_-^j\right),\end{aligned} \tag{A.93}$$

where the term proportional to κ is equal to zero which one can see when again using the cyclic properties of the trace and the fact that the Pauli spin operators $\hat{\sigma}_i$ commute with the operator $\hat{a}$. As before, we now insert the driven Tavis-Cummings Hamiltonian which leads to

$$\begin{aligned}\langle\dot{\hat{\sigma}}_-^j\rangle &= -\mathrm{i}\Delta_c\mathrm{Tr}\left(\left[\hat{a}^\dagger\hat{a},\hat{\rho}\right]\hat{\sigma}_-^j\right)-\mathrm{i}\sum_k\frac{\Delta_s^k}{2}\mathrm{Tr}\left(\left[\hat{\sigma}_z^k,\hat{\rho}\right]\hat{\sigma}_-^j\right)\\ &+\sum_k g_k\mathrm{Tr}\left([\hat{\sigma}_-^k\hat{a}^\dagger-\hat{\sigma}_+^k\hat{a},\hat{\rho}]\hat{\sigma}_-^j\right)+\eta\mathrm{Tr}\left([\hat{a}^\dagger-\hat{a},\hat{\rho}]\hat{\sigma}_-^j\right)\\ &+\frac{\gamma_\parallel}{2}\sum_k\mathrm{Tr}\left([2\hat{\sigma}_-^k\hat{\rho}\hat{\sigma}_+^k-\hat{\sigma}_+^k\hat{\sigma}_-^k\hat{\rho}-\hat{\rho}\hat{\sigma}_+^k\hat{\sigma}_-^k]\hat{\sigma}_-^j\right)+\frac{\gamma_\perp}{2}\sum_k\mathrm{Tr}\left([\hat{\sigma}_z^k\hat{\rho}\hat{\sigma}_z^k-\hat{\rho}]\hat{\sigma}_-^j\right),\end{aligned} \tag{A.94}$$

where the terms proportional to Δ_c and η are zero as well. For the terms containing the sum over k only the terms $k=j$ are relevant because for $k\neq j$ the spin operators commute and these terms are zero. Therefore, we from now on set $k=j$ and drop the sum. For better readability the index j will be dropped from now on as well.

Die approbierte gedruckte Originalversion dieser Diplomarbeit ist an der TU Wien Bibliothek verfügbar
The approved original version of this thesis is available in print at TU Wien Bibliothek.
TU Bibliothek Your knowledge hub WIEN

By evaluating the commutators we get

$$\begin{aligned}\langle\dot{\hat{\sigma}}_-\rangle =& -\mathrm{i}\frac{\Delta_s}{2}\mathrm{Tr}\left(\hat{\sigma}_z\hat{\rho}\hat{\sigma}_- - \hat{\rho}\hat{\sigma}_z\hat{\sigma}_-\right)\\ &+ g\left[\mathrm{Tr}\left(\hat{\sigma}_-\hat{a}^\dagger\hat{\rho}\hat{\sigma}_- - \hat{\rho}\hat{\sigma}_-\hat{a}^\dagger\hat{\sigma}_-\right) - \mathrm{Tr}\left(\hat{\sigma}_+\hat{a}\hat{\rho}\hat{\sigma}_- - \hat{\rho}\hat{\sigma}_+\hat{a}\hat{\sigma}_-\right)\right]\\ &+ \frac{\gamma_\parallel}{2}\mathrm{Tr}\left(2\hat{\sigma}_-\hat{\rho}\hat{\sigma}_+\hat{\sigma}_- - \hat{\sigma}_+\hat{\sigma}_-\hat{\rho}\hat{\sigma}_- - \hat{\rho}\hat{\sigma}_+\hat{\sigma}_-\hat{\sigma}_-\right) + \frac{\gamma_\perp}{2}\mathrm{Tr}\left(\hat{\sigma}_z\hat{\rho}\hat{\sigma}_z\hat{\sigma}_- - \hat{\rho}\hat{\sigma}_-\right),\end{aligned} \tag{A.95}$$

where one sees that the first term proportional to g is zero again. Now we use the cyclic properties of the trace which gives

$$\begin{aligned}\langle\dot{\hat{\sigma}}_-\rangle =& -\mathrm{i}\frac{\Delta_s}{2}\mathrm{Tr}\left(\hat{\sigma}_-\hat{\sigma}_z\hat{\rho} - \hat{\sigma}_z\hat{\sigma}_-\hat{\rho}\right) - g\mathrm{Tr}\left(\hat{a}\hat{\sigma}_-\hat{\sigma}_+\hat{\rho} - \hat{a}\hat{\sigma}_+\hat{\sigma}_-\hat{\rho}\right)\\ &+ \frac{\gamma_\parallel}{2}\mathrm{Tr}\left(2\hat{\sigma}_+\hat{\sigma}_-\hat{\sigma}_-\hat{\rho} - \hat{\sigma}_-\hat{\sigma}_+\hat{\sigma}_-\hat{\rho} - \hat{\sigma}_+\hat{\sigma}_-\hat{\sigma}_-\hat{\rho}\right) + \frac{\gamma_\perp}{2}\mathrm{Tr}\left(\hat{\sigma}_z\hat{\sigma}_-\hat{\sigma}_z\hat{\rho} - \hat{\sigma}_-\hat{\rho}\right).\end{aligned} \tag{A.96}$$

By using the well known Pauli spin operator commutation relation $[\hat{\sigma}_i, \hat{\sigma}_j] = 2\mathrm{i}\epsilon_{ijk}\hat{\sigma}_k$ one easily find the relations $[\hat{\sigma}_\pm, \hat{\sigma}_z] = \mp 2\hat{\sigma}_\pm$ and $[\hat{\sigma}_+, \hat{\sigma}_-] = \hat{\sigma}_z$ (where the spin raising and lowering operators are given by $\hat{\sigma}_\pm = \frac{1}{2}(\hat{\sigma}_x \pm \mathrm{i}\hat{\sigma}_y)$). Furthermore, we use the fact that $\hat{\sigma}_i\hat{\sigma}_j = \delta_{ij} + \epsilon_{ijk}\hat{\sigma}_k$ form which $\hat{\sigma}_-\hat{\sigma}_- = 0$ follows. This leads to

$$\begin{aligned}\langle\dot{\hat{\sigma}}_-\rangle =& -\mathrm{i}\frac{\Delta_s}{2}\mathrm{Tr}\left([\hat{\sigma}_-, \hat{\sigma}_z]\hat{\rho}\right) - g\mathrm{Tr}\left(\hat{a}[\hat{\sigma}_-, \hat{\sigma}_+]\hat{\rho}\right)\\ &+ \frac{\gamma_\parallel}{2}\mathrm{Tr}\left(-\hat{\sigma}_-(\hat{\sigma}_z + \hat{\sigma}_-\hat{\sigma}_+)\hat{\rho}\right) + \frac{\gamma_\perp}{2}\mathrm{Tr}\left(\hat{\sigma}_z(2\hat{\sigma}_- + \hat{\sigma}_z\hat{\sigma}_-)\hat{\rho} - \hat{\sigma}_-\hat{\rho}\right)\\ =& -\mathrm{i}\Delta_s\langle\hat{\sigma}_-\rangle + g\langle\hat{a}\hat{\sigma}_z\rangle - \frac{\gamma}{2}\langle\hat{\sigma}_-\rangle - \gamma_\perp\langle\hat{\sigma}_-\rangle,\end{aligned} \tag{A.97}$$

where we used the relations $\hat{\sigma}_-\hat{\sigma}_z = \hat{\sigma}_-$ and $\hat{\sigma}_z\hat{\sigma}_- = -\hat{\sigma}_-$ as well.

Last but not least we want to derive the equation of motion for the operator $\hat{\sigma}_z^j$. The starting point is, as before,

$$\begin{aligned}\mathrm{Tr}\left(\dot{\hat{\rho}}\hat{\sigma}_z^j\right) =& -\frac{\mathrm{i}}{\hbar}\mathrm{Tr}\left([\hat{H}, \hat{\rho}]\hat{\sigma}_z^j\right) + \kappa\mathrm{Tr}\left([2\hat{a}\hat{\rho}\hat{a}^\dagger - \hat{a}^\dagger\hat{a}\hat{\rho} - \hat{\rho}\hat{a}^\dagger\hat{a}]\hat{\sigma}_z^j\right)\\ &+ \frac{\gamma_\parallel}{2}\sum_k \mathrm{Tr}\left([2\hat{\sigma}_-^k\hat{\rho}\hat{\sigma}_+^k - \hat{\sigma}_+^k\hat{\sigma}_-^k\hat{\rho} - \hat{\rho}\hat{\sigma}_+^k\hat{\sigma}_-^k]\hat{\sigma}_z^j\right) + \frac{\gamma_\perp}{2}\sum_k \mathrm{Tr}\left([\hat{\sigma}_z^k\hat{\rho}\hat{\sigma}_z^k - \hat{\rho}]\hat{\sigma}_z^j\right).\end{aligned} \tag{A.98}$$

One sees that the term proportional to κ is zero again. Moreover, by using the cyclic properties of the trace one sees that the last term is zero as well. Inserting the driven Tavis-Cummings Hamiltonian leads to

$$\begin{aligned}\langle\dot{\hat{\sigma}}_z^j\rangle =& -\mathrm{i}\Delta_c\mathrm{Tr}\left(\left[\hat{a}^\dagger\hat{a}, \hat{\rho}\right]\hat{\sigma}_z^j\right) - \mathrm{i}\sum_k \frac{\Delta_s^k}{2}\mathrm{Tr}\left(\left[\hat{\sigma}_z^k, \hat{\rho}\right]\hat{\sigma}_z^j\right) + \sum_k g_k\mathrm{Tr}\left([\hat{\sigma}_-^k\hat{a}^\dagger - \hat{\sigma}_+^k\hat{a}, \hat{\rho}]\hat{\sigma}_z^j\right)\\ &+ \eta\mathrm{Tr}\left([\hat{a}^\dagger - \hat{a}, \hat{\rho}]\hat{\sigma}_z^j\right) + \frac{\gamma_\parallel}{2}\sum_k \mathrm{Tr}\left([2\hat{\sigma}_-^k\hat{\rho}\hat{\sigma}_+^k - \hat{\sigma}_+^k\hat{\sigma}_-^k\hat{\rho} - \hat{\rho}\hat{\sigma}_+^k\hat{\sigma}_-^k]\hat{\sigma}_z^j\right),\end{aligned} \tag{A.99}$$

Die approbierte gedruckte Originalversion dieser Diplomarbeit ist an der TU Wien Bibliothek verfügbar
The approved original version of this thesis is available in print at TU Wien Bibliothek.
TU Bibliothek Your knowledge hub WIEN

where the terms proportional to Δ_c and η are zero because of the aforementioned reasons. As before, for the terms containing the sum over k only the terms $k = j$ are relevant because for $k \neq j$ the spin operators commute and these terms are zero. Therefore, we from now on set $k = j$ and drop the sum. For better readability we drop the index j from now on as well. By evaluating the commutators we get

$$\begin{aligned}\langle\dot{\hat{\sigma}}_z\rangle = &-\mathrm{i}\frac{\Delta_s}{2}\mathrm{Tr}\left(\hat{\sigma}_z\hat{\rho}\hat{\sigma}_z - \hat{\rho}\hat{\sigma}_z\hat{\sigma}_z\right) + g\left[\mathrm{Tr}\left(\hat{\sigma}_-\hat{a}^\dagger\hat{\rho}\hat{\sigma}_z - \hat{\rho}\hat{\sigma}_-\hat{a}^\dagger\hat{\sigma}_z\right)\right.\\ &\left.-\mathrm{Tr}\left(\hat{\sigma}_+\hat{a}\hat{\rho}\hat{\sigma}_z - \hat{\rho}\hat{\sigma}_+\hat{a}\hat{\sigma}_z\right)\right] + +\frac{\gamma_\parallel}{2}\mathrm{Tr}\left(2\hat{\sigma}_-\hat{\rho}\hat{\sigma}_+\hat{\sigma}_z - \hat{\sigma}_+\hat{\sigma}_-\hat{\rho}\hat{\sigma}_z - \hat{\rho}\hat{\sigma}_+\hat{\sigma}_-\hat{\sigma}_z\right),\end{aligned} \tag{A.100}$$

where one sees that the first term is zero. Using the cyclic properties of the trace and the aforementioned spin operator commutator relations gives

$$\begin{aligned}\langle\dot{\hat{\sigma}}_z\rangle =&g\left[\mathrm{Tr}\left(\hat{a}^\dagger\hat{\sigma}_z\hat{\sigma}_-\hat{\rho} - \hat{a}^\dagger\hat{\sigma}_-\hat{\sigma}_z\hat{\rho}\right) - \mathrm{Tr}\left(\hat{a}\hat{\sigma}_z\hat{\sigma}_+\hat{\rho} - \hat{a}\hat{\sigma}_+\hat{\sigma}_z\hat{\rho}\right)\right]\\ &+\frac{\gamma_\parallel}{2}\mathrm{Tr}\left(2\hat{\sigma}_+\hat{\sigma}_z\hat{\sigma}_-\hat{\rho} - \hat{\sigma}_z^i\hat{\sigma}_+\hat{\sigma}_-\hat{\rho} - \hat{\sigma}_+\hat{\sigma}_-\hat{\sigma}_z\hat{\rho}\right)\\ =&g\left[\mathrm{Tr}\left(\hat{a}^\dagger[\hat{\sigma}_z,\hat{\sigma}_-]\hat{\rho}\right) - \mathrm{Tr}\left(\hat{a}[\hat{\sigma}_z,\hat{\sigma}_+]\hat{\rho}\right)\right] + \frac{\gamma_\parallel}{2}\mathrm{Tr}\left([\hat{\sigma}_+,\hat{\sigma}_z]\hat{\sigma}_-\hat{\rho} + \hat{\sigma}_+[\hat{\sigma}_z,\hat{\sigma}_-]\hat{\rho}\right)\\ =&-2g\left(\langle\hat{a}^\dagger\hat{\sigma}_-\rangle + \langle\hat{a}\hat{\sigma}_+\rangle\right) + \frac{\gamma_\parallel}{2}\mathrm{Tr}\left(-2\hat{\sigma}_+\hat{\sigma}_-\hat{\rho} - 2\hat{\sigma}_+\hat{\sigma}_-\hat{\rho}\right)\\ =&-2g\left(\langle\hat{a}^\dagger\hat{\sigma}_-\rangle + \langle\hat{a}\hat{\sigma}_+\rangle\right) - \gamma_\parallel\langle\hat{\sigma}_z\rangle - \gamma_\parallel,\end{aligned} \tag{A.101}$$

where in the last step we used $\hat{\sigma}_+\hat{\sigma}_- = \frac{1}{2}\left(\hat{\sigma}_z + 1\right)$.

To sum up, we get the following coupled differential equations

$$\begin{aligned}\langle\dot{\hat{a}}\rangle &= -\mathrm{i}\Delta_c\langle\hat{a}\rangle + \sum_j g_j\langle\hat{\sigma}_-^j\rangle + \eta - \kappa\langle\hat{a}\rangle\\ \langle\dot{\hat{\sigma}}_-\rangle &= -\mathrm{i}\Delta_s\langle\hat{\sigma}_-\rangle + g\langle\hat{a}\hat{\sigma}_z\rangle - \left(\frac{\gamma_\parallel}{2} + \gamma_\perp\right)\langle\hat{\sigma}_-\rangle\\ \langle\dot{\hat{\sigma}}_z\rangle &= -2g\left(\langle\hat{a}^\dagger\hat{\sigma}_-\rangle + \langle\hat{a}\hat{\sigma}_+\rangle\right) - \gamma_\parallel\left(1 + \langle\hat{\sigma}_z\rangle\right).\end{aligned} \tag{A.102}$$

Die approbierte gedruckte Originalversion dieser Diplomarbeit ist an der TU Wien Bibliothek verfügbar
The approved original version of this thesis is available in print at TU Wien Bibliothek.
TU Bibliothek Your knowledge hub WIEN

TU WIEN Bibliothek Your knowledge hub
Die approbierte gedruckte Originalversion dieser Diplomarbeit ist an der TU Wien Bibliothek verfügbar
The approved original version of this thesis is available in print at TU Wien Bibliothek.

Bibliography

[1] J. C. Maxwell, "VIII. a dynamical theory of the electromagnetic field," *Philosophical Transactions of the Royal Society of London*, vol. 155, pp. 459 – 512, Dec. 1865.

[2] A. Einstein, "Über einen die erzeugung und verwandlung des lichtes betreffenden heuristischen gesichtspunkt," *Annalen der Physik*, vol. 322, no. 6, pp. 132–148, 1905.

[3] A. Pais, "How einstein got the nobel prize: Why did the nobel committee for physics wait so long before giving einstein the prize, and why did they not award it for relativity?," *American Scientist*, vol. 70, no. 4, pp. 358–365, 1982.

[4] P. A. M. Dirac and N. H. D. Bohr, "The quantum theory of the emission and absorption of radiation," *Proceedings of the Royal Society of London. Series A, Containing Papers of a Mathematical and Physical Character*, vol. 114, pp. 243–265, Mar. 1927.

[5] R. Feynman, *QED: the Strange Theory of Light and Matter*. Universities Press (India) Pvt. Limited, 1985.

[6] R. P. Feynman, "The development of the space-time view of quantum electrodynamics," *Science*, vol. 153, no. 3737, pp. 699–708, 1966.

[7] J. Schwinger, "Relativistic quantum field theory," *Science*, vol. 153, no. 3739, pp. 949–953, 1966.

[8] S. Tomonaga, "Development of quantum electrodynamics," *Physics Today*, vol. 19, no. 9, pp. 25–32, 1966.

[9] S. Haroche, "Nobel lecture: Controlling photons in a box and exploring the quantum to classical boundary," *Rev. Mod. Phys.*, vol. 85, pp. 1083–1102, Jul 2013.

[10] D. J. Wineland, "Nobel lecture: Superposition, entanglement, and raising schrödinger's cat," *Rev. Mod. Phys.*, vol. 85, pp. 1103–1114, Jul 2013.

[11] J. I. Cirac and P. Zoller, "Quantum computations with cold trapped ions," *Phys. Rev. Lett.*, vol. 74, pp. 4091–4094, May 1995.

Die approbierte gedruckte Originalversion dieser Diplomarbeit ist an der TU Wien Bibliothek verfügbar
The approved original version of this thesis is available in print at TU Wien Bibliothek.
TU Bibliothek Your knowledge hub WIEN

[12] J. Majer, J. M. Chow, J. M. Gambetta, J. Koch, B. R. Johnson, J. A. Schreier, L. Frunzio, D. I. Schuster, A. A. Houck, A. Wallraff, and et al., "Coupling superconducting qubits via a cavity bus," *Nature*, vol. 449, p. 443–447, Sep 2007.

[13] D. Loss and D. P. DiVincenzo, "Quantum computation with quantum dots," *Phys. Rev. A*, vol. 57, pp. 120–126, Jan 1998.

[14] J. R. Petta, A. C. Johnson, J. M. Taylor, E. A. Laird, A. Yacoby, M. D. Lukin, C. M. Marcus, M. P. Hanson, and A. C. Gossard, "Coherent manipulation of coupled electron spins in semiconductor quantum dots," *Science*, vol. 309, no. 5744, pp. 2180–2184, 2005.

[15] D. Englund, B. Shields, K. Rivoire, F. Hatami, J. Vučković, H. Park, and M. D. Lukin, "Deterministic coupling of a single nitrogen vacancy center to a photonic crystal cavity," *Nano Letters*, vol. 10, no. 10, pp. 3922–3926, 2010. PMID: 20825160.

[16] S. Putz, *Circuit Cavity QED with Macroscopic Solid-State Spin Ensembles*. Springer International Publishing, 2017.

[17] K. Sandner, *Cavity quantum electrodynamics with ultracold atoms and superconducting resonators*. PhD thesis, Universität Innsbruck, 2012.

[18] D. O. Krimer, S. Putz, J. Majer, and S. Rotter, "Non-markovian dynamics of a single-mode cavity strongly coupled to an inhomogeneously broadened spin ensemble," *Physical Review A*, vol. 90, Oct 2014.

[19] S. Putz, D. Krimer, R. Amsüss, A. Valookaran, T. Nöbauer, J. Schmiedmayer, S. Rotter, and J. Majer, "Protecting a spin ensemble against decoherence in the strong-coupling regime of cavity qed," *Nature Physics*, vol. 10, p. 720–724, Aug 2014.

[20] T. Astner, S. Nevlacsil, N. Peterschofsky, A. Angerer, S. Rotter, S. Putz, J. Schmiedmayer, and J. Majer, "Coherent coupling of remote spin ensembles via a cavity bus," *Physical Review Letters*, vol. 118, Apr 2017.

[21] S. Putz, A. Angerer, D. O. Krimer, R. Glattauer, W. J. Munro, S. Rotter, J. Schmiedmayer, and J. Majer, "Spectral hole burning and its application in microwave photonics," *Nature Photonics*, vol. 11, pp. 36–39, Jan. 2017.

[22] A. Angerer, S. Putz, D. O. Krimer, T. Astner, M. Zens, R. Glattauer, K. Streltsov, W. J. Munro, K. Nemoto, S. Rotter, J. Schmiedmayer, and J. Majer, "Ultralong relaxation times in bistable hybrid quantum systems," *Science Advances*, vol. 3, no. 12, p. e1701626, 2017.

Die approbierte gedruckte Originalversion dieser Diplomarbeit ist an der TU Wien Bibliothek verfügbar
The approved original version of this thesis is available in print at TU Wien Bibliothek.
TU Bibliothek Your knowledge hub WIEN

[23] A. Angerer, T. Astner, D. Wirtitsch, H. Sumiya, S. Onoda, J. Isoya, S. Putz, and J. Majer, "Collective strong coupling with homogeneous rabi frequencies using a 3d lumped element microwave resonator," *Applied Physics Letters*, vol. 109, p. 033508, Jul 2016.

[24] A. Angerer, K. Streltsov, T. Astner, S. Putz, H. Sumiya, S. Onoda, J. Isoya, W. J. Munro, K. Nemoto, J. Schmiedmayer, and et al., "Superradiant emission from colour centres in diamond," *Nature Physics*, vol. 14, p. 1168–1172, Sep 2018.

[25] R. H. Dicke, "Coherence in spontaneous radiation processes," *Phys. Rev.*, vol. 93, pp. 99–110, Jan 1954.

[26] J. D. Jackson, *Classical electrodynamics*. New York, NY: Wiley, 3rd ed. ed., 1999.

[27] C. Gerry and P. Knight, *Introductory Quantum Optics*. Cambridge University Press, 2004.

[28] M. O. Scully and M. S. Zubairy, *Quantum Optics*. Cambridge University Press, 1997.

[29] M. Fox, *Quantum optics : an introduction*. Oxford New York: Oxford University Press, 2006.

[30] S. Haroche, *Exploring the quantum : atoms, cavities and photons*. Oxford New York: Oxford University Press, 2006.

[31] E. Jaynes and F. Cummings, "Comparison of quantum and semiclassical radiation theories with application to the beam maser," *Proceedings of the IEEE*, vol. 51, no. 1, pp. 89–109, 1963.

[32] M. Tavis and F. W. Cummings, "Exact solution for an n-molecule—radiation-field hamiltonian," *Phys. Rev.*, vol. 170, pp. 379–384, Jun 1968.

[33] H. J. Carmichael, *Statistical Methods in Quantum Optics 1: Master Equations and Fokker-Planck Equations*. Berlin, Heidelberg, New York: Springer-Verlag, 1999.

[34] A. Angerer, *Non-linear Dynamics in Cavity QED: Beyond Two Coupled Springs*. PhD thesis, TU Wien, 2019.

[35] R. Fitzpatrick, *Oscillations and waves : an introduction*. Boca Raton: CRC Press Taylor & Francis Group, 2013.

Die approbierte gedruckte Originalversion dieser Diplomarbeit ist an der TU Wien Bibliothek verfügbar
The approved original version of this thesis is available in print at TU Wien Bibliothek.
TU Bibliothek Your knowledge hub WIEN

[36] T. Astner, J. Gugler, A. Angerer, S. Wald, S. Putz, N. J. Mauser, M. Trupke, H. Sumiya, S. Onoda, J. Isoya, and et al., "Solid-state electron spin lifetime limited by phononic vacuum modes," *Nature Materials*, vol. 17, p. 313–317, Feb 2018.

[37] M. W. Doherty, N. B. Manson, P. Delaney, F. Jelezko, J. Wrachtrup, and L. C. Hollenberg, "The nitrogen-vacancy colour centre in diamond," *Physics Reports*, vol. 528, p. 1–45, Jul 2013.

[38] T. Nöbauer, K. Buczak, A. Angerer, S. Putz, G. Steinhauser, J. Akbarzadeh, H. Peterlik, J. Majer, J. Schmiedmayer, and M. Trupke, "Creation of ensembles of nitrogen-vacancy centers in diamond by neutron and electron irradiation," *arXiv preprint arXiv:1309.0453*, 2013.

[39] N. M. Atherton, *Principles of electron spin resonance*. New York: Ellis Horwood PTR Prentice Hall, 1993.

[40] D. Goldfarb and S. Stoll, *EPR spectroscopy: fundamentals and methods*. John Wiley & Sons, 2018.

[41] F. Jelezko and J. Wrachtrup, "Single defect centres in diamond: A review," *physica status solidi (a)*, vol. 203, no. 13, pp. 3207–3225, 2006.

[42] F. Pobell, *Matter and Methods at Low Temperatures*. Berlin, Heidelberg: Springer Berlin Heidelberg, 2007.

[43] J. O'Sullivan, O. W. Kennedy, K. Debnath, J. Alexander, C. W. Zollitsch, M. Šimėnas, A. Hashim, C. N. Thomas, S. Withington, I. Siddiqi, K. Mølmer, and J. J. L. Morton, "Random-access quantum memory using chirped pulse phase encoding," *arXiv preprint arXiv:2103.11697*, 2021.

[44] T. Nöbauer, A. Angerer, B. Bartels, M. Trupke, S. Rotter, J. Schmiedmayer, F. Mintert, and J. Majer, "Smooth optimal quantum control for robust solid-state spin magnetometry," *Physical Review Letters*, vol. 115, Nov 2015.

[45] B. Julsgaard and K. Mølmer, "Dynamical evolution of an inverted spin ensemble in a cavity: Inhomogeneous broadening as a stabilizing mechanism," *Physical Review A*, vol. 86, Dec 2012.

[46] M. Gross and S. Haroche, "Superradiance: An essay on the theory of collective spontaneous emission," *Physics Reports*, vol. 93, pp. 301–396, Dec. 1982.

[47] P. Goy, L. Moi, M. Gross, J. M. Raimond, C. Fabre, and S. Haroche, "Rydberg-atom masers. II. triggering by external radiation and application to millimeter-wave detectors," *Phys. Rev. A*, vol. 27, pp. 2065–2081, Apr 1983.

Die approbierte gedruckte Originalversion dieser Diplomarbeit ist an der TU Wien Bibliothek verfügbar
The approved original version of this thesis is available in print at TU Wien Bibliothek.
TU Bibliothek Your knowledge hub WIEN

[48] J. Choi, S. Choi, G. Kucsko, P. C. Maurer, B. J. Shields, H. Sumiya, S. Onoda, J. Isoya, E. Demler, F. Jelezko, and et al., "Depolarization dynamics in a strongly interacting solid-state spin ensemble," *Physical Review Letters*, vol. 118, Mar 2017.

[49] D. M. Lukin, A. D. White, R. Trivedi, M. A. Guidry, N. Morioka, C. Babin, n. O. Soykal, J. Ul-Hassan, N. T. Son, T. Ohshima, and et al., "Spectrally reconfigurable quantum emitters enabled by optimized fast modulation," *npj Quantum Information*, vol. 6, Sep 2020.

[50] C. A. Brasil, F. F. Fanchini, and R. de Jesus Napolitano, "A simple derivation of the lindblad equation," *Revista Brasileira de Ensino de Física*, vol. 35, pp. 01–09, Mar. 2013.

[51] D. Manzano, "A short introduction to the lindblad master equation," *AIP Advances*, vol. 10, p. 025106, Feb. 2020.

Die approbierte gedruckte Originalversion dieser Diplomarbeit ist an der TU Wien Bibliothek verfügbar
The approved original version of this thesis is available in print at TU Wien Bibliothek.
TU Bibliothek Your knowledge hub WIEN

Die approbierte gedruckte Originalversion dieser Diplomarbeit ist an der TU Wien Bibliothek verfügbar
The approved original version of this thesis is available in print at TU Wien Bibliothek.

Acknowledgments

Despite the difficult times because of the Corona pandemic I really enjoyed the time I spent at the Atominstitut in the atomchip group. The time was very instructive, I learned very very much in the last year. This ranges from simple soldering together electrical parts (which I did for the first time) to more difficult things like setting up the communication between an AWG and the PC. Besides that I learned a lot of new interesting physics regarding our topic. All this would not been able without the help of the following people.

First, I want to thank the leader of the lab Andreas Angerer who introduced me in NV experiments and who guided me through the different difficulties which arose during the last year. His immense knowledge ranging from programming over cryostat operations to quantum physics was very impressive and helpful. He was always willing to discuss things with me with helped me a lot to understand the underlying physical concepts better.

Moreover, I want to thank Wenzel Kersten, who had always an open ear for my questions and was willing to answer every one of them no matter how stupid they probably were. He introduced me in how to handle the Matlab scripts used for the different measurement runs and showed me how to interpret the obtained data correctly. By doing so, I gained very much knowledge about our measurement scheme and the underlying physics.

Next, I want to thank Andrew Kanagin with whom I had some fruitful discussions as well. Besides that he helped me with answering questions regarding the English language. The barbecues and other cooking events he organized were a welcoming opportunity to get better in touch with others and made the time here even nicer.

Additionally, I want to thank Jörg Schmiedmayer for the opportunity to work in his group and for letting us follow our own ideas.

Finally, I want to thank my parents, my brother and my girlfriend, without them it would be impossible to finish my studies. They always encouraged and supported me on my way. Without them I would not be there where I am today. For that I owe my family my deepest gratitude.

Die approbierte gedruckte Originalversion dieser Diplomarbeit ist an der TU Wien Bibliothek verfügbar
The approved original version of this thesis is available in print at TU Wien Bibliothek.
TU Bibliothek Your knowledge hub WIEN